UNIVERSIDADE DE LISBOA
FACULDADE DE CIÊNCIAS
DEPARTAMENTO DE FÍSICA

Decoding gait phases from neural activity in rat

Ana Filipa Sousa Silva

Mestrado Integrado em Engenharia Biomédica e Biofísica
Perfil em Engenharia Clínica e Instrumentação Médica

Dissertação orientada por:
Prof. Dr. Tomislav Milekovic
Prof. Dr. Hugo Ferreira

2017

Abstract

Introduction. Clinical assistance when it comes to nerve damage and spinal cord trauma falls short, and rehabilitation and recovery can sometimes be impossible due to the inability to self-regenerating. The brain spinal interface (BSI) is a concept that arises when exploring epidural electrical stimulation as a potential technique that is able to restore locomotion after a spinal cord injury. BSI's in monkeys and humans have already been proven successful, however not in rats. The rat model is significantly different from the other ones, especially when it comes to its neural organization and complexity. For this reason we searched for proof that it is also possible to decode gait phases from neural activity in rat. This thesis was originated from the work done in a six month internship in Gregoire Courtine laboratory, based in Switzerland.

Background. In rats the area that is known to encode information about movement is the primary sensorimotor cortex. This information is passed on through the descending neural pathway in the medulla and then on to the efferent nerves that trigger the necessary muscle groups that enforce motion and ensure time specific flexion and extension. In case of a spinal cord injury and subsequent lower limbs paralyses, the nerves are severed in such a way that this signal is lost. The BSI aims to capture gait related neural activity by implanting a 32-channel microelectrode array (Tucker-Davis Technologies (TDT), Alachua, FL, USA) in the right sensorimotor cortex and use classification methods to obtain quantitative prediction outputs. For the purposes of this thesis these outputs were the conditions of foot strike and foot off.

Methods. We implanted two female Lewis rats designated by r263 and r328 and used a dedicated motion capture system (Vicon Motion Systems®) to record 3D kinematics and video. After sufficient recovery time after the surgery we proceeded to do the overground recordings. Each recording session consisted of one rat performing a full length runway walk walking quadrupely. We had 24 sessions for r263 and 31 for r328. From the Vicon files we extracted the real time of left foot off and left foot strike. The data sets containing the neural activity were pre-processed, and at the end we preserved 31 channels and extracted three different signal components (LPC, TRFT-low, TRFT-high). For each event (left foot off, left foot strike and baseline) we had a total of 93 extracted features that were used to train a regularized discriminant analysis classifier. Using cross-validation we trained different classifiers using different combinations of model parameters and choose the mutual information values to be our predictor for the optimum detection model.

Results & Discussion. From the three extracted signal components, the TRFT-low showed the most information around the time of the event. The highest mutual information value found was of 0.617, considering that 1 was the highest possible number. We also built a decoder for predicting right side events, however it had a performance around 25-30 percent lower, comparatively to the left side prediction. This is justified by the fact that the implant was placed on the right sensorimotor cortex. The idea of a BSI, proves to be feasible on the rat model since it is possible to decode gait primitives using neural activity recorded from the sensorimotor cortex.

Key words: spinal cord injury; neurorehabilitation; epidural electrical stimulation; brain spinal interface; LFPs; decoder; foot strike; foot off.

Resumo

Introdução. A assistência médica prevista em casos de traumatismo na medula espinhal é escassa, o que em conjunto com a incapacidade de autorregeneração do sistema nervoso central, implica que a recuperação após trauma seja lenta e muitas vezes impossível. O conceito de uma interface cérebro-espinhal aparece quando exploramos o potencial da estimulação elétrica epidural como técnica de restauração da locomoção após trauma na medula espinhal. Esta técnica já provou ser eficaz em macacos, porém não em ratos. O modelo do rato é significativamente diferente, especialmente quando consideramos a complexidade da sua organização neuronal. Partindo desta problemática procurámos descobrir se é possível decodificar fases da marcha a partir da atividade neuronal em ratos. Este projeto foi desenvolvido durante um estágio de seis meses no laboratório de Gregoire Courtine, localizado no EPFL (École Polytechnique Fédérale de Lausanne), Suíça. Este laboratório especializa-se em neuro-reabilitação e neuro-regeneração. Ao longo desta dissertação será feita a análise e discussão deste projeto.

Revisão da literatura. A marcha humana é produzida por uma série de contrações de músculos extensores e flexores a um ritmo predeterminado. Duas fases podem ser identificadas, uma fase de apoio seguida de uma fase de balanço.

Os mecanismos que controlam a locomoção ainda não são completamente conhecidos, e a maioria da evidência encontrada surge de estudos realizados em modelos animais. No entanto, podem fornecer alguma orientação. Atualmente, sabe-se que não é necessário controlo supra-espinhal para produzir o ritmo básico da marcha, e que este padrão pode ser gerado por circuitos neuronais que existem na medula espinhal. Porém, várias estruturas do cérebro controlam e regulam as variantes da marcha em situações que envolvem uma marcha mais precisa e criteriosa. Os propriocetores musculares também têm um papel importante neste processo. Contudo considera-se que a marcha de um ser humano está mais dependente de um controlo cerebral.

O córtex motor tem um papel de supervisão durante o decorrer da marcha e é a estrutura com o maior nível de abstração em termos da sua atividade elétrica, comparativamente a outras estruturas envolvidas na marcha. Apresenta muita atividade, especialmente quando um movimento requer a ativação de vários grupos musculares.

Aquando de uma lesão espinhal, técnicas de reabilitação como a fisioterapia e a estimulação elétrica são utlizadas com algum grau de sucesso. Geralmente, o foco da reabilitação encontra-se em readquirir alguma qualidade de vida e destreza motora por parte do doente. No entanto nos casos em que a gravidade da lesão é tal que não existem células neuronais que mantenham qualquer ligação da espinhal medula as perspetivas de reabilitação tornam-se significativamente inferiores. Técnicas que potenciem a plasticidade neuronal e técnicas que viabilizem a regeneração neuronal devem ser então exploradas. A interface cérebro-espinhal utiliza a estimulação elétrica neuronal, controlando o seu ritmo, recorrendo a primitivas descodificadas de atividade neuronal que identificam momentos específicos do ciclo da marcha. Procuramos então obter uma prova de conceito, de que é possível obter variáveis discretas de locomoção a partir de atividade neuronal usando o modelo do rato.

Métodos. A área que é conhecida por codificar informações sobre a locomoção no rato é o córtex sensoriomotor primário. Esta informação é transmitida através do caminho descendente do córtex sensoriomotor através da medula para os nervos eferentes que acionam os grupos musculares necessários na locomoção, garantindo a flexão e a extensão faseadas dos membros inferiores. Nos casos

onde há uma lesão na medula espinhal e subsequente paralisia dos membros inferiores, a gravidade dos danos neuronais impedem a transmissão do sinal. O objetivo da interface cérebroespinal é capturar a atividade neuronal relacionada com a locomoção implantando uma matriz de microeléctrodos de 32 canais no córtex sensorimotor primário direito e usando métodos de classificação para prever momentos específicos do ciclo da marcha, que neste caso foram: o aplanamento e o impulso do pé. A nomenclatura usada para estes dois momentos foi de *foot strike* e *foot off* , respetivamente.

Dois ratos fêmeas da raça Lewis designados por r263 e r328 receberam o implante cortical. Após o tempo de recuperação recomendado pós-cirurgia, prosseguimos com os ensaios, que consistiam na execução de aproximadamente um metro e meio de caminhada quadrupede. Um sistema de captura e análise de movimentos tridimensionais (Vicon Motion Systems®) foi utilizado para gravar as variáveis cinemáticas e o vídeo. No total, considerámos vinte e quatro sessões para r263 e trinta e uma sessão para r328. Após a análise das variáveis obtidas pelo sistema *Vicon*, extraímos o tempo real dos dois momentos do ciclo da marcha: *foot strike* e *foot off*. Os potenciais de campo locais (*LFPs*) obtidos durante os ensaios foram processados de modo a obter três componentes diferentes do signal: uma no domínio do tempo (LPC), e outras duas no domínio das frequências (TRFT-low and TRFT-high). Primeiramente, o sinal sofreu *common average re-referencing* e os ensaios e canais anormais foram removidos. Depois, para obtermos a LPC aplicamos um filtro Savitzky-Golay de segunda ordem. As outras duas componentes foram obtidas através da utilização de uma transformada de Fourier. A identificação da banda de frequência de TRFT-high e TRFT-low foi feita olhando para os valores de SNR (*Signal-to-noise ratio*). Para r263 TRFT-high estava entre os 3 e 15 Hz e TRFT-low entre os 39 e os 747 Hz. Para r328 TRFT-high estava entre os 3 e 21 Hz e TRFT-low entre os 105 e os 693 Hz. No final, para cada evento (*foot strike*, *foot off* e *baseline*) um total de 93 características foram extraídas sendo usadas para treinar um classificador de análise discriminante regularizado. Usando o método de validação cruzada, treinamos diferentes classificadores com diferentes combinações de parâmetros e selecionámos os valores de informação mútua como preditor do modelo que seria o ótimo. Toda a análise relativa à atividade neuronal foi feita com o auxílio do software Matlab®.

Resultados & Discussão. Dos três componentes de sinal extraídos, TRFT-low demonstrou possuir a informação mais relevante em torno do momento de cada evento. O valor mais alto de informação mútua obtido para eventos relativos ao lado esquerdo da marcha foi de 0,617, considerando 1 o máximo. Relativamente aos eventos do lado direito, o desempenho do algoritmo foi 25-30% mais baixo, comparativamente. Facto este que pode ser justificado visto que o implante foi colocado no córtex sensório-motor direito. A continuação deste trabalho, requer mais ensaios e se possível num maior número de ratos. Conjuntamente, um algoritmo mais sofisticado e com uma maior precisão deve ser estudado. Também é importante continuar os esforços no sentido de perceber a dinâmica neuronal e de que maneira todos os sistemas se integram para garantir funções motoras num estado saudável de modo a otimizar a abordagem terapêutica em patologias que comprometem estes sistemas.

Conclui-se dizendo que a ideia de uma interface cérebroespinal revela-se viável usando o modelo do rato, uma vez que é possível descodificar primitivas de marcha utilizando a atividade neuronal registada a partir do córtex sensório-motor. No entanto, isto foi apenas o primeiro passo no desenvolvimento de uma interface cérebroespinal completamente funcional.

Palavras-chave: lesão na medula espinhal; neuro-reabilitação; estimulação elétrica neuronal; interface cérebroespinal; potenciais de campo locais; classificador; *foot strike*; *foot off*.

Contents

Abbreviations

ASIA – American Spinal Cord Association
BSI – Brain Spinal Interface
CNS – Central Nervous System
EES – Epidural Electrical Stimulation
EMG – Electromyography
FFT – Fast Fourier Transform
LFO – Left Foot Off
LFP – Local Field Potential
LFS – Left Foot Strike
LPC – Low-Pass Component
MLR – Mesencephalic Locomotor Region
MUA – Multi-Unit Activity
RFO – Right Foot Off
RFS – Right Foot Strike
SCI – Spinal Cord Injury
SNR – Signal-to-Noise Ratio

List of Figures

List of Tables

Chapter 1

Introduction

The vertebrate spinal column accommodates the spinal canal, which encircles and protects the spinal cord. The central nervous system is responsible for superior cognitive functions and it houses the brain and the spinal cord. The spinal cord connects to the peripheral nervous system and therefore is essential to all somatosensory mechanisms. A spinal cord injury (SCI) takes place when there is trauma to the spinal nerves, usually as a result of excessive force applied, laceration or a neurodegenerative disease. Damage to the axons usually impairs the corresponding muscles and nerves bellow the injury site, and this is problemsome because the central nervous system is generally incapable of self-repair. There are different levels of SCI and severity degrees, the level refers to the location of injury and are denoted by the vertebrae name and severity says to which degree the sensory and motor function is still possible[1].

A SCI has a major impact in a person's life and also the life of its caretakers, because it becomes impossible for them to resume their daily life and perform the same activities, autonomously. Also the economic and social implications are severe. In case of an incomplete injury some functions can be restored through intense physical rehabilitation. Electrical stimulation of nerves may repair some motor and sensory functions however, it depends on the level and type of SCI. To date there is still no way to reverse the damage to the spinal cord, but major research fields focus on the subject, some more focused on rehabilitation and others on increasing quality of life. The answer to this problem may come from neural engineering efforts, electrical stimulation, prostheses or brain-machine interfaces.

Epidural electrical stimulation (EES) was first used as a pain management therapy, but with time its potential as a rehabilitation technique was revealed, since it can be used to promote spinal neuroplasticity. Here, a microchip is implanted over the dura mater bellow the site of injury, and delivers electric current. Over time this allows for re-arrangements of the connections between neurons. However, by itself, EES only has had clinical human trials where this technique is used as a way to increase a patient's general health and quality of life[2].

In recent years there has been major breakthroughs in the different fields regarding research on recovering from a SCI and more and more stakeholders seem to be getting involved. Although recovery from SCI seems to be more feasible, complete reversal of paralysis still appears to be a farfetched notion. The answer appears to lie in combining multiples techniques and therapies that provide a safe eco-system that can be translated to humans, from stem cells research to technology advancements.

In 2012, Gregoire Courtine lab [3], showed that by combining excitatory drugs, epidural electrical stimulation and intensive training, using the rat model, it was possible to restore voluntary control of locomotion after SCI. Since then, it has broaden its research and focused immensely in improving the stimulation protocols. Now, this Switzerland based lab, has explored different techniques

in mice, rats, monkeys and humans, and developed new technologies and models in its efforts of finding an answer to SCI.

Another idea that has been explored is an interface that makes use of neural information to trigger and tune EES bypassing the injury and therefore better mimicking natural locomotion processes. This is referred to as a brain-spinal-interface (BSI), which incorporates different technologies. Here, a microchip is implanted in the primary motor cortex to record neural activity and a spinal electrode array is also implanted under the lesion site. Then, an algorithm decodes from the neural activity, locomotor primitives which are used to control stimulation protocols and trigger the spinal implant to deliver electrical current to recruit paralyzed hind limb muscles after SCI, with pharmacology aid to ensure the chemical synaptic transmission[4].

This is a step in human Neuro-rehabilitation, since we know that in primates the brain does control movements and we want to reconnect the motor cortex to the sub lesion therefore we aim to use signals from the motor cortex and regain the information bridge. It already has been successfully done in monkeys, however more advances can be made by using the rat model where more immunohistochemistry techniques are available and the timetable is significantly reduced which also means less costs[4].

The concept of a rat BSI, although theoretical as a whole, in its individual parts has already shown to be feasible in other projects. However there is still the question of whether or not decoding from neural activity in rats is viable as the rat's brain is immensely less organized and the low complexity degree is an obstacle for it to be used in an online system[5]. Before starting this endeavour, we needed to find proof of concept that it is possible to decode gait phases from neural activity in rat, offline. More specifically: **Can we accurately decode the time of the two stages of gait from the neural activity of an intact rat?**

The work done for my thesis was in search for this answer, where I did a six month internship supervised by Tomislav Milekovic in Georgine Courtine's laboratory situated in École Polytechnique Fédérale de Lausanne, Switzerland. I did this thesis as a student of *Faculdade de Ciências, Universidade de Lisboa* under main supervision of Professor Hugo Ferreira, member of the *Faculdade de Ciências da Universidade de Lisboa* faculty. Figure 1.1, schematizes what led to the development of this project.

Neurorehabilitation after SCI

A spinal cord injury takes place when there is trauma to the spinal nerves. Generally the central nervous system is incapable of self-repair, as a result the corresponding muscles and nerves bellow the injury site become impaired. To date there is still no way to completely reverse nerve damage, however major scientific breakthroughs are being made across many fields.

Epidural electrical simulation

Epidural electrical stimulation was first used as a pain management therapy, but its potential as a neurorehabilitation tecnhique was soon discovered. Here, a microchip is implanted over the dura mater bellow the site of injury, and delivers electric current. In 2012, Gregoire Courtine lab [1], showed that by combining excitatory drugs , epidural electrical stimulation and intensive training, it was possible to restore voluntary control of locomotion after SCI, using the rat model.

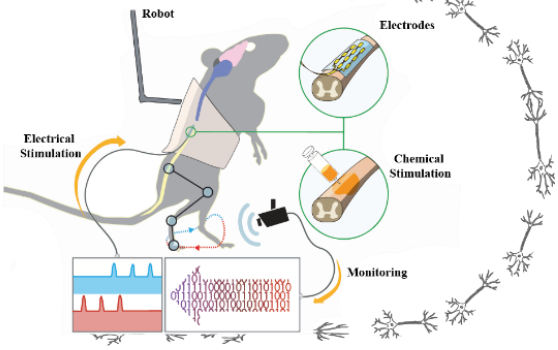

Brain-spinal interface

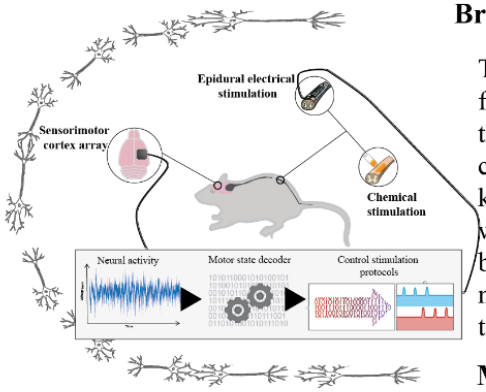

The idea of a rat BSI is to use gait-related information captured from neural activity recorded from the motor cortex to stimulate the spinal cord and recruit paralysed hindlimb muscles after spinal cord injury. This is a step in human neurorehabilitation, since we know that in primates the brain does control movements and we want to reconnect the motor cortex to the sub-lesion. It already has been successfully done in monkeys however by using the rat model more immunohistochemistry techniques are available, and the whole process in less time consuming and costly.

Motor state decoder

The lower complexity degree and organization of the rat's brain poses the question of wether or not is feasible to use neural activity to decode gait primitives. Before starting this endeavour, we needed to find proof-of-concept that it is possible to accurately decode gait phases from neural activity in rat, offline.

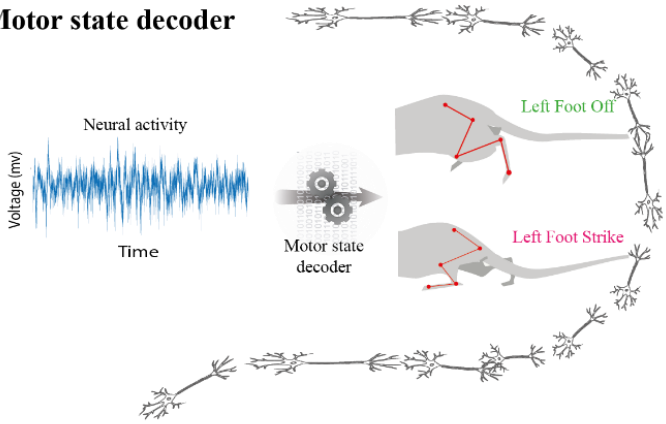

Can we accurately decode the time of the two stages of gait from the neural activity of an intact rat?

Figure 1.1: Infographic of the problematic that lead to the elaboration of the project.

Chapter 2

Background

The nervous system is responsible for the activation of certain muscles and their fine control ensuring the coordination of voluntary and involuntary movements. It is possible to determine which corticospinal structures are involved in the planning and organization of movement using various imaging techniques. However there is still a lot of debate on the role of which structure and on the overall functional structure and its feedback system. In order for us to reach feasible and efficient neurorehabilitation techniques we need to fully grasp the complexity of the nervous system at a micro and macro scale in regards to its role in movement behaviours. In this chapter we will discuss and present some of the existing current hypothesis and theories and also examine the injury setting.

1. Corticospinal locomotion structures

The nervous system is comprised of the central nervous system which includes the spinal cord and the brain, and the peripheral nervous system with all the extensions of the neural structures which includes the somatic and autonomic divisions. For the purposes of this work, we will focus on structures that are a part of the locomotion system.

1.1. The brain

The brain is divided into three main structures: the cerebellum, the cerebrum and the brainstem. The brainstem extends from the upper cervical spinal cord into the cerebrum and posterior to the brainstem lies the cerebellum, as it shows in Figure 2.1.

The brainstem is divided into medulla oblongata, pons and midbrain (also known as mesencephalon). The pyramidal decussation happens below the pons, here most motor fibers that pass from the motor area of the cortex to the medulla oblongata to the spinal cord cross over at the midline (see Figure 2.1). The cerebellum consists of 2 hemispheres with a midline structure connecting them, the vermis. The cerebellum is involved in modulating motor control to provide extremely coordinated body movements.

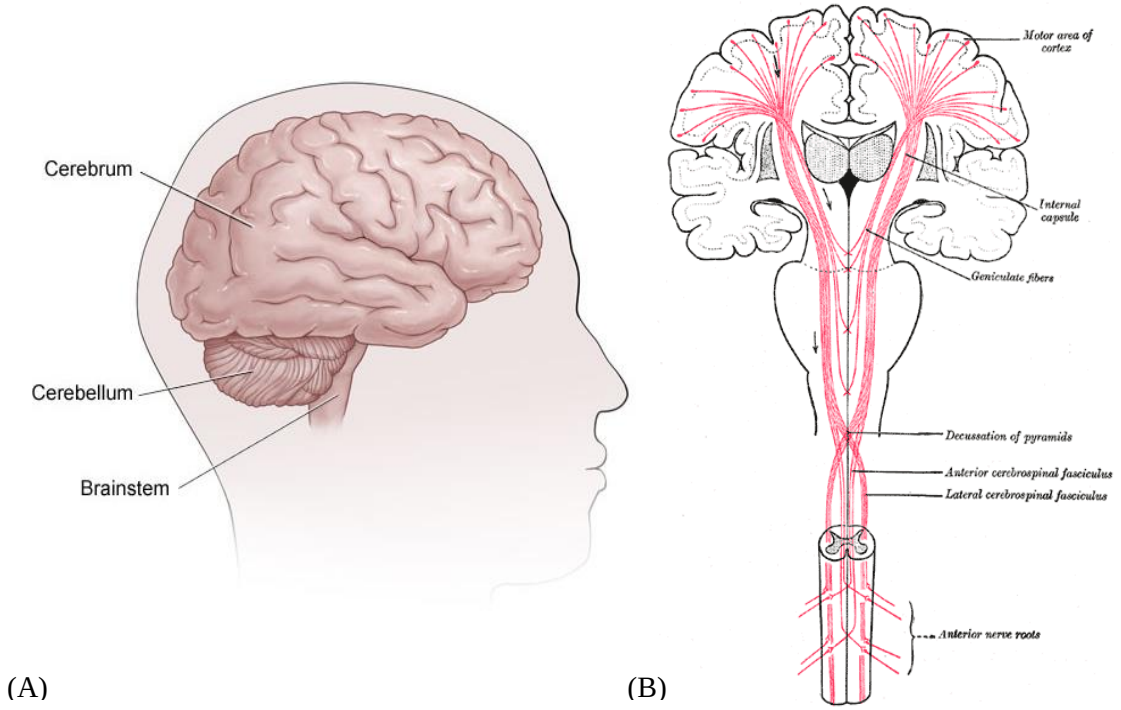

Figure 2.1: (A) The human brain and their three main divisions: Cerebellum, cerebrum and the brainstem. Adapted from [6]. *(B) The decussation of motor fibers. Adapted from* [7].

The cerebrum is the main component of the brain and is structurally divided into four lobes: the frontal lobe, the parietal lobe, the temporal lobe and the occipital lobe. Functionally we have the telencephalon and the diencephalon. The telencephalon has the cortex, the subcortical fibers and the basal nuclei, and the diencephalon has the thalamus and the hypothalamus. The basal nuclei or basal ganglia is deeply connected with the motor cortex and the premotor cortex and has a fundamental role in the modulation of movements[1].

1.1.1. Motor cortex

Voluntary movements require the participation of the motor cortex in order to achieve specific coordinated movements. The motor cortex is located in the frontal lobe, anterior to the central sulcus and it is a functional area of the cerebrum. It is divided in three areas, the premotor cortex, the supplementary motor area and the primary motor cortex. More specifically, the primary motor cortex, is located on the precentral gyrus and on the anterior paracentral lobule on the medial surface of the brain. It is organized in a somatotopically way and as we move across the precentral gyrus from dorsomedial to ventrolateral, we find areas that coordinate torso, arm, hand and face movements, respectively. The premotor cortex and supplementary motor area also have their own somatotopic maps. In terms of its cytoarchitecture the motor cortex is divided into six layers. Each of these layers contain different proportions of pyramidal and non-pyramidal cells. The main difference between them is that axons from non-pyramidal cells terminate locally and pyramidal cells have long axons that go down to the spinal cord. The motor cortex connects to other areas of the cortex directly through the thalamus

and receives input from the cerebellum and the basal ganglia indirectly through the thalamus, see Figure 2.2.

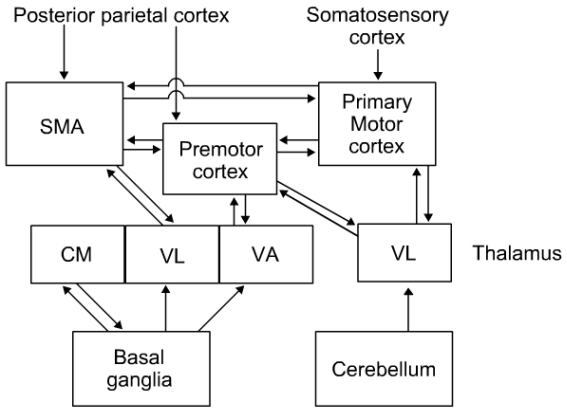

Figure 2.2: Main connections of the motor cortex. Ventral Lateral nuclei (VL). Ventral anterior nuclei (VA).Centrum medianum nuclei (CM).Adapted from [8].

1.1.2. Mesencephalic locomotor region

The mesencephalic locomotor region was first introduced when studies showed that electrical stimulation of that particular area triggered walking and galloping in cats. It is located in the mesencephalon, which is part of the brainstem, and its neurons descend through the medulla and connect with the motor neurons supplying the trunk and proximal limb flexors and extensors[1].

1.2.Spinal cord structure

The spinal cord is a structure protected by bones of the vertebral column. It is divided into four parts: cervical, thoracic, lumbar and sacra and is externally protected by three membranes of the central nervous system, the pia mater, arachnoid and dura mater. There are fissures from each side of the cord where the ventral and dorsal rootlets emerge to form the spinal nerves. In its essence the spinal cord is composed of grey matter that is surrounded by white matter at its circumference. The grey matter shows a crescent shape and the proportions between the grey matter and white matter vary according to its location within the spinal cord. The proportion of white matter diminishes towards the end of the cord and the grey matter becomes a single mass where parallel spinal roots form a structure called cauda equina. The white matter is divided into dorsal, dorsolateral, lateral ventral and ventrolateral funiculi. The grey matter is divided into the dorsal horn, intermediate grey, ventral horn and a centromedial region surrounding the central canal.

From the dorsal rootlets, the dorsal horn and the dorsolateral white matter extend and converge into two bundles and enter the dorsal root ganglion (DRG) in the intervertebral foramen. When the dorsal and ventral roots merge they form the spinal nerve. Spinal nerves end up forming plexuses and from there the peripheral nerves emerge and innervate the whole body[1].

Ascending and descending pathways connect the spinal cord to other parts of the central nervous system. Ascending pathways are responsible of carrying sensory information and leave the spinal cord

through the dorsal roots. Descending pathways carry motor information and leave the spinal cord through the ventral roots.

Spinal interneuronal networks modulate the fine control of spinal motor and somatosensory functions. The role and the different classes of inter neuronal networks are not completely understood by now, however a wide range of interneuron types have been identified by their neurochemical features using imunohistochemical techniques. In the spinal cord there are propriospinal connections. These pathways establish connections between different groups of neurons and transmit information between descending pathways and intrinsic spinal neurons. Information about proprioception comes from muscles, tendons and joints. The axons of sensory nerves that relay the information from spindles to spinal cord are one of the fastest conducting type of nerves. Spindles are groups of muscle encapsulated by connective tissue and connected to two types of sensory fibers. They are also innervated by small motoneurons and axons referred to as gamma efferents. By contracting or relaxing the muscle fibers within the spindles the information about the condition of the muscle is modulated with no need of the spinal cord. In muscle tendons the golgi tendon organs monitor the stretch enforced on the tendon. The central branch of the axon that carries the information from the spindles splits after entering the spinal cord through the posterior horn synapsing right onto moto neurons to commence the monosynaptic reflex or onto interneurons to exert more complex control over locomotor activity[1].

1.3. Meninges

There are three tissue layers that cover the brain and the spinal cord called meninges: the pia matter, arachnoid and the dura mater. The pia covers the Central Nervous system (CNS) and conforms to its grooves and folds and it is rich with blood vessels that descend into the nervous sytem. Around the pia, there is cerebrospinal fluid in a space called the subarachnoid space which is then covered by the arachnoid mater. The last meninge located just on the inside layer of the skull and spinal cord, is the dura mater. Between the arachnoid mater and the dura mater we have the subdural space. Figure 2.3 schematizes the meninges and structures that surround the CNS.

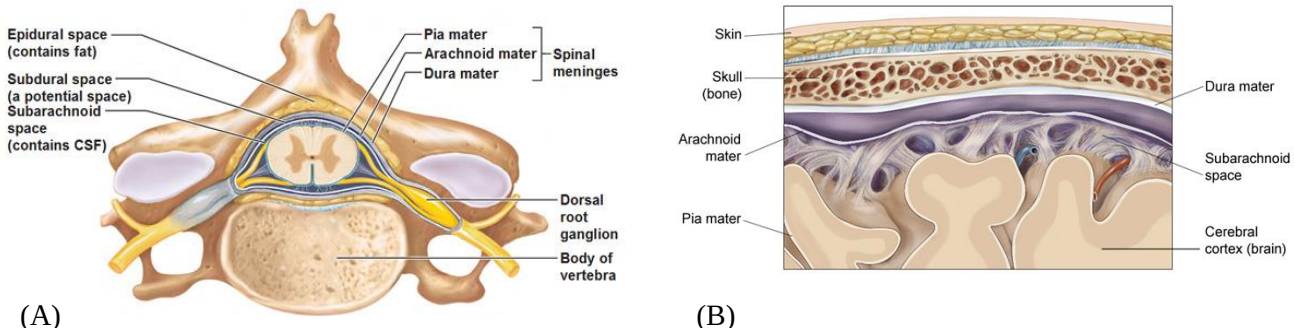

Figure 2.3: (A) Cross-section of meninges and skull. Adapted from [9]. *(B) Cross section of the spinal cord and vertebra. Adapted from* [10].

1.4. Nerve cells

Neurons or nerve cells are the basic unit of the nervous system. A human brain has on the order of 10^{11} nerve cells. There are 2 different types of cells in the nervous system: nerve cells or neurons and glial cells or glia.

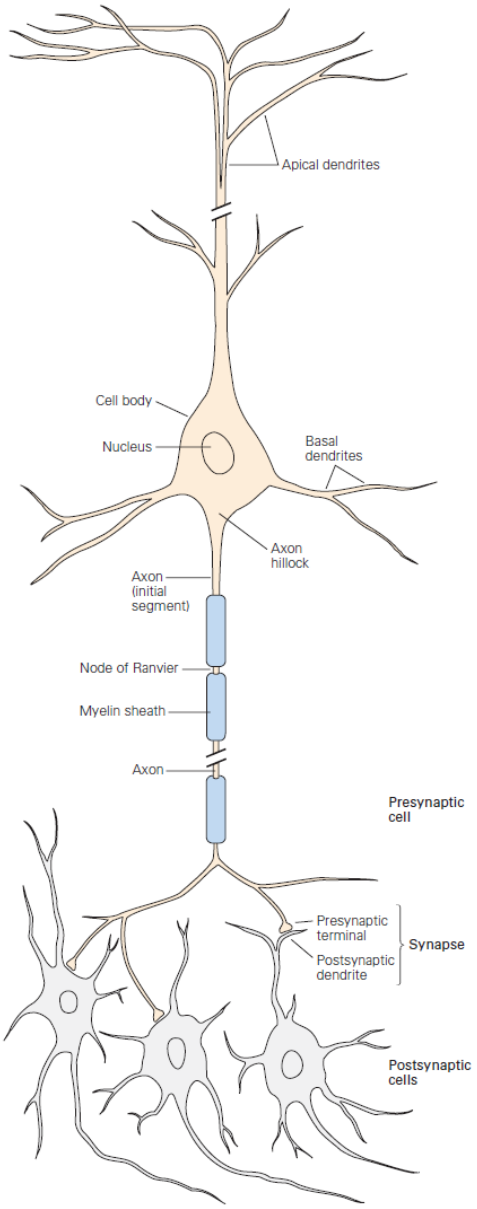

Figure 2.4: Schematics of a neuron. Adapted from [5].

The main structures that define a neuron are: the cell body, dendrites, axon and presynaptic terminals, see Figure 2.4. The cell body is the metabolic center, it contains the nucleus, which contains the genes of the cell, and the endoplasmic reticulum, an extension of the nucleus where the cell's proteins are synthesized. Leaving the cell body we have axons and dendrites. Dendrites are small, thin extensions that are responsible for receiving incoming signals from other cells. Axons are bigger, more defined extensions that carry signals to other neurons. The axon then branches out and connects with other neurons through the presynaptic terminals. The synapse is then defined as the place of communication between neurons. Along the axon we have myelin sheaths composed by a lipid substance, myelin that act as a nerve insulation system. The gaps between the myelin wrappings are called the nodes of Ranvier.

Glial cells outnumber neurons[5]. Glial cells are around nerve cells bodies, axons and dendrites. They differ from nerve cells since they don't form dendrites or axons and are not electrically excitable. They can be divided into microglia and macroglia, with different structures and functionalities[5].

1.4.1. Action potentials

From the axon, electrical signals can be triggered and propagated through the neural network. In the cells, there are voltage-gated ion channels, the potassium and sodium channels, which are voltage sensitive. They are distributed along in unmyelinated sections of the axon, in the nodes of Ranvier and in the cell's body. The Hodgkin-Huxley model (see Figure 2.5) describes the electric currents created when there is a change in ion concentrations.

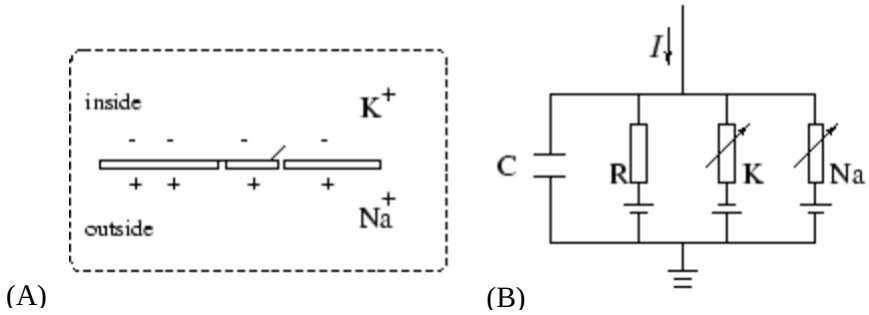

Figure 2.5: Diagram for the Hodgkin-Huxley model. Adapted from [11]. *(A) Iionic concentrations inside and outside the cell. (B) Representative circuit of all nerve cell currents. Adapted from* [11].

Differences in ionic concentrations create concentration gradients that can originate action potentials, which are responsible for conveying messages throughout the nervous system. The transmission of an action potential down an axon occurs the following way, see Figure 2.6:

- The inside of the nerve cell is at its resting potential, -70 mV, however when it receives a stimulus causing the sodium (Na^+) channels to open, its potential can go up to -55 mV. This is defined as the action threshold value.
- If reached the action threshold, more sodium channels open. This influx of sodium drives the cell potential up to about +30 mV. This part of the process is called depolarization.
- The sodium channels close and the potassium (K^+) channels open. Since the K+ channels are much slower to open, the depolarization has time to be completed. An action potential is created.
- After an action potential is reached the potassium channels stay open and the membrane begins to repolarize back towards its rest potential.
- The repolarization typically overreaches to about -90 mV. This is called hyperpolarization. Hyperpolarization prevents the neuron from receiving another stimulus during this time, or at least raises the threshold for any new stimulus. This

is important when preventing any stimulus already sent up an axon from triggering another action potential in the opposite direction during the refractory period.

- Eventually the membrane goes back to its resting state of -70 mV.

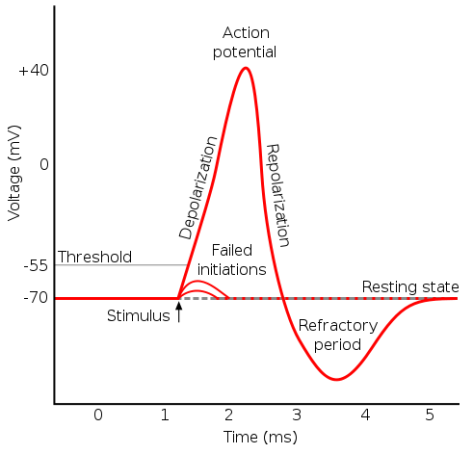

Figure 2.6: Action potential and its correspondent before and after phases. Adapted from [12].

1.4.2. The motor unit

The elementary unit of muscle control is the motor unit. The muscle fibers and the motor neuron which innervates it comprise the motor unit. Generally, muscle contractions involve many motor units. In Figure 2.7, we see that the axon of the motor neuron leaves the spinal cord through the ventral root then it extends until it reaches the muscle and branches out, innervating multiple muscle fibers. When the motor neuron achieves an action potential it releases a neurotransmitter at the neuromuscular synapse (site of connection between the neuron and the muscle) which triggers an action potential through the fibers in a similar fashion to axon depolarization and activates the cross-bridge cycle. The innervation number denotes the number of muscle fibers innervated by one motor neuron. The smaller the number the more fineness of control of the muscle there is [5].

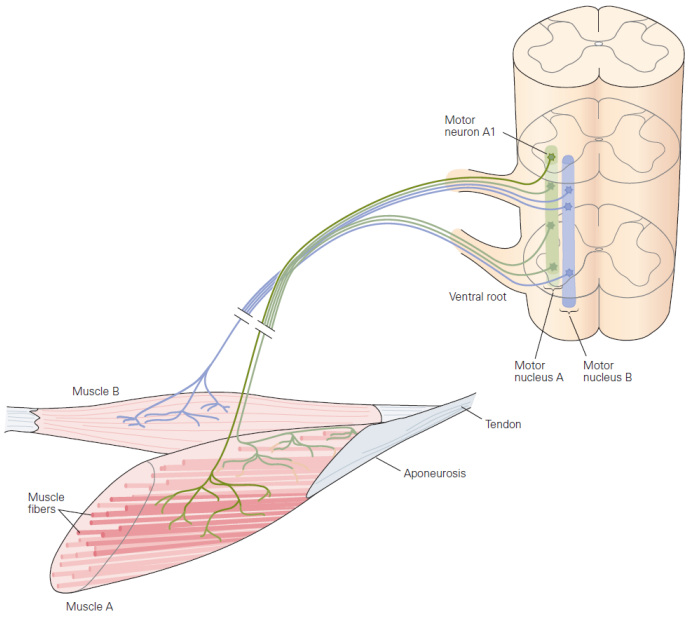

Figure 2.7: Motor unit. Motor neuron and the muscle fibers it innervates. Adapted from [5].

There are three types of muscle: cardiac muscle, skeletal muscle and smooth muscle. Skeletal muscle is a form of striated muscle tissue which is innervated by the somatic nervous system. The skeletal muscle fibers are called myocytes, see Figure 2.8. The myocyte is involved by a cell membrane called the sarcolemma and the sarcoplasm surrounds the myofribils which are long tubular structures which exists at the total length of the myocyte being attached to the sarcolemma at either end. In each myofribil there are smaller structures called myofilaments. Tick myofilaments are mostly composed of myosin proteins and thin filaments of actin proteins. The interactions between these filaments cause muscle contraction and relaxation in a physiological process called the cross bridge cycle [1].

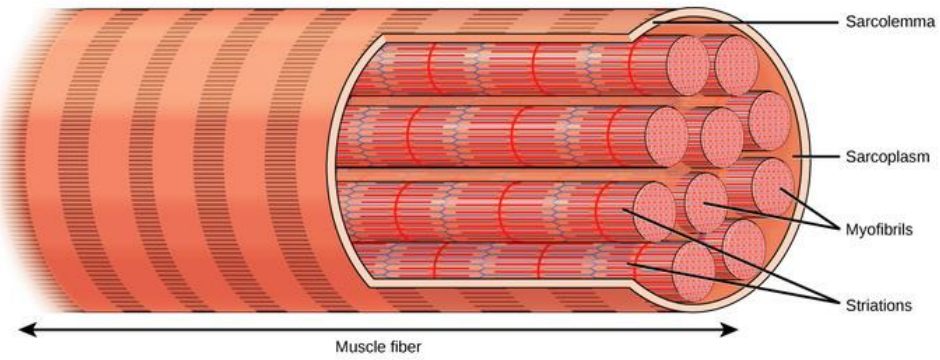

Figure 2.8: Skeletal muscle fiber and its constituents. Adapted from [13].

2. Locomotion

The neural mechanisms that control walking are not yet fully understood, and research has been done in order to understand how nerve cells generate the rhythmic motor patterns associated with locomotion and how sensory information regulates these patterns in different environments. Most evidence there is comes from experiments using cats or rodents and therefore do not completely translate into humans, nonetheless they can provide insight.

The neural control of quadrupedal stepping can be studied under different experimental settings. Spinal preparations require that the spinal cord is transected, separating the spinal segments that innervate the hind limbs. Within spinal preparations we have acute spinal preparations where adrenergic drugs, which trigger spontaneous generation of locomotor activity, are administered right after the procedure. In chronic spinal preparation, no drugs are administrated and the animals are studied weeks after the transection, since daily training can restore locomotor activity. In decerebrate preparations the brainstem is transected at the midbrain level. This one allows research into the role of the cerebellum and brain stem, since it disconnects the spinal centers from the cerebral cortex. Depending on the level of decerebration, stimulation of the mesencephalic locomotor region might be needed to induce a stepping behaviour. Then, there are deafferented preparations where the dorsal roots that carry all sensory information are transected and immobilized preparations that are used to investigate the synaptic events associated with locomotor activity, where an inhibitor is administered blocking synapses at the neuromuscular junction. Finally we have neonatal rodent preparations where the spinal cord is removed in the days following the birth, and placed in a saline preparation combined with a stimulant. The leg motor neurons then generate bursts of activity, and this allows for pharmacological studies.

Early studies using cats with spinal cord transections showed that rhythmic motor patterns could be exhibited without supraspinal sensory input. Subsequently it was shown that quadrupeds with complete paralysis of the hind legs can over time regain hind leg stepping. In stepping behaviours, electromyography data shows similar muscle activity patterns to the ones from non-transected animals. When using immobilized decerebrate animals we also know that the quality of gait varies depending on the amount of supraspinal and afferent sensory input that is still existent. Although the spinal cord itself has the ability to generate locomotor patterns under specific circumstances the overall fine tuning and control seems to be dependent on other neural structures.

In summary, considering all the data, there is sufficient prove to make these four following statements [5]:

1. Supraspinal commands are not necessary for producing the basic motor pattern for stepping.

2. The basic rhythmicity of stepping is produced by neuronal circuits contained entirely within the spinal cord.

3. The spinal circuits can be modulated by tonic descending signals from the brain.

4. The spinal pattern-generating networks do not require sensory input but nevertheless are strongly regulated by input from limb proprioceptors.

2.1.The human step cycle

The rhythmic movements of the legs during stepping are produced by contractions of many extensor and flexor muscles, each precisely timed and scaled to achieve a specific task in the act

of locomotion. The human step cycle (see Figure 2.9) can be divided into two distinct phases. Swing, when the foot is off the ground, it can be divided in two different stages [5]:

- Flexion, there is flexion at the hip, knee and ankle.
- First extension the knee and leg begin to extend moving the foot ahead of the body and preparing the leg to accept weight in anticipation of foot contact. The hip continues to flex.

And stance, when the foot is in contact with the ground, with also two different stages:

- Second extension, the knee and ankle joints flex, even though extensor muscles are contracting. A lengthening contraction of ankle and knee extensor muscles occurs because weight is being transferred to the leg. The spring-like yielding of these muscles as weight is accepted allows the body to move over the foot.
- Third extension, the hip, knee, and ankle extend to provide a propulsive force to move the body forward.

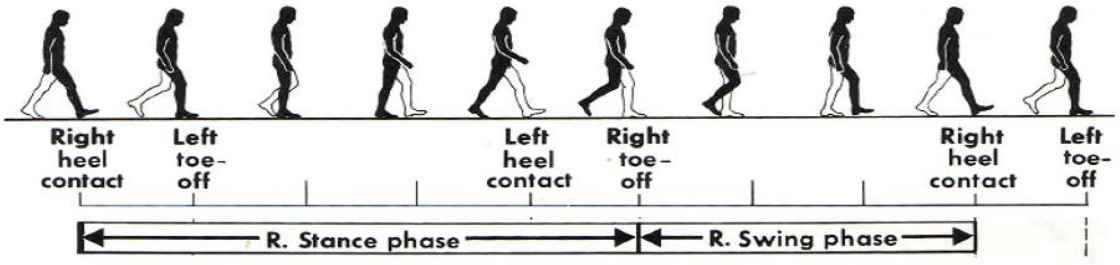

Figure 2.9: Human gait phases from the right leg. Adapted from [14].

2.2. Central pattern generators

The term Central Pattern Generator (CPG) is used when referring to the whole circuitry of neurons within the central nervous system that has the ability to generate rhythmic patterns of motor activity without sensory input from peripheral receptors. Motor neurons from CPGs that generate simple motor patterns can depolarize spontaneously. The most complex ones require the activation of different groups of neurons.

There is not a clear consensus whether central pattern generators actually exist in humans or not. We know that patients who suffered a spinal cord injury are not able to walk automatically afterwards. However from studying babies in development stages we also know that there is a primitive walking reflex when newborns are held upright, that allows for them to perform stepping at a stage when they cannot even support their own bodyweight. This phenomenon disappears soon after and around the first year it is introduce as a voluntary behaviour, at a time when the systems that control balance are more developed. We also know that in humans the locomotor spinal networks are more dependable on supraspinal input [5] [15].

2.2.1. Fine control of locomotor patterns

The visual, vestibular and somatosensory systems provide input that is used to regulate stepping patterns. Proprioceptors in joints and muscles automatically regulate stepping. Cutaneous receptors in the skin give feedback and adjust the stepping patterns to the environment.

Studies with decerebrated cats show that electrical stimulation of the Mesencephalic locomotor region (MLR) initiates stepping. The intensity of this stimulation does not modify the pattern, but the speed of the walk. The mesencephalic motor neurons connect with neurons in the medullary reticular formation whose axons descend in the ventrolateral region of the spinal cord.

Adrenergic drugs can initiate stepping patterns, but it is not what triggers it in nature. Administration of glutamate receptor agonists initiate locomotor activity similarly to when the MLR is stimulated. It is concluded that regarding the descending systems that initiate movement, glutamatergic pathways are involved.

The cerebellum fine tunes locomotor patterns by regulating the timing and intensity of descending signals. Neurons in the dorsal tract are strongly activated by numerous leg proprioceptors and therefore provide the cerebellum with detailed information about the mechanical state of the hind legs. In contrast, neurons in the ventral tract are activated primarily by interneurons in the CPG, thus providing the cerebellum with information about the state of the spinal locomotor network. The cerebellum also receives input from the motor cortex and other forebrain regions related to locomotor function.

The motor cortex uses visual information in complex stepping patterns (walking in irregular terrain, stepping over obstacles). A considerable amount of neurons is activated in the motor cortex, which project to the spinal cord, and may regulate interneurons in the CPG for locomotion and adjust timing and magnitude of a specific locomotor task.

Planning and coordination of visually guided movements involves the posterior parietal cortex. Neurons from this structure seem to increase their activity when an animal approaches an obstacle in their path. For quadrupeds, the posterior parietal cortex stores information in the visual working memory, in order to regulate hind limb movements since they usually are not in the animal's vision field.

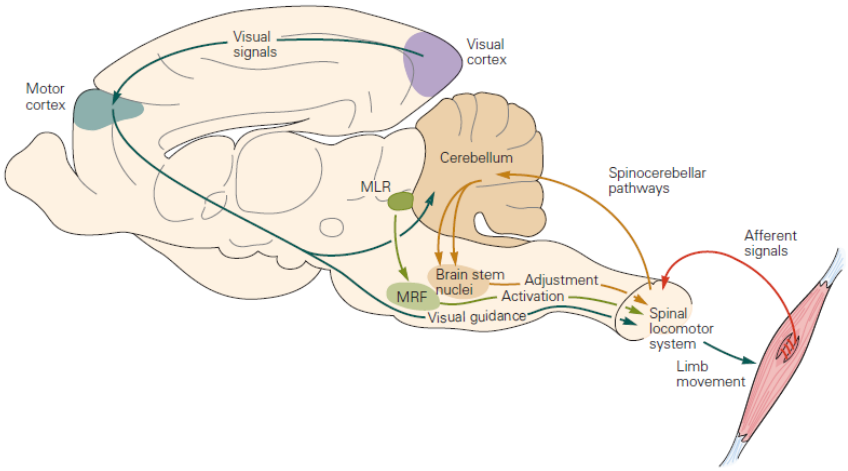

Figure 2.10: Functional organization of supraspinal structures in locomotion. Adapted from [5].

We can divide supraspinal systems into three different functional areas: one activates the spinal locomotor system, initiates walking, and controls the overall speed of locomotion; another one refines the motor pattern in response to feedback from the limbs; and a third one that visually guides limb movement (see Figure 2.10). Descending pathways are necessary for initiation and adaptive control of stepping and fine control of stepping movements involves the motor cortex, cerebellum and various sites in the brain stem.

2.3.Encoding of movement by the motor and premotor cortex

The motor cortex role in the underlying processes of movement is one of supervision, and it is the highest hierarchical structure of motor related neuronal activity. The firing rates of neurons is well observed in the motor cortex, especially when multiple muscle groups are required to perform a certain movement. However, the level of abstraction that we get from looking at this activity is higher in the motor cortex than it is in other lower levels as the spinal cord.

The firing rates of the three different areas of the motor cortex are associated with specific events. The neurons from the primary motor cortex fire 5-100 ms before the movement itself and these action potentials encoded the force, direction, extent and speed of the movement.

The premotor cortex is associated with more complex movements and postures. This area signals the preparation of movement, various sensory aspects associated with particular motor acts and the association of contextual external information with specific movements. The supplementary motor area seems to be connected to the choice of movements based on previously obtained information of movement sequences. It is involved in the transformation of kinematic information into dynamic information and in the mental rehearsal of sequences of movements.

3. Spinal cord injury and Neurorehabilitation

Spinal cord injuries are usually the result of trauma or diseases such as polio and spina bifida and have serious implications on the individual lifestyle and quality-of-life. The type of injury is denominated by the lowest level of the spinal cord that still has normal function. For example a C4 injury means that above that cervical nerve, all spinal cord nerves are still completely functional and the referred one included. Figure 2.11 illustrates different sites of injuries and the corresponding degree of paralysis.

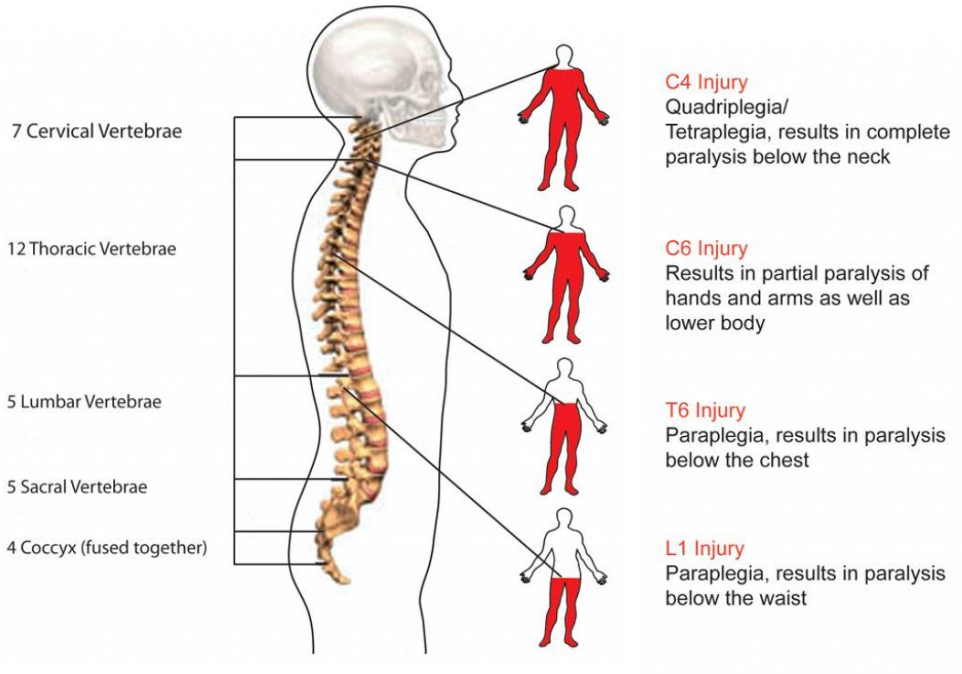

Figure 2.11: Diagram of different paralysis types as a result of a SCI. Adapted from [16].

The injury can also be classified as complete or incomplete depending on the degree to which the spinal cord is severed. If there is still a neural bridge after the injury is considered an incomplete lesion and if there is no nerve connections left it is a complete lesion. Also, when referring to spinal injuries there is a distinction between lesions that cause sensory loss and motor loss, since the ventral roots might be damaged but not at the same level as the dorsal ones or vice versa.

3.1. Clinical neurorehabilitation

A SCI triggers changes within the sensorimotor system. The subsequent impairment depends on both level and completeness of injury. We will focus on the basic and clinical research to re-establish sensorimotor systems involved in functional movements.

According to the level of severity of the lesion, there are guidelines for patients to undergo different available treatments. The rehabilitation goals also differ since it is important to be mindful and have realistic recovery expectations depending on the lesion characteristics. Figure 2.12, synthesizes the degree of injury (according to the ASIA scale[17]), the treatment approach and the rehabilitation goals.

(A)

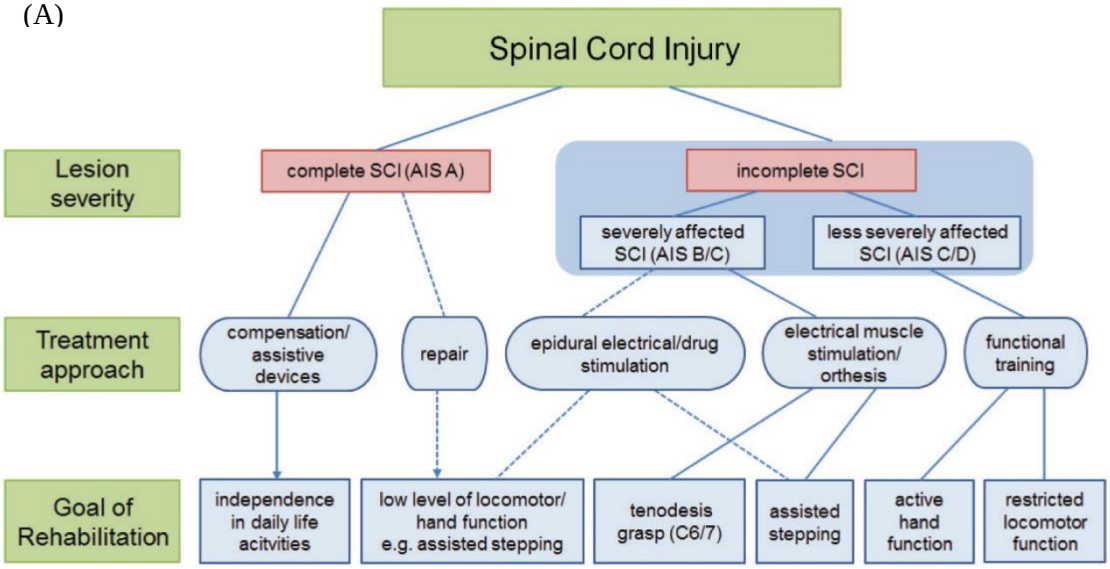

(B)

ASIA grade	Clinical state (below level of injury)
A	Complete: No preservation of function below level of injury, and no sacral sparing (S4-S5).
B	Incomplete: Sensory but not motor function is preserved below the neurological level and includes the sacral segments S4-S5.
C	Incomplete: Motor function is preserved below the neurological level, and more than half of key muscles below the neurological level have a muscle grade less than 3.
D	Incomplete: Motor function is preserved below the neurological level, and at least half of key muscles below the neurological level have a muscle grade of 3 or more.
E	Normal: motor and sensory function are normal.

Figure 2.12: (A) Rehabilitation guidelines after a SCI. Adapted from [17]. *(B) Classification of spinal cord injury according to the American Spinal Injury Association. Adapted from* [18].

In incomplete injuries, neuroplasticity after SCI plays a major role in the rehabilitation of functional movements. It occurs at several anatomical levels of the CNS, such as the spinal cord, the brain stem and the cortex. By unloading the body with assistance, neuroplasticity can be facilitated through the training of movements and by electrical stimulation techniques. However, proprioceptive input to the spinal cord is essential when triggering a locomotor electromyographic pattern during training, since the resulting movements need to evoke appropriate afferent input to the spinal cord to promote neuroplasticity.

Electrical stimulation of the spinal cord was first introduced as a pain relief treatment. Here, an electrode array is implanted in the epidural space of the spinal cord connected to a wire that connects to an electrical impulse generator. It reliefs pain by modifying the pain signal before it reaches the brain. Not all patients experience the benefits of this treatment. Furthermore, research has shown that epidural electrical stimulation delivered bellow the site of injury can also trigger locomotor patterns, as discussed previously on this chapter.

Around sixty percent of patients with SCI have complete injuries[18]. Perspectives for regaining function in this individuals are less and more complex. Nevertheless some preclinical approaches to restore function are being researched.

A complete injury deprives spinal neuronal networks of the descending input that is necessary to trigger their activation. Studies using animal models show that after complete transection of the spinal cord, this lack of excitatory drive from supraspinal centres can be compensated pharmacologically, by electrical stimulation, or by natural sensory afferent input. Even though these studies show promising results, translation to humans have shown less satisfactory results. Still, these techniques show promise and an answer may lie in combining them with axonal regeneration tactics[18].

Some approaches to induce neural repair in the spinal cord were moderately successful in rodents. Schwann cells, which are a type of macroglia cells from the peripheral nervous system, have demonstrated the ability to form tissue bridges after complete lesions. There have been studies that reported regeneration of a few millimetres in axons in rodents, which is still a long way from what a human injured spinal cord needs[18]. In addition, the risk of tumour formation cannot be ignored and axons need to guaranteedly, form the correct connections.

Although this is a growing field of research, there are many other major challenges surrounding clinical translation. Most studies in animal models rely on techniques that need incomplete lesions where there is residual tissue bridges. Also, when it comes to animal models, we see that different species have different possible degrees of recovery. We know that primates have a higher degree of recovery when compared to rodents, since their corticospinal tract has a higher degree of midline crossing collaterals resembling humans better[18]. Finally, quadrupedal locomotion allows for more post-lesion training activities when compared to human bipedal walking.

3.2.Training, pharmacological treatments and epidural electrical stimulation

Rats with paralyzing lesions showed the ability to exert supraspinally controlled hindlimb movement after several weeks of training with an electrochemical neural prostheses that encouraged reorganization of the neural circuitry [3]. In addition, Harkema et al. proved in 2011 that epidural electrical spinal cord stimulation in human patients with complete spinal cord injuries can provide a certain degree of supraspinal control of the legs. At the end of the trials individuals were able to voluntary execute toe extension, ankle dorsi-flexion and leg flexion with help of epidural electrical stimulation[2].

The recruitment of neural pathways is possible with imposed electrical stimulation of the spinal cord. One of the possible explanations for this is that a combination of chemical drugs and electrical epidural stimulation of the lumbosacral spinal cord can force the activation of pathways that trigger CPG networks modulated by sensory information obtained from afferent connections.

3.2.1. Optimum stimulation protocols

The neuro-restorative effects of epidural electrical stimulation can be increased by using optimum stimulation protocols. In earlier studies, as the ones mentioned above electrical epidural stimulation was provided at a constant predetermined frequency and amplitude. Also the array was implanted over the midline on certain segments of the spinal cord with no specific distribution of the electrodes.

Gait patterns can be modulated by tuning EES parameters using feedback control systems [19]. The influence of different EES amplitudes, pulses widths and frequencies on locomotor movements is substantial and through an online monitoring platform, adjustment of EES can provide a less robotic a more accurate and stable walking pattern. For example, the manipulation of the stimulation frequency within certain values can control step height in real time.

The advantages of real-time control mechanisms is potentiated with spatially selective electrodes that are tailored to the anatomy of the spinal cord and vertebra structures. With the identification of the specific muscle groups that are involved in the flexion and extension phases of gait in conjunction with their respective spinal cord dorsal roots, we have better models of stimulating arrays [20].

3.3. Brain spinal interface

The brain spinal interface (see Figure 2.13) is a pre-clinical concept. It is mainly a combination of different already existent technologies. After a complete/incomplete spinal cord lesion two implants are placed in the subject, one electrode array in the cortex, preferably in an area with a high degree of locomotor information such as the motor cortex in human and another electrode array in the spinal cord bellow the site of injury. The cortical array records electric potentials and through a radio frequency transmitter sends them to an external processing unit that decodes from this signals the specific intended gait phase. These triggers are then used to activate electrical stimulation protocols for the different muscle groups involved in the extension and flexion phases of the gait cycle. Also pharmacological excitatory drugs are administrate to ensure the chemical synaptic transmission. This so called motor state decoder is an algorithm that through statistical methods is able to identify specific patterns of data in neural activity recordings and correspond them to stages of the gait cycle, because the neural activity used here is typically recorded from the motor cortex and we know that motor cortex encodes the intention of movement.

There are different approaches that one can use when trying to record neural activity. The chosen approach should considerer the level of specificity that needs to exist for the purpose of the study. The obtained signal depends on the place of implantation of the electrodes. Figure 2.14, schematizes this different techniques and signals.

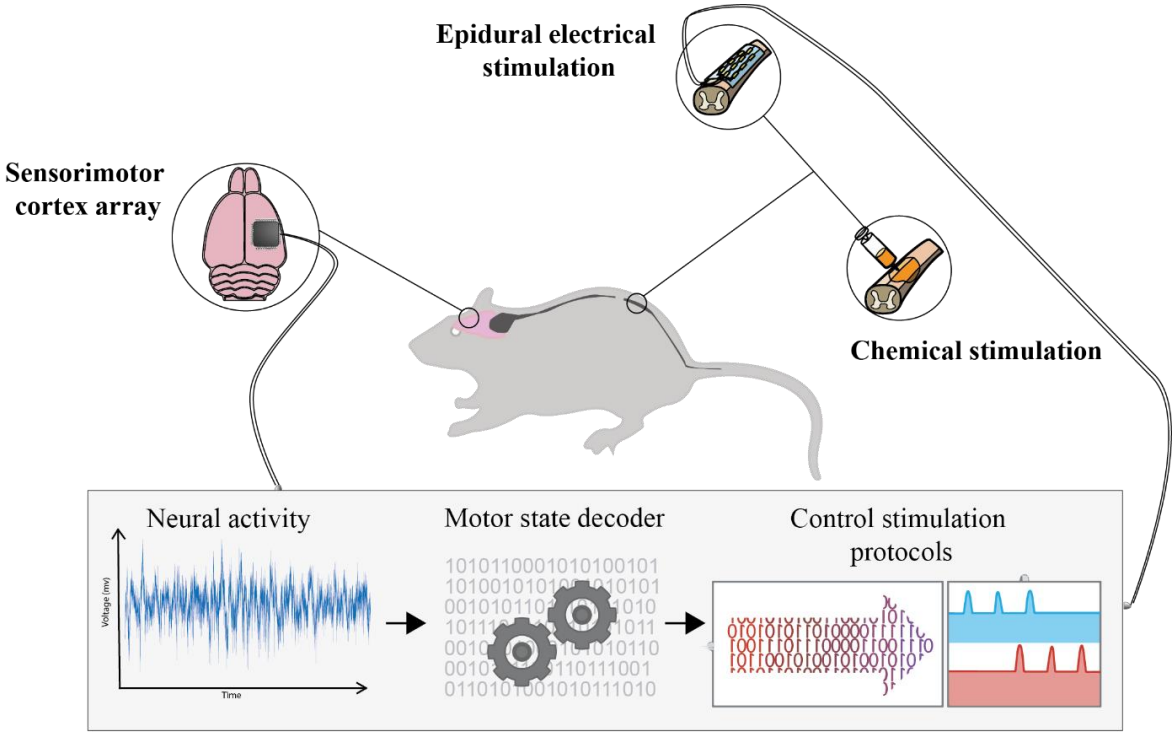

Figure 2.13: Brain spinal interface concept using the rodent model

In a macroscopic scale, electrodes are placed on top of the skin non-invasively and the techniques are called electroencephalography and magnetoencephalography which record the signals through the meninges, skull and skin and therefore implies a high degree of noise and poor resolution, comparatively. In electroencephalography we have the summed electrical currents associated with the firing of neurons and in magnetoencephalography the magnetic fields produced by these electrical currents. In one degree deeper we have electrocorticography where the electrodes are implanted on top of the meninges that envelope the brain. Another technique is Local Field Potentials where the electrodes are implanted right on the cortex piercing the nerve cells. The level of resolution is high and the signal corresponds to the sum of the electrical currents from nearby neurons within a spatial reach of a few hundred. The frequency range goes from 0.5 Hz to 300 Hz. This signal, as it provides information from a collective number of neurons, gives us a good understanding of more complex processes and cognitive functions.

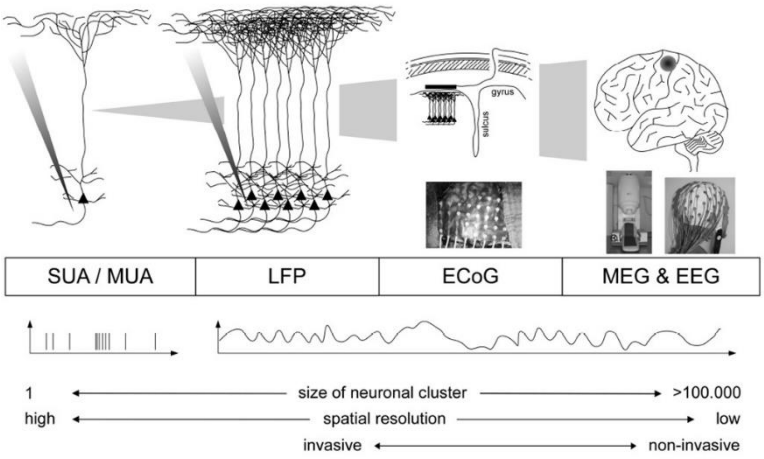

Figure 2.14: Schematics of different neural activity recording techniques. The scale of the recorded neurons increase from left to right. Adapted from [21].

Spikes or action potentials, can also be recorded using microelectrodes. We can refer to them as single unit when it corresponds to activity from one individual neuron recorded using microelectrodes or multi-unit when they were recorded using an array of microelectrodes that record from different neurons. Different techniques are known for the extraction of single unit spikes.

4. Detection algorithms

The motor state decoder is essentially, a predictive algorithm. We can construct a model that has the ability to make predictions on data using computational statistics. Several science fields specialize in building and optimizing of these models/algorithms and its applications are numerous. There are mainly two different types of learning methods that we will consider: supervised learning and unsupervised learning.

Depending on the type of problem and data, some approaches are more adequate than others, see Figure 2.15. Supervised learning implies that there is input and output data apriori that will be used to build the algorithm, and thus will be able to predict new results from unseen new input data. Then considering whether the desirable output we want to predict is continuous or categorical variables we have regression or classification methods, respectively. The second type of learning method is unsupervised learning that does not have the output data as its teacher. This works by clustering the data [22].

These two types are not completely separate from each other, for example, unsupervised learning can be used followed by supervised learning [22].

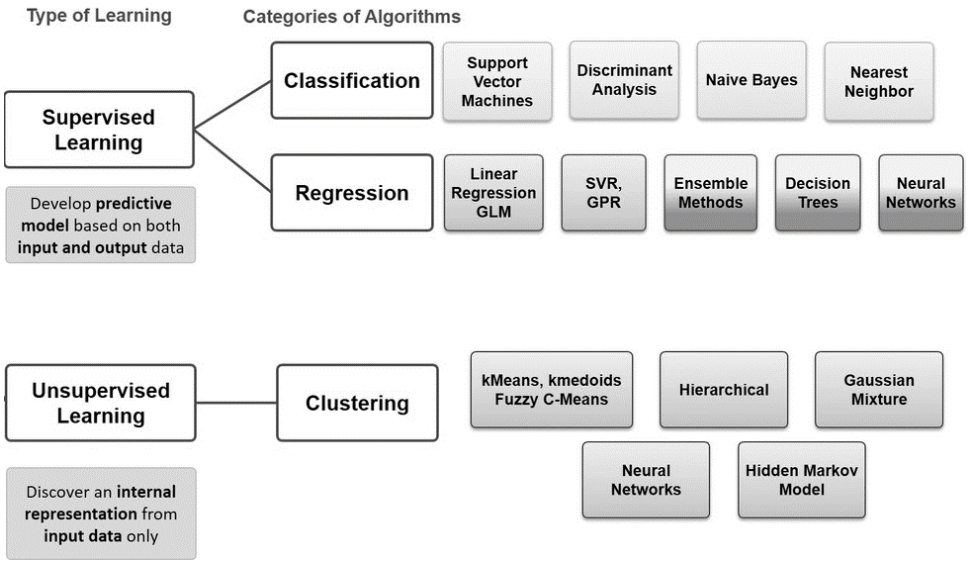

Figure 2.15: Schematics showing different types and categories of learning algorithms. Adapted from [23].

Chapter 3

State-of-the-art

1. Brain machine interfaces in healthcare

There has been a lot of recent developments in research regarding the control of external devices using one's own brain. The applications for these type of devices are extensive and provide a very important step in medical devices. However the demand and the consequent fast pace of new equipments and techniques available is not only due to medical purposes but also due to their vast application in other areas, from gaming devices to security and marketing[24]. Brain computer interfaces (BCIs) for medical purposes can also be used, as a mean of communication for patients with speech impairments, or for movement rehabilitation and assistance in patients with movement disabilities. Different types of invasive and non-invasive neural activity recording techniques can provide us with different types of signals that contain useful information on neural states. The five types of signals that one can get from invasive techniques are: Local Field Potentials (LFPs), Single Unit Activity (SUA), Multi-Unit Activity (MUA), electrocorticographic oscillations (from electrodes on the cortical surface) and calcium channel permeability[25]. From non-invasive techniques we have seven types of brain signals: slow cortical potentials, sensorimotor rhythms, P300 event related potential, steady-state visual evoked potentials, error-related negative evoked potentials, blood oxygenation levels and cerebral oxygenation changes [26]. These different signals have been widely used and have already reported levels of accuracy and robustness.

For assistance purposes, most existent studies show the ability of a person or monkey to control or manipulate a robotic upper limb with previous training sessions where the subject imagines the movement by looking at a screen demonstration or by observing the robotic component perform it. Brain computer interfaces can also have an important role in neurorehabilitation when combined with functional electrical stimulation, since they can therefore provide a bridge between existent supraspinal commands and efferent nerve fibers.

In 2008, Miller et al showed in monkeys with temporarily paralysed forearm muscles that it was possible to use recordings from their motor cortex to provide control protocols over functional electrical stimulation to forearm muscles. A Wiener cascade decoder used approximately 100 neural signals to predict kinetic forces. A multi-electrode array was implanted in the area that encoded hand movements information on the primary motor cortex and spike sorting was performed based on the shapes of the waveforms and inter-spike intervals.

In 2016, Bouton et al showed that it was possible, through learning algorithms, to record MUA from the motor cortex and control forearm muscles using a custom-built neuromuscular electrical stimulation system (NMES) in a quadriplegic patient[27]. The NMES was an array of 130 electrodes embedded into a flexible sleeve that was wrapped around the arm (see Figure 3.1). The patient had to do six selected movements indicated by a computer screen, intercalated with rest periods. One decoder was trained for each individual task using a support vector machine algorithm.

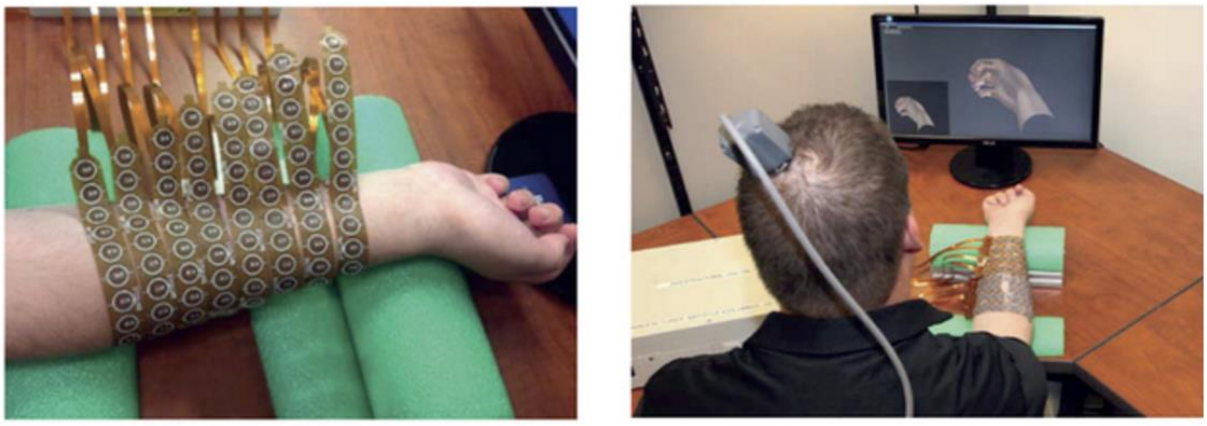

(A) (B)

Figure 3.1: (A) Neuromuscular electrical stimulation system (NMES). Adapted from [27]. *(B) Patient with NMES, implanted cortex array and computer monitor giving instructions Adapted from* [27].

1.1. Brain spinal interfaces for neurorehabilitation

Very few studies have actually been done, combining brain machine interfaces with functional electrical stimulation designed for locomotion restoration. In 2014 [28], a brain-machine-muscle neuro-prosthetic device was attempted and its feasibility tested in six rats. A micro-wire array consisting of one stimulation array, seven neural recording electrodes, one reference electrode and one common terminal electrode was implanted. Neural recordings were mainly obtained from layers V/VI of the motor cortex. Ten to twenty walking sessions with a one minute duration of neural activity were recorded after the implantation surgery. The rats underwent a second surgery for a spinal cord transection and after three to four days of recovery they were attached to a body weight support system which allowed only forelimb walking.

Here a neural signal processing system was built to decode the locomotor primitives form the neural activity. The system had an online spike detection circuit and a signal processing unit. Various spike detection methods were implemented, but lastly the one that showed better performance was the median value spike threshold method. The neuroprocessor run baseline firing rate calculations of the given signal to obtain the threshold value and when the smoothed average spike count was higher than the pre-stored threshold count, the system would prompt stimulation procedures, as shown in Figure 3.2. The electrical stimulation circuit provided biphasic pulses. Different stimulation parameters were tested in order to find the best ones, which proved to be 3 pulses with frequency of 100Hz, for 0.5 ms time each. This allowed rhythmic bilateral hind leg movements.

To test this concept, firstly the procedure was done in an offline mode, without using any stimulation, and the predicted steps were compared to the actual observed steps. Eleven out of fourteen steps were correctly identified (79% accuracy) with a mean time delay of 113.41 ms. Then in real time functioning, the decoder could predict and properly stimulate and trigger locomotion. However after the complete spinal cord transection, accurate locomotor information could no longer be predicted from neural activity obtained from the primary sensorimotor cortex.

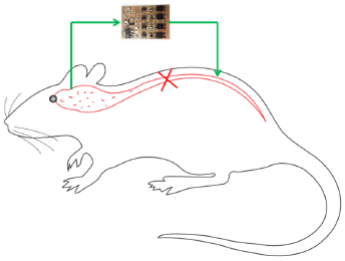

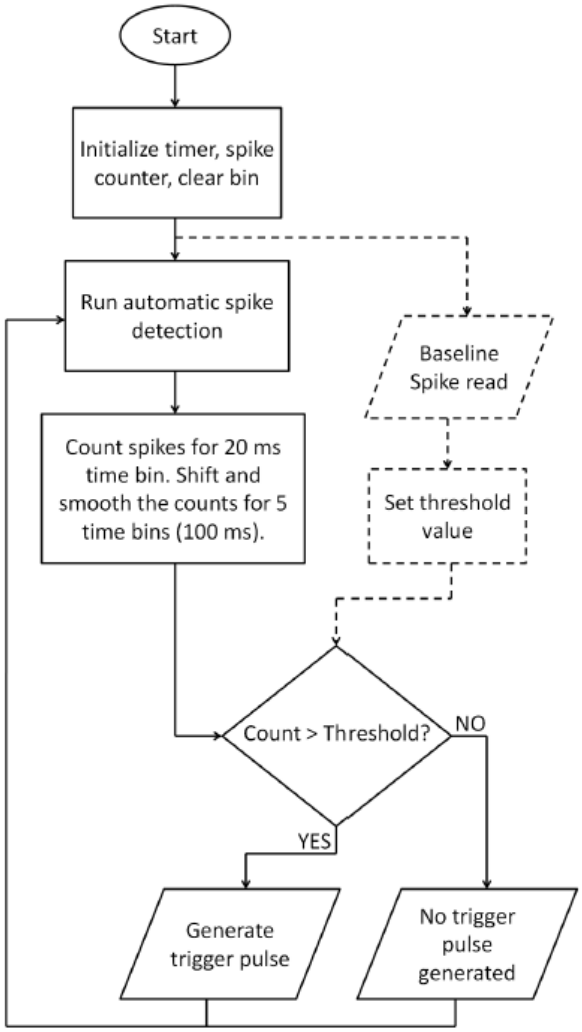

(B)

Figure 3.2: (A) Brain-to-muscle interface. Adapted from [28]. *(B) A diagram of the program flow chart from brain-to-muscle study. Adapted from* [28].

Another brain-spinal interface in monkeys has been successfully developed in the Courtine lab which translates motor intention from motor cortex signals and triggers electrical spinal cord stimulation protocols. The concept is described in Figure 3.3, and consists of an e-dura array [29] that records neural signals and transmits it wirelessly to a computer, that decoded locomotor states and triggers spatially selective electric current pulses executed by the implanted spinal cord stimulation array in a close loop system that monitors the subsequent movements and the electromyography signals.

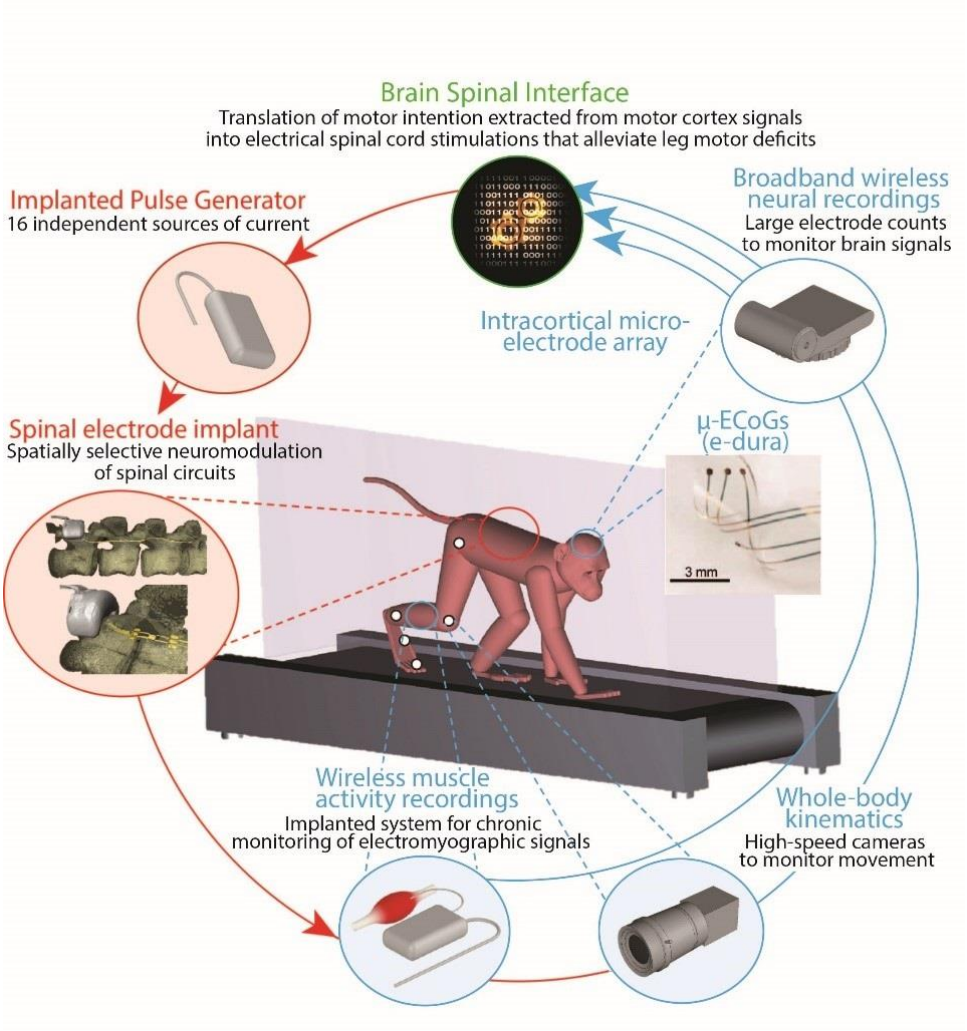

Figure 3.3: Brain spinal interface developed by the Courtine lab in monkeys.

2. State of the art of motor states detection algorithms

2.1. Extracting neural information on locomotion from cortical recordings in rats

Motor cortical neurons encode different variables that can be used for epidural electrical stimulation in rodent models. Although Brain-Machine-Interfce(BMI) research has been largely neglected in this field, some efforts have been made.

In 2009 [30], multiple movement related variables such as robot attachment point position, velocity, and hind limb state were predicted in rats using regression algorithms. Here, it was found that proximal variables were better decoded than distal ones, from the motor sensorimotor cortex, having better kinematics reconstruction at the pelvis level. The study used neural firing patterns has its input information and experiments were made using four rats walking with a robot attached to their pelvis. Also the performance of decoding was compared with reported decoding performance from the DRG neurons and it showed that decoding from the DRG had increased performance, demonstrating that the activity form cortical neurons is more abstract.

In 2012 [31], a study using six rats that had to perform a behavioural task which consisted of pressing a pedal upon hearing an audio cue, used single neuron activity to predict three events. This events were the audio cue, the start of the pressing of the button and the end of pressing the button and peri-event time histograms were used to predict them by showing neuron firing times in a specific time window around the event. Principal component analysis was previously performed to the data. In addition, the kinematics of the trajectory performed by the rat during the behavioural task was decoded using a Wiener filter weighted on the spiking activity of all the neurons recorded simultaneously from the hind limb sensory motor cortex. The model was trained using 50 % percent of the data and tested on the remaining 50% using the cross-validation method.

In 2015 [32], another study performed experiments on six rats trying to decoded several movement related variables from recorded neural activity. These rats were implanted with a recording array in the left motor cortex which recorded single and multi-unit activity, and also with ten bipolar electrodes in the hind limb muscles of the right hind limb to view electromyographic signals. The behavioural tasks were standing, stepping on a treadmill, walking overground and climbing staircases all with a bipedal posture backed by a body weight support system. Firing rates of stable neural units were used to build classifiers of gait phases, stance or swing, or types of tasks, treadmill, runway and staircase using the support vector machine learning method. Also hind limb kinematics gathered as Cartesian coordinates where decoded using the same method. The study concluded affirming that brain machine interfaces can be more accurately built by estimating gait phases instead of continuous variables such as limb or joint positions since they provide more robust control strategies for stimulation protocols.

2.2. Robustness and long-term performance of the decoder

The long-term performance of a decoder depends on the stability of the neural signals used as input information. The non-stationarity of neural signals presents itself as a challenge when using techniques as spike sorting, since the shapes of the waveforms of action potentials change over time due to shifts in membrane conductance's during extended burst firing sequences and electrode position changes. This makes the case for further studying the performance of decoders using LFPs and unsorted spikes when decoding movement variables.

It is reported that LFPs are significantly more stable than spikes[33] but still less accurate. However, performance of detection algorithms that use LFPs as input neural information is still significant enough to ensure precise decoding[34].

For regression type problems, the Kalman filter and its optimized versions have the highest reported communication rate neural prosthesis to date [35], [36]. In terms of motor states classification problems, the linear discriminant analysis classifier and the quadratic discriminant analysis classifier have the most consistent performance overall [22], being consistently ranked among the top three classifiers for multiclass classification.

Chapter 4

Decoding gait phases from local field potentials in rats

As stated in previous chapters, to prove that the BSI was feasible in the rat model we needed to first, find out if we could build a motor state decoder that from neural activity could decode specific gait phases accurately.

The cerebral cortex of the human brain is divided into four lobes each responsible for distinct functions as described in Chapter 2. The frontal lobe houses the motor cortex, which only controls movement. The rat's brain is organized in different functional areas from the human brain, and the area that is known to encode information about movement is the primary sensorimotor cortex represented in Figure 4.1 by M1.This functional area is the highest hierarchical structure of both motor and sensory related neuronal activity. For decoding purposes we needed, at least, of local field potentials, so the cortical implant should be piercing the nerve cells of sensorimotor cortex. Also, since the electrode was intended to be implanted in the right cortex (which encodes left side locomotor activity), it made sense to start with the left hind limb. We chose the hindlimb and not the forelimb since the BSI is to be primarily developed for locomotion restoration and translation must be kept in mind.

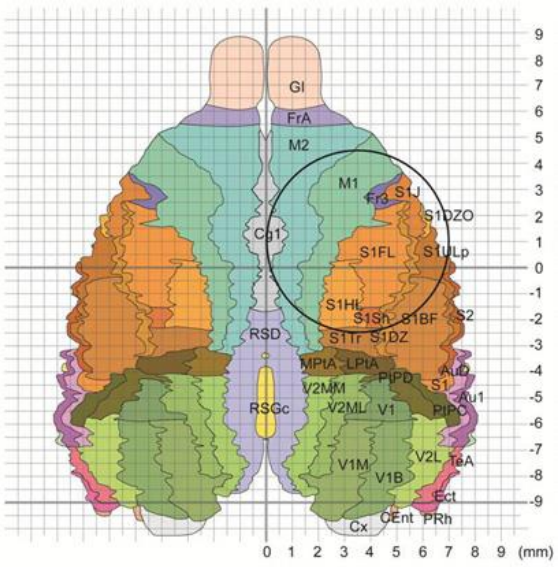

Figure 4.1: Rat's functional brain cortex areas viewed from vertex. The black circle locates the sensorimotor cortex. Adapted from[37].

Considering the rat step cycling , we choose two key moments, the beginning of the stance phase where the foot is in contact with the ground, which we called foot strike, and the beginning of the swing phase where the foot has just left the ground entirely, which we called foot off. In summary, as an input

of the detection algorithm we would have the data from the local field potentials and as an output we need to have the left foot off moment and the left foot strike moment (Figure 4.2).

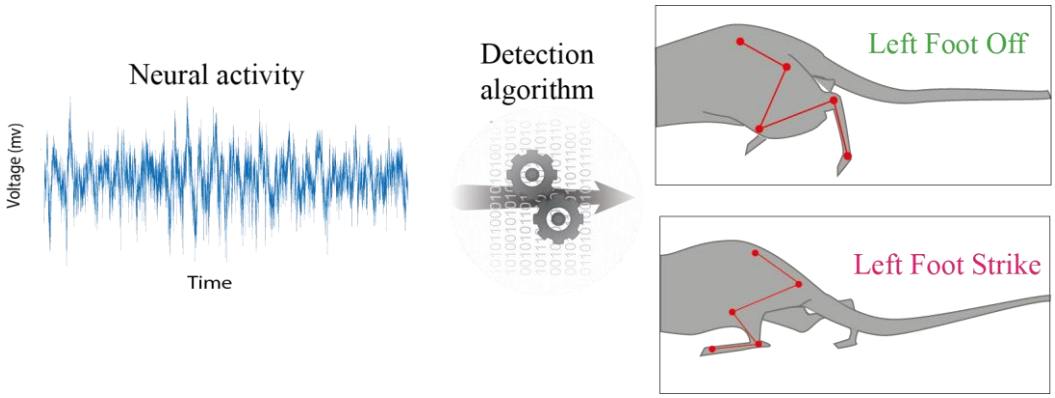

Figure 4.2: Detection algorithm with its input and output.

4.1. Detection algorithms

4.1.1. Supervised Learning Methods

Methods of supervised learning use examples to train the prediction of outputs. The independent variables from classical statistics are viewed and referred to as inputs, predictors or features and the dependent variables are the responses or prediction output. The prediction output can be quantitative or qualitative. We have binary qualitative responses or multi-label ones. All variables that come from prediction functions are represented by a hat accent.

4.1.2. Discriminant Analysis

If the predictor of our detection model, takes values into a discrete set, and the input values can be separated by a finite number of regions our problem becomes one of classification. When these regions are separated by boundaries that are linear, we have linear methods for classification. These approaches are members of a class of methods that model a discriminant function $\delta\kappa(\chi)$ for each class, and then classify x to the class with the largest value for its discriminant function.

Considering that we have classes $\kappa = 1, 2, \ldots, K$, a Linear Discriminant Analysis classifier and a Quadratic Discriminant Analysis classifier, make predictions simply by using the Bayes' rule and selecting the class κ that maximizes this conditional probability[22].

$$P(\mathcal{Y} = \kappa \mid X) = \frac{P(X \mid \mathcal{Y} = \kappa)}{P(X)} = \frac{P(X \mid \mathcal{Y} = \kappa)}{\sum l \, P(X \mid \mathcal{Y} = l) \, .P(\mathcal{Y} = l)} \quad (4.1.)$$

$P(X \mid Y = \kappa)$ is modelled as an estimated multivariate Gaussian distribution [22]with a density function of

$$P(X \mid Y = \kappa) = \frac{1}{(2\pi)^n |\sum_\kappa^{1/2}|} \exp\left(-\frac{1}{2}(X - \mu_\kappa)^t \sum_\kappa^{-1}(X - \mu_\kappa)\right) \quad (4.2.)$$

μ_κ - mean of each class,
$\sum_\kappa^{-1}$ - inverse covariance matrix.

The mean of the class distribution is estimated by the class sample mean and the covariance by the class sample covariance, in the following way[22]

$$\widehat{\mu} = \frac{1}{N}\sum_1^N x^n \quad (4.3.)$$

$$\widehat{\sum} = \frac{1}{N}\sum_{n-1}^N (x^n - \widehat{\mu})(x^n - \widehat{\mu})^T \quad (4.4.)$$

N – sample size.

For the linear discriminant analysis classifier (LDA) the classes share a covariance matrix which makes the decision boundary surface linear. The quadratic discriminant analysis (QDA) model assumes that the classes are conditionally independent since the covariance matrices are diagonal and generates quadratic boundaries between classes[22].

To classify new data we can apply each of the class Gaussian distributions and calculate the probability. To determine the correspondent class we either chose the class with the highest probability or use a threshold value.

4.1.3. Stability and accuracy of LDA and QDA

The LDA and the QDA classifiers have good track records. Both techniques are widely used and produce stable results. The reasoning for this might be that the data supports better, simple decision boundaries. This favours these methods that have linear and quadratic boundaries, respectively, assuming that the Gaussian distribution is stable[22].

4.1.4. Regularized Discriminant Analysis

When our number of features is much higher than our number of samples we have a high dimensionality problem, which can cause overfitting and high variance problems. To overcome this issue we can use a linear classifier with quadratic regularization. Because the dimension of the covariance matrix is $X\,\rho$, where ρ is the feature dimension, in cases where the features' dimension is much bigger than the number of samples the covariance matrix becomes singular. To correct this we use regularization to shrink $\widehat{\sum}$ towards its diagonal.

$$\hat{\Sigma}(\gamma) = (1-\gamma)\,\hat{\Sigma} + \gamma\, diag(\hat{\Sigma}) \qquad (4.5.)$$

$\gamma \epsilon [0,1]$.– regularization coefficient,
$\hat{\Sigma}$ – covariance matrix.

In this technique, the regularization parameter is usually computed using a cross-validation procedure, which searches the classification accuracy using a finite range of γ values and finds the value in this range that maximizes it.

4.1.5. Cross-Validation

Cross-validation is the most widely used method for estimating prediction error. Typically estimates well only the expected prediction error.[22] K-fold cross-validation uses a part of the data to fit the model and another part to test it, computing the prediction error of the fitted model. The original dataset is divided into equal k=1,2,..N folds and *t* folds are used for training the model and the other N-*t* are used for validating the model. N is the total number of trials. Every data fold is used for validating the model through different iterations and at the end the error is estimated conjointly. Figure 4.3 shows an example of a dataset division where N=4 and k=2.

1	2	3	4
Training set	Training set	Validation set	Validation set

1	2	3	4
Validation set	Validation set	Training set	Training set

Figure 4.3: Example of a dataset division for the purposes of cross-validation.

When choosing the size of the training set, we know that if k=N it is unbiased for the true prediction error but has high variance and the computational time is high. However, if we considerably decrease k, we have lower variance but bias is a problem. Figure 4.4 shows in a hypothetical situation how the choice of k, and subsequently of the training set size, can overestimate the expected error. The final compromise is taken when considering the goal of the study.

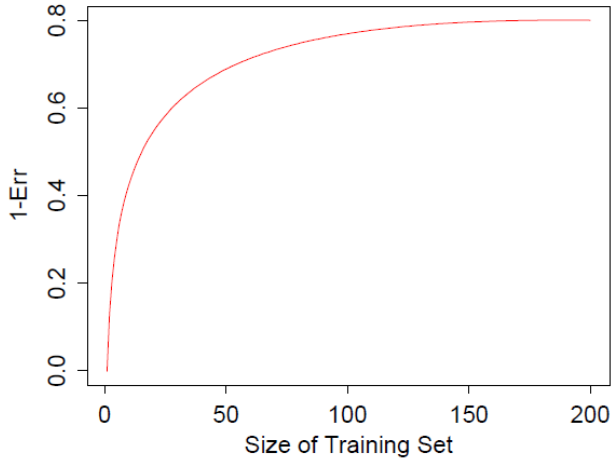

Figure 4.4: Learning curve for a classifier with 200 observation. Err is the estimated average error. Adapted from [22].

4.1.6. Mutual information value

Although we can use the conventional prediction error as a value of the accuracy of the model we can also calculate directly its performance by measuring the mutual information value that compares the time of real events and the time of detected events from one dataset. The mutual information value is given by,

$$I(X,Y) = \sum_X \sum_Y p(x,y) \log_2\left(\frac{p(x,y)}{p(x)p(y)}\right) \quad (4.6.)$$

X, Y – sets of all possible states of real and detected events
$p(x,y)$ – joint probability of x and y happening jointly
$p(x)$ and $p(y)$ – probability of specific event.

It ranges from 0 to 1, and the maximum is achieved when the detected events and real events perfectly match within a chosen time window.

Chapter 5

Methods

1. Rat model and surgical procedures

As mentioned before the rat animal model was suitable for this study due to its accessibility to a range of immunohistochemistry techniques needed to explore the levels of neural restoration. Two female Lewis rats designated by r263 and r328, were used for the experiments. Under general anesthesia, a craniotomy was performed over the right sensorimotor cortex. A ZIF-Clip, 32-channel microelectrode array (Tucker-Davis Technologies (TDT), Alachua, FL, USA) was inserted with the help of a hydraulic 33 microdrive using stereotaxic coordinates and spatio-temporal neuronal characteristics to localize layer V. The row spacing of the microwire array was 250 μm, while the column spacing was 375 μm. To ensure fixation to the skull cranial screws and dental cement were placed. The wires were subsequently covered with dental cement. The array component that connects to the headstage of the ZIP-Clip was left uncovered and projected upwards. Also bipolar electrodes were implanted into the hindlimb muscles in order to record electromyography activity.

All procedures were conducted in accordance with Swiss federal legislation and under guidelines established at EPFL, and approved by local Swiss Veterinary office.

2. Acquisition system

The headstage component was connected to a dedicated neurophysiology RZ5 workstation (TDT, Alachua, FL, USA). Here the pre-amplifier had a high-pass filter at 3Hz. The signals were digitized with a 16 bit resolution at approximately 12 kHz and stored not synchronously with other data. Whole body kinematics was recorded using the high-speed motion capture system Vicon from Vicon Motion Systems®, which combines 12 infrared cameras (200 Hz). Reflective markers were placed in both right and left hindlimbs, positioned on the crest, hip, knee, ankle and fifth metatarsal, making a total of 10 markers. The 3D kinematics reconstruction was done offline with the help of the Vicon Nexus software. The electromyography signals were amplified and band pass filtered, however for this study they were not used therefore not analysed.

The staging of this experiment was already a key feature of the laboratory, which combines all the before mentioned acquisition systems and inter usable task specific modules. In this case only a 1.5 meters length horizontal runway was necessary.

3. Training and overground recordings

Before surgery each rat was handled for one week in order to get accustomed to the laboratory environment, runway and human interaction. After surgery both rats underwent several sessions of recordings after some necessary recovery time. One session consisted of a rat performing a full length runway quadruple walk using motivation from the trainer when needed. The data from each session was stored for offline use and at this initial stage a low pass 5khz filter was applied before saving, using the Matlab® software. At the end, the data used for the duration of the study was from the best data set

obtained from different days of recordings, meaning that all data references from now on correspond to the same day of recordings.

4. Data processing

All data processing was done using Matlab® software. The initial datasets contained 32 channels of raw neural recordings, sampled at 12 kHz. Recordings for rat r328 contained 31 sessions and 24 sessions for rat r263. For each session there was also Vicon files containing video and marker position recordings captured from the right hindlimb and from the left hindlimb.

Firstly we analysed the Vicon files to do the reconstruction of the leg kinematics trajectories. Also it was necessary to obtain the real time of the gait events. Here, with the software's help we extracted the time of right foot off, right foot strike, left foot off and left foot strike storing them into excel files.

Both datasets containing neural activity and excel files with real event time were imported into Matlab. This data was re-arranged and synchronized. The analysis for the neural data started with common average re referencing to the channels. This entails calculating the mean of the signal over each channel and removing it from every channel for every session.

Afterwards we decomposed the signal into baseline and left foot off and left foot strike, right foot off and right foot strike trials (also referred to as triggered events). We cut the original signal using time widows of 1s around the time of the real events. The remaining part of the signal was concatenated and used as baseline. The value used for the time window varied according to how we intended to process it. This allowed us to look at the Signal-to-noise ratio (SNR), looking at the ratio between the trials with events and baseline for each channel. From here we determined which channels were the best, removing the worst from the common average re-referencing means and which trials contained too many artefacts and therefore should be removed.

At the end, three signal components were extracted, see Figure 5.1. Firstly, we used a second order Savitzky Golay filter with a nominal 3 db cut off frequency and a filter width of half a second [38] to extract one component in the time domain, that was designated of Low-pass Component (LPC). We extracted the other two components in the time-frequency domain using a time resolved Fourier transform, with a Hamming window. Since recordings from each electrode had been digitized at 12 kHz, spectral amplitudes could only be calculated up to 6000 Hz (Nyquist frequency). We looked at the SNR values across the different frequency ranges and selected the two with the highest SNR, obtaining TRFT-low and TRFT-high. The frequency ranges obtained for this two components are detailed in Chapter 6.

4.1. Savitzky Golay filtering

A low pass filter can be used to smooth noisy data. The Savitzky Golay filter, also known as least squares or Digital smoothing polynomial, performs a least squares fit of a set of points (filter width) to a polynomial and takes the calculated central point of the fitted polynomial curve as the new data point[39]. The smoothed data point is obtained by the following equation,

$$(y_k)_s = \frac{\sum_{i=-n}^{n} A_i y_{k+i}}{\sum_{i=-n}^{n} A_i} \qquad (5.1.)$$

k – index of central point

n – number of points to the left and right of central point

A_i – weighting coefficients of polynomial

$(y_k)_s$ - new smoothed data point.

This filter doesn't have its properties defined in the Fourier domain, and derives directly from a particular formulation of the data smoothing problem in the time domain. However its smoothing operation of this filter reduces the high-frequency components of the signals and passes the low-frequencies with little change. This algorithm is not very aggressive, therefore doesn't cause a significant loss of information.

4.2. Time resolved Fourier Transform

The Fourier transform decomposes a signal in time into a function of frequencies, extracting series of cosines and sines which compose the function. The fast fourier transform (FFT) is a discrete fourier transform algorithm which reduces the number of computations needed to obtain the frequency domain representation of the original signal [40].

The signal from each session underwent the fast fourier transform in chunks of 1/6 of a second with a Hamming window that slid according to a step value that was half the window size for baseline and for the triggered parts of the signal a step of 1/64 seconds.

A Hamming window is defined by the following equation,

$$W(n) = \alpha - \beta \cos\left(2\pi \frac{n}{N}\right), \ 0 \leq n \leq N \qquad (5.2.)$$

with α = 0.54 and β = 0.46 and a window length of $L = N + 1$, and N the number of samples and n the individual elements[40].

After a time resolved Fourier Transform, the amplitudes of every frequency bin are normalized by dividing them by the average baseline amplitude of the same frequency bin in the respective session[41].

5. Signal-to-noise ratio analysis

The metric used to compare each of the four triggered related neuronal activities and the baseline neuronal activity was the signal-to-noise ratios (SNR). This was calculated in the following way,

$$SNR\ (t, ch)_{\substack{EVENT \\ VS \\ BASELINE}} = \frac{|\mu_{EVENT}\ (t,ch) - \mu_{BASELINE}|}{\sigma_{EVENT}(t,ch) + \sigma_{BASELINE}} \qquad (5.3.)$$

t – Time within the event time window,

ch - channel,

μ_{EVENT} - mean of respective event neuronal activity,

$\mu_{BASELINE}$ – mean of baseline neuronal activity,

σ_{EVENT} – standard deviation of respective event neuronal activity,

$\sigma_{BASELINE}$ – standard deviation of baseline neuronal activity.

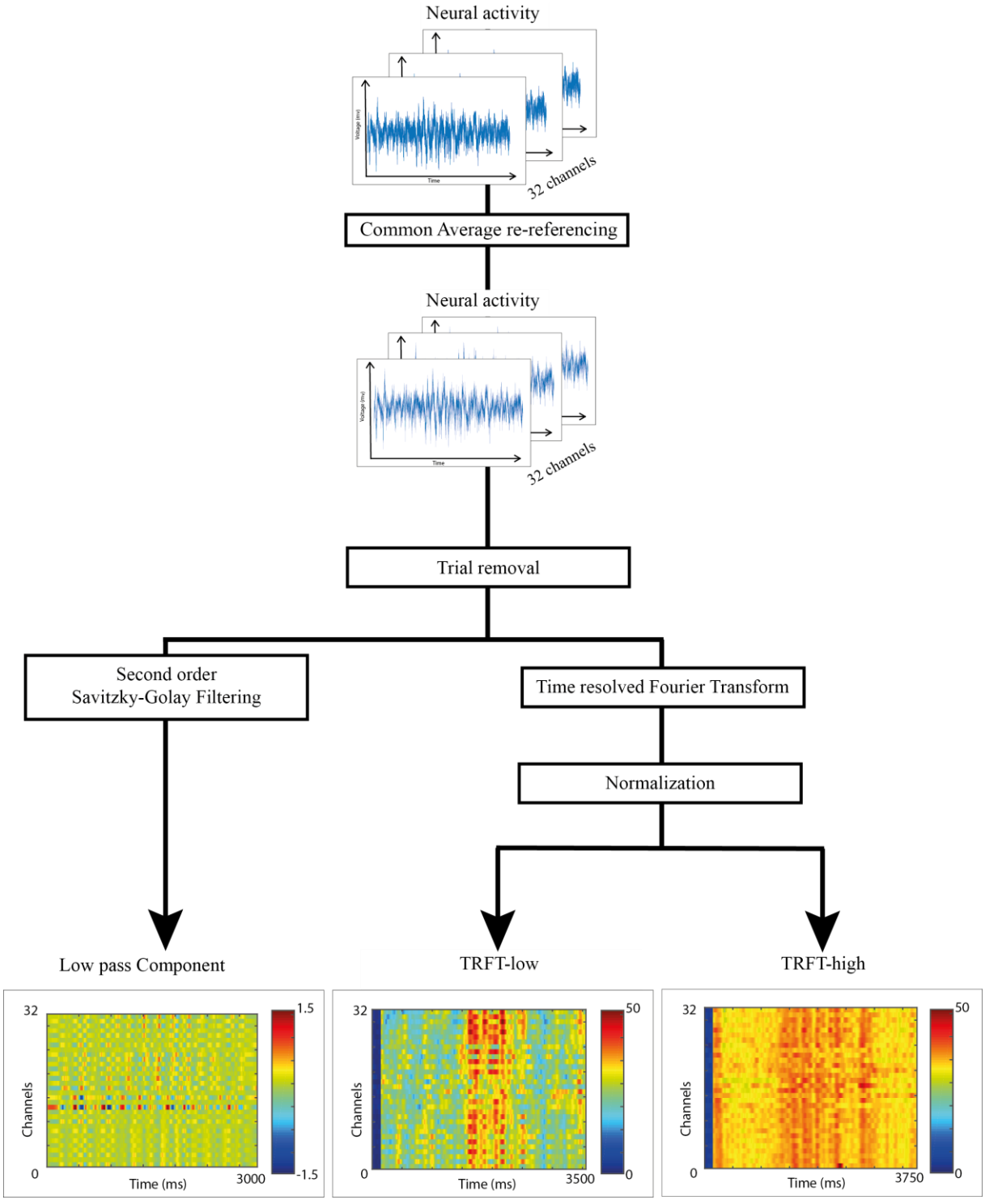

Figure 5.1: Schematics of Data Processing methods

6. Extracted features and classification

The goal was to classify 3 different classes of data, left foot off, left foot strike and baseline. We had 93 different features from each event, since we extracted 3 different components from the original signal that was recorded over 32 channels, and one channel was removed in order to ensure linear independency, leaving 31 channels. We took 15 equidistant time points of the signal starting 250 ms prior to each event and ending at the time of the event, making 1395 different values for each class, see Figure 5.2. We calculated each class mean and respective standard deviation and obtained the z-scores, using the following equation.

$$Z = \frac{X - E(X)}{\sigma(X)} \qquad (5.4.)$$

$E(X)$ – mean of the population

$\sigma(X)$ – standard deviation of the population

As this classifier is built by fitting a multivariate Gaussian distribution to each of the classes, see equation 4.2., we calculated the estimated mean (equation 4.3.) and covariance matrix (equation 4.4.) that underwent a regularization procedure, see equation 4.5, to improve its accuracy in a new independent dataset.

We obtain the class probabilities for each event, choosing a threshold value of 0.95 as the probability which represented the occurrence of the events, also ensuring that a refractory period of 150 ms was respected, so that the detection of events would only be quantified if the same class event hadn't been detected within that specified period. Figure 5.2 outlines the classification procedures described.

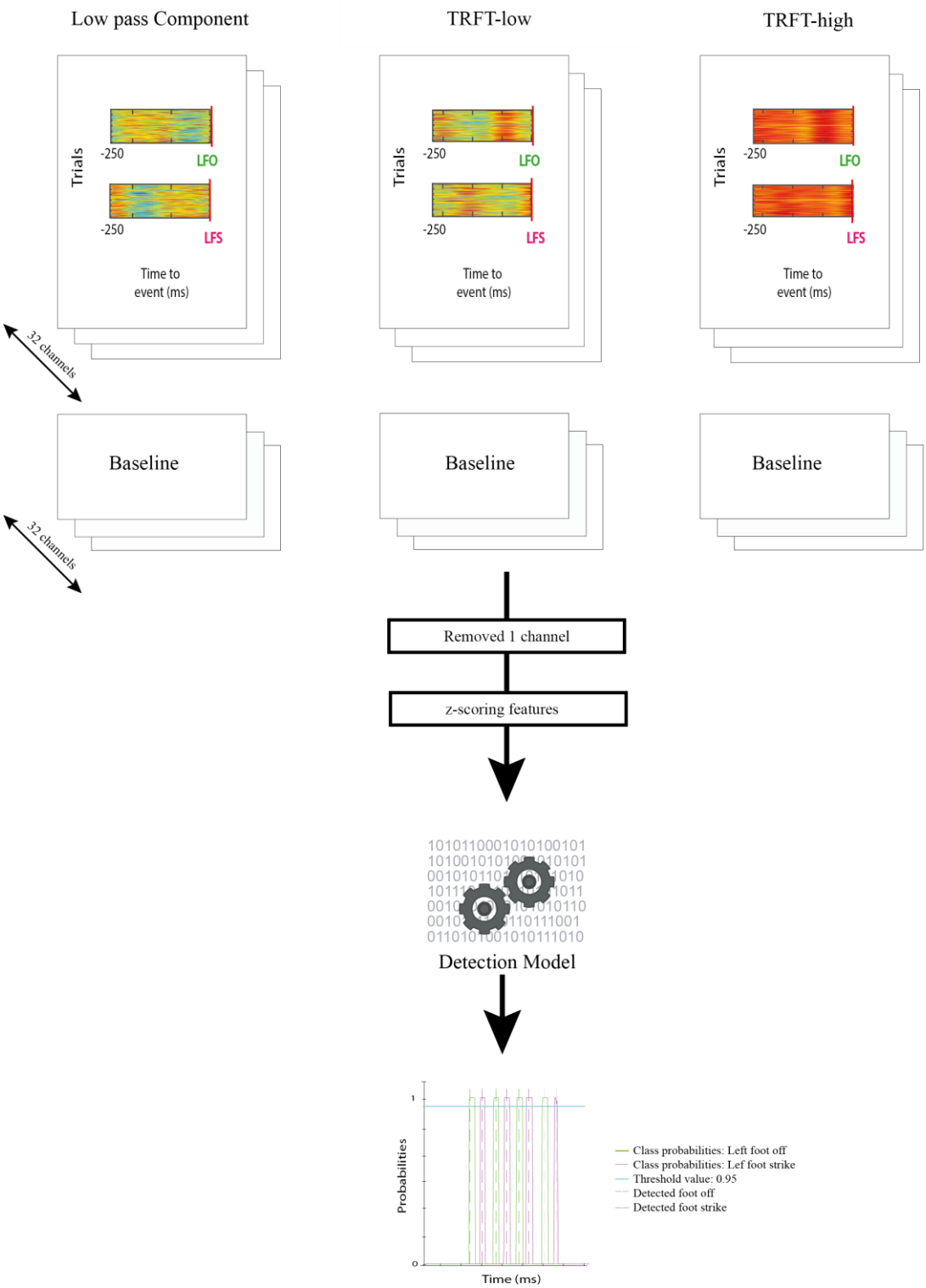

Figure 5.2: Classification procedures.

7. Model selection and Cross-validation

The cross-validation was performed three times. We divided the entire dataset into two, three and ten equally sized parts, and did the whole procedure for the three different divisions in search for the best model. For each data division we held out one part for the testing set and used the rest for the training set, see Figure 5.3, and then we looped trough the parts, to change the part which was used as the testing set.

To find the best prediction model, we trained classifiers with different combinations of model parameters, namely: feature length values, ranging from 0 ms to 1000 ms; number of features from each channel, 1 to 15 points; regularization coefficients, ranging from 0 to 1. Each combination was trained on the training trials and tested on the testing trials, where the cardinal number for true positives, false positives, false positives and false negatives was saved. After all the iterations we calculated the combined mutual information value (see equation 4.6.). The mutual information value infers to the number of detected events within a specific tolerance window around the time of the real event, which stretched from 10 to 60 ms.

The best prediction model and set of parameters, was found by finding the highest mutual information value obtained.

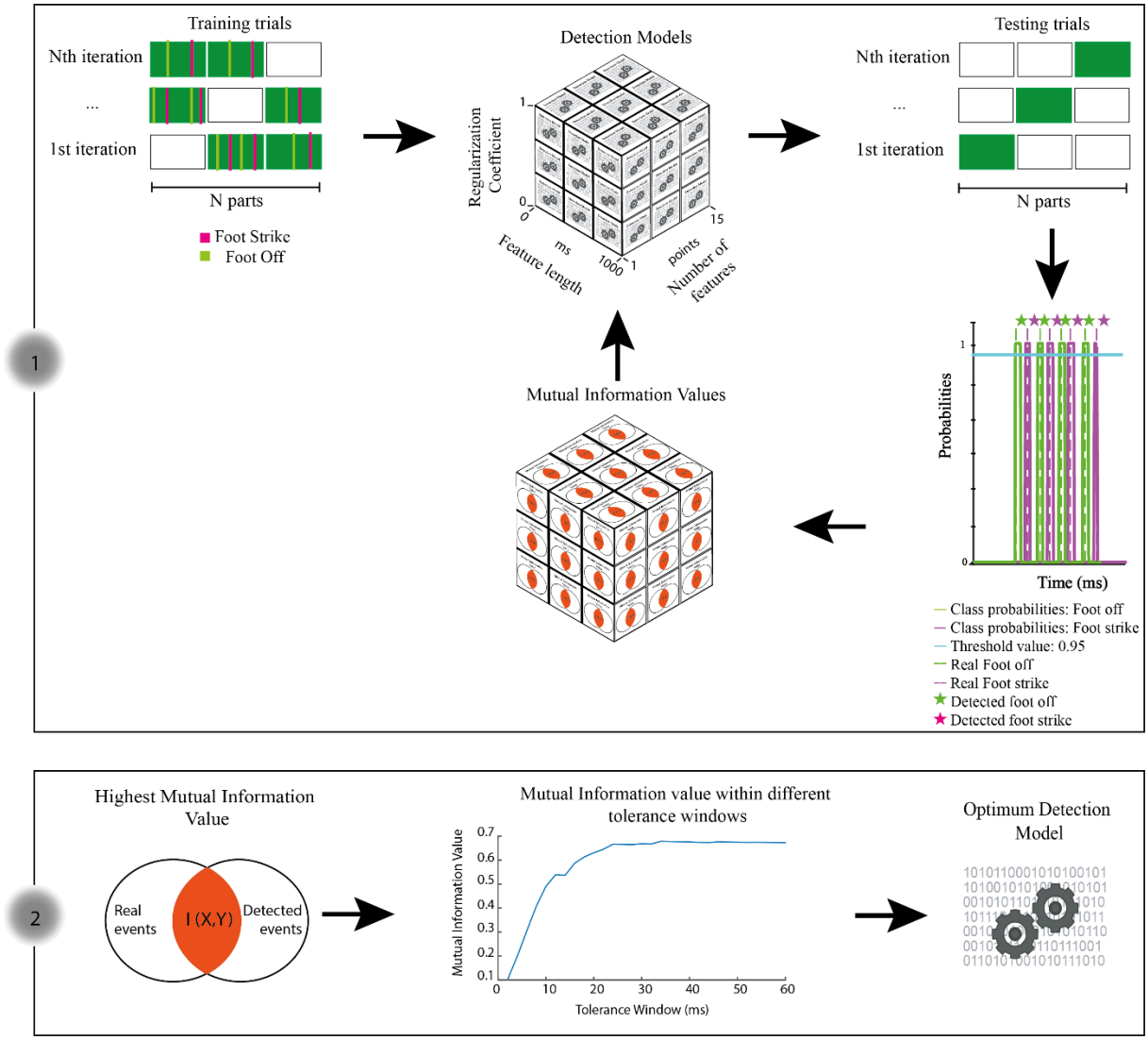

Figure 5.3: Part 1 represents Cross-validation procedures and part 2 the selection of the optimum detection model.

8. Time correction

After choosing the optimal prediction model, we searched for the difference that still remained between our decoded events and real events. This difference was calculated as the median of all the differences of same sequenced events. For both rats there was still a significant difference, smaller than the 60 ms window however, still significant enough considering that a gait cycle was around 250 ms. In order to correct this we implemented this time bias into the triggers array that was used to train the classifier, by incrementing it. Afterwards a new model was formed, which accounted for the default difference.

Chapter 6

Results

1. Extracted features from recorded neuronal activity

A preliminary overview of the signals across the channels showed that it would be difficult to use spiking activity as input data into the decoder since it didn't seem to show any recognisable spiking activity patterns around the time of each event. Other, non-related-to-gait-activity patterns were clearly superimposed.

Looking at the spectrograms of the trials, which corresponds to the signal around the time of the event, per channel, we saw the need to remove some abnormal channels from the common average referencing procedure. For r263, we removed channel 13 and 30. For r328, channel 32 was removed and also session 2 was removed since it showed too many artefacts, see Appendix A.1.

After extracting the two different components (one through the low pass filter and another from the TRFT, see Methods), we looked at the SNR values of each component for every channel around the triggers, in order to determine whether or not both components showed relevant and therefore usable information for the four events, in the context of our problem. The SNR values of all four events from the two components, for both rats are in Appendix A.2.1. and in Appendix A.2.2.

From the component that was obtained after performing a time resolved fourier transform to the data, we extracted other two components, with different frequency ranges, by looking at the SNR averaged over all channels and conditions across all frequency bands. The maximum values at the lower end of the spectrum identified the TRFT-low frequency range, and the maximum values at the higher end of the spectrum identified the TRFT-high frequency range. Below, in Figure 6.1 and Figure 6.2 is plotted the SNR averaged over all channels and conditions of a specific bottom and top frequency. In Table 6.1, the frequency ranges for TRFT-low and TRFT-high for both rats are listed. For r263 the SNR maximum was between 3 and 15 Hz for the TRFT-low, and for the TRFT-high it was between 39 and 747 Hz. The SNR maximum for r328 was 3 to 21 Hz for the TRFT-low and 105 to 693 Hz for the TRFT-high.

Table 6.1 : Frequency ranges for the TRFT-low and TRFT-high, for r263 and r328

	TRFT-low	TRFT-high
r263	3 - 15 Hz	39 -747 Hz
r328	3 - 21 Hz	105 - 693 Hz

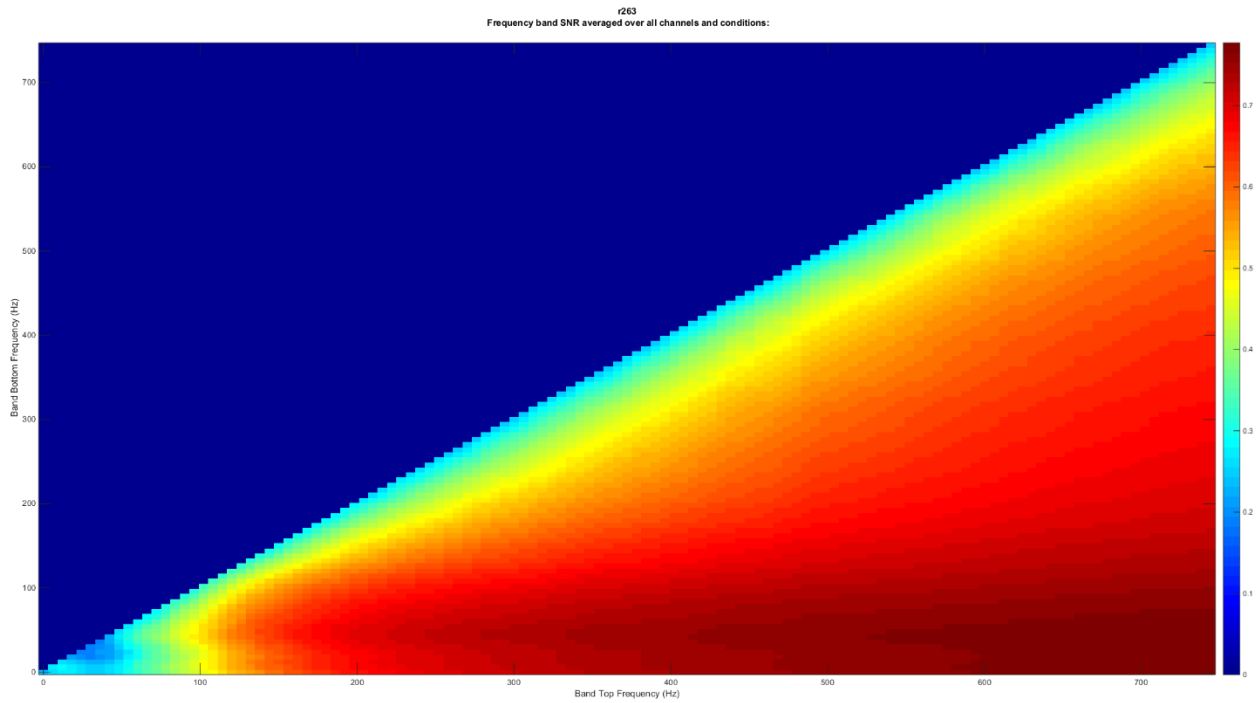

Figure 6.1: Frequency band SNR averaged over all channels and conditions of r263

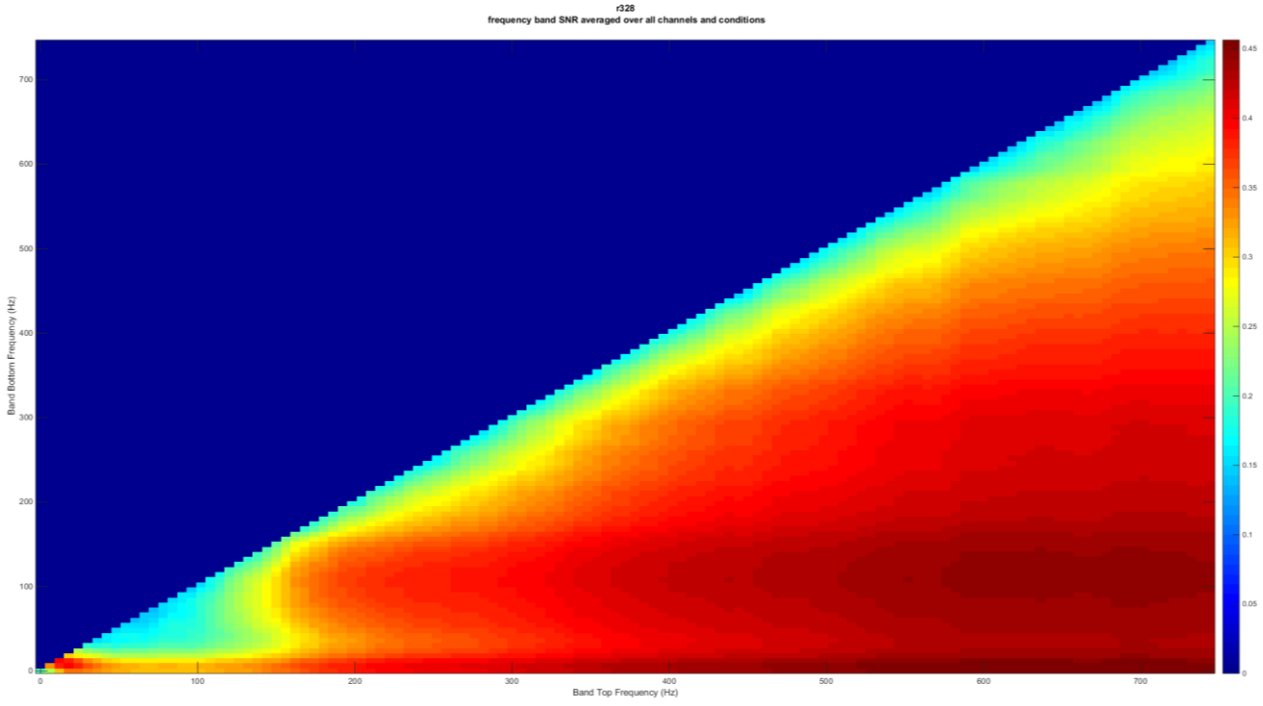

Figure 6.2: Frequency band SNR averaged over all channels and conditions of r328

2. Decoding left side events

2.1. Model selection and cross-validation

The iterations to determine which model gave a higher mutual information value were performed by the methods described above. The various values of mutual information and their various corresponded combinations for rat 328 and 263 left side events decoding, are shown in Appendix B.1. .

From the parameters tested we inferred which combination or combinations corresponded to the model that allowed the highest mutual information value. For the left side events of rat 263, Table 6.2 shows the parameters values and its mutual information value, which corresponded to the maximum mutual information value found.

Table 6.2: Optimum combination of parameters for decoding model, of rat 263 left side events, and its mutual information value.

		Division of data in 3 parts
r263	Feature Length (ms)	250
	Number of features from each channel	15
	Regularization coefficient	0
	Mutual Information Value using a 60 ms tolerance window	0.3966

As for the left side events of rat 328 there was more than one combination (see Table 6.3) for the maximum value therefore the choice fell upon the one that required a lower computational time, since the division in 10 parts required more than triple the time than the one using thirds of the data, during cross-validation procedures.

Table 6.3: Optimum combination of parameters for decoding model, of rat 328 left side events, and its mutual information value and computation time.

		Division of data in 3 parts	Division of data in 10 parts
r328	Feature Length (ms)	250	250
	Number of features from each channel	15	15
	Regularization coefficient	0	0
	Mutual Information Value using a 60 ms tolerance window	0.6017	0.6017
	Computational Time	medium	high

2.2. Time correction

Lastly, after the appropriate model was built we determined if there still was a difference between the real events time and the time of the detected events. Both rats still exhibit a significant difference, as it is described in Table 6.4, calculated as described in the above Methods correspondent section.

Table 6.4: List of time values that correspond to the difference between the time of the real events and the detected events time, for left foot off and left foot strike.

	Left foot off	Left foot strike
r263	25 ms	30 ms
r328	25 ms	25 ms

This time values were implemented as a time bias correction variable and the new classification model was tested again for the time bias between the real and detected triggers.

Table 6.5: List of time values after first time correction that correspond to the difference between the time of the real events and the detected events time, for left foot off and left foot strike.

	Left foot off	Left foot strike
r263	0 ms	0 ms
r328	0 ms	0 ms

2.3. Decoding left foot off and left foot strike

After building the decoding model and optimizing it, it is time to put it to action. By showing the class probabilities correspondent to the left foot off and left foot strike as an independent variable dependent on time and the chosen threshold of 0.95 we obtained the decoded events (explained in the Methods section above). In order to have a visual guide of how well the decoded events match the real events and to look for error anomalies we overlapped the decoded events with the correspondent real events. In Figure 6.3 and Figure 6.4 we can see four sessions that exemplify the output of the decoder from rat 263 and 328.

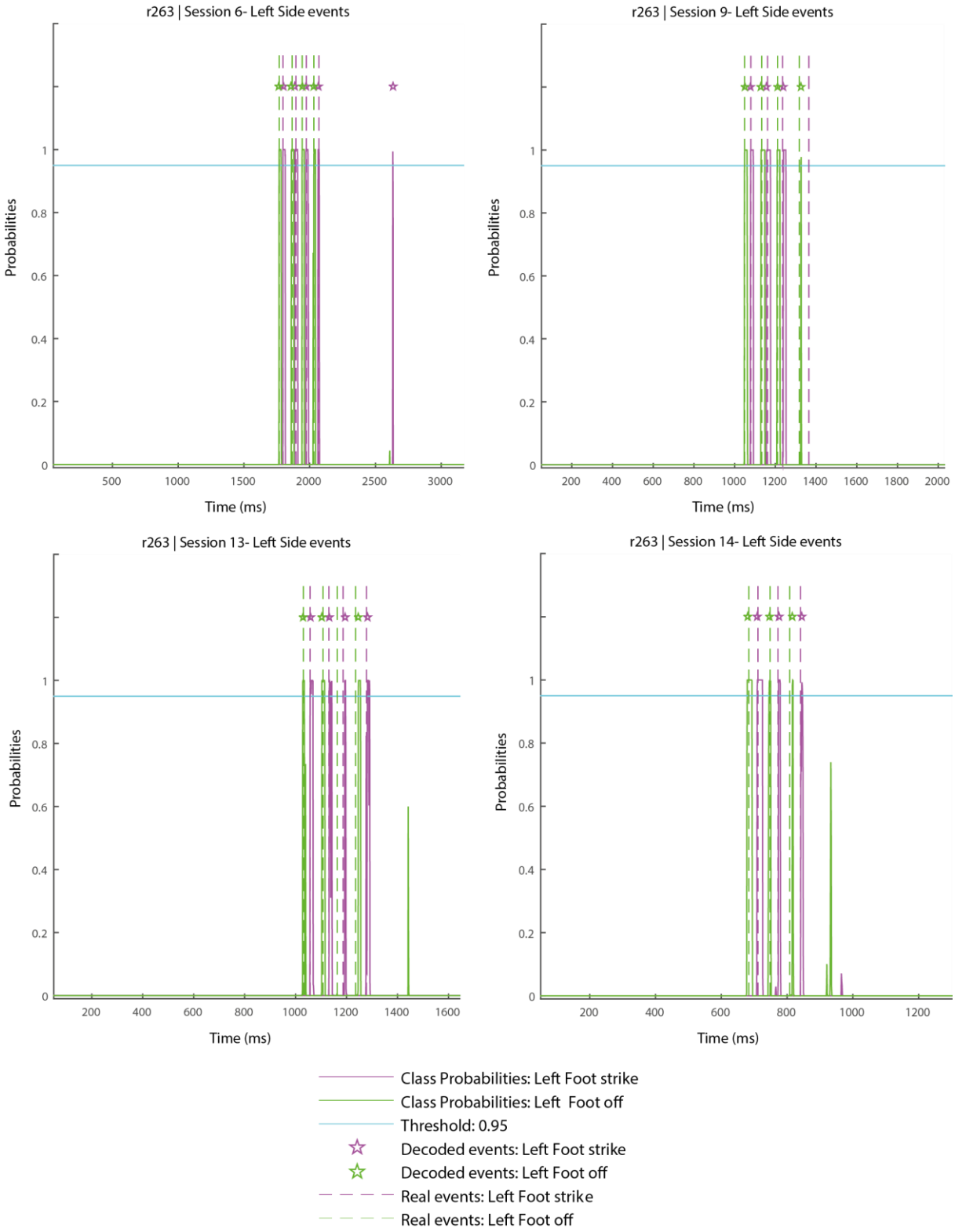

Figure 6.3: Class Probabilities of left side events from rat 263

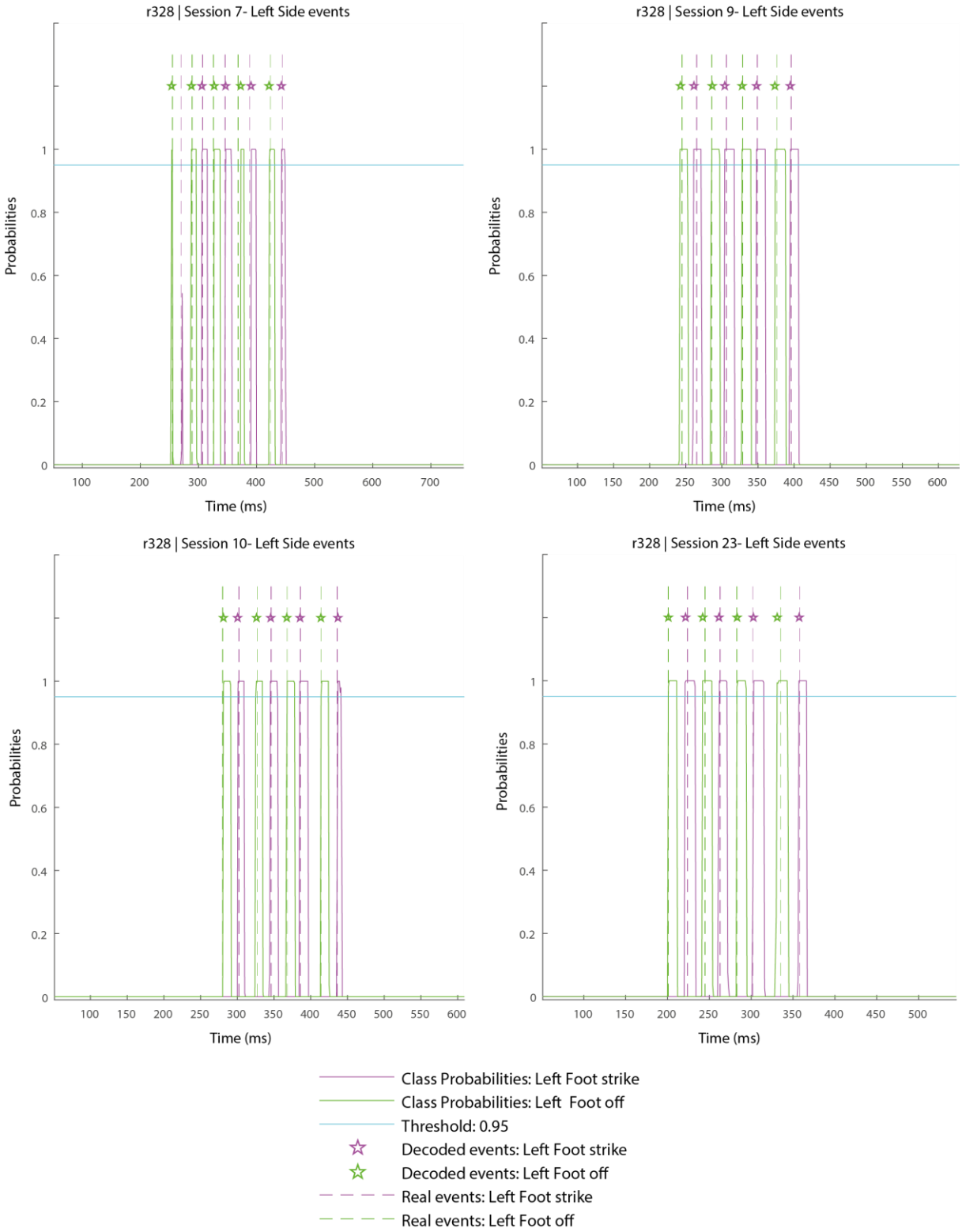

Figure 6.4: Class Probabilities of left side events from rat 328

3. Decoding right side events

3.1. Model selection and cross-validation

After building a decoding model for the left side events there was also the question of whether or not right side events could be decoded with some level of accuracy. All the combinations and their calculated mutual information values are shown in Appendix B.2. . The combination of optimal parameters and the corresponded mutual information value, which is the highest found, are detailed in Table 6.6 and Table 6.7.

Table 6.6: Optimum combination of parameters for decoding model, of rat 263 right side events, and its mutual information value.

		Division of data in 3 parts
r263	Feature Length (ms)	250
	Number of features from each channel	15
	Regularization coefficient	0
	Mutual Information Value using a 60 ms tolerance window	0.3014

Table 6.7: Optimum combination of parameters for decoding model, of rat 328 right side events, and its mutual information value.

		Division of data in 3 parts
r328	Feature Length (ms)	250
	Number of features from each channel	15
	Regularization coefficient	0
	Mutual Information Value using a 60 ms tolerance window	0.4458

3.2. Time correction

The time correction made concerning the right side events calculated as describe in the Methods section of the detected events is specified in Table 6.8.

Table 6.8: List of time values that correspond to the difference between the time of the real events and the detected events time, for right foot off and right foot strike.

	Right foot off	Right foot strike
r263	40 ms	20 ms
r328	25 ms	30 ms

Identically to the left side events the time differences were tested a second time and the values obtained are in Table 6.9.

Table 6.9: List of time values after first time correction that correspond to the difference between the time of the real events and the detected events time, for right foot off and right foot strike.

	Right foot off	Right foot strike
r263	-5 ms	5 ms
r328	0 ms	0 ms

3.3. Decoding right foot off and right foot strike

The class probabilities of the right side events across time are in Figure 6.5 and Figure 6.6. There we can see the class probabilities, the decoded events and the real events. Out of the 4 sessions shown, there is one error from each rat. Both errors occur in the beginning of session 4 (see Figure 6.5) and session 13 (see Figure 6.6).

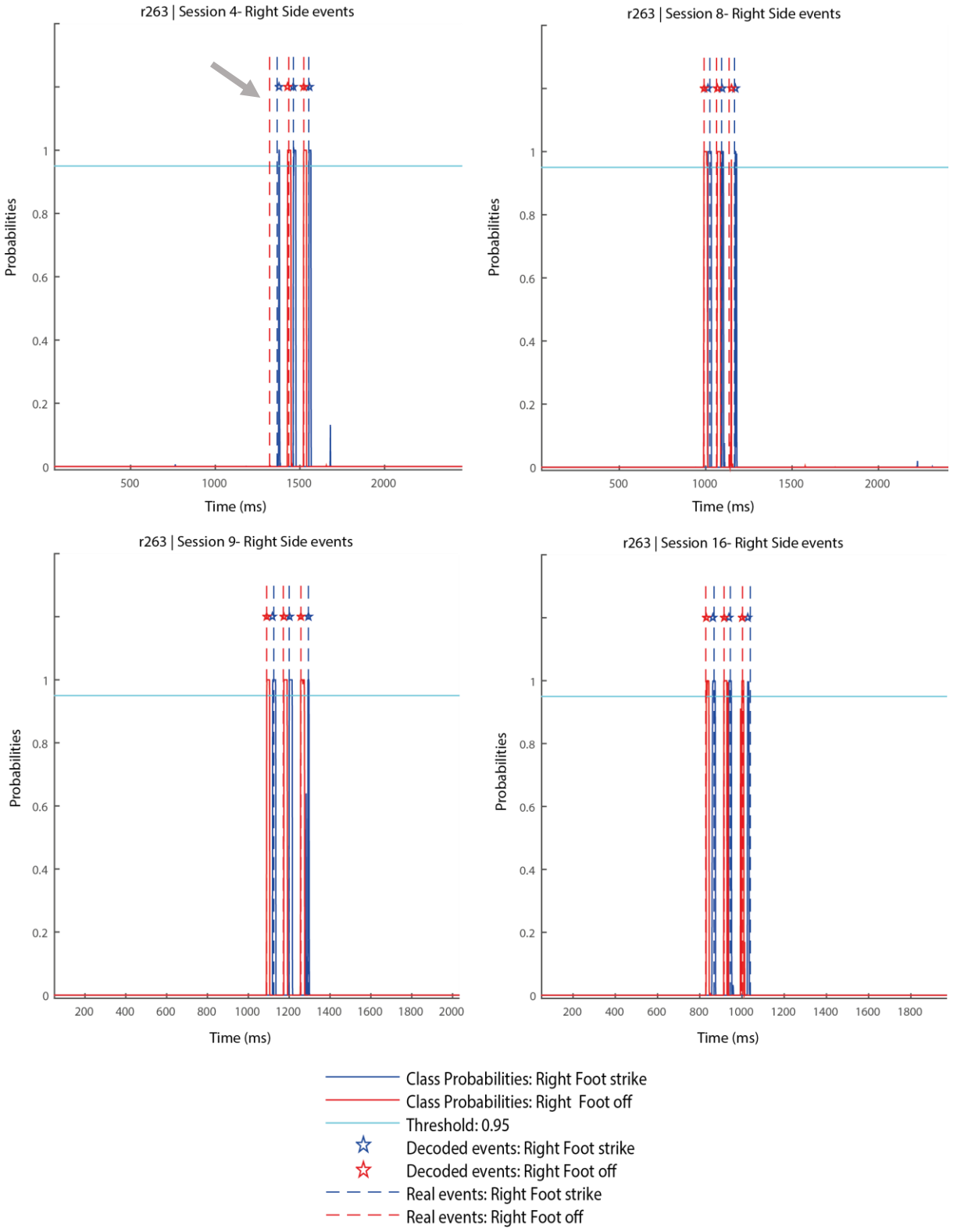

Figure 6.5: Class Probabilities of right side events from rat 263. The grey arrow points to a classification mistake.

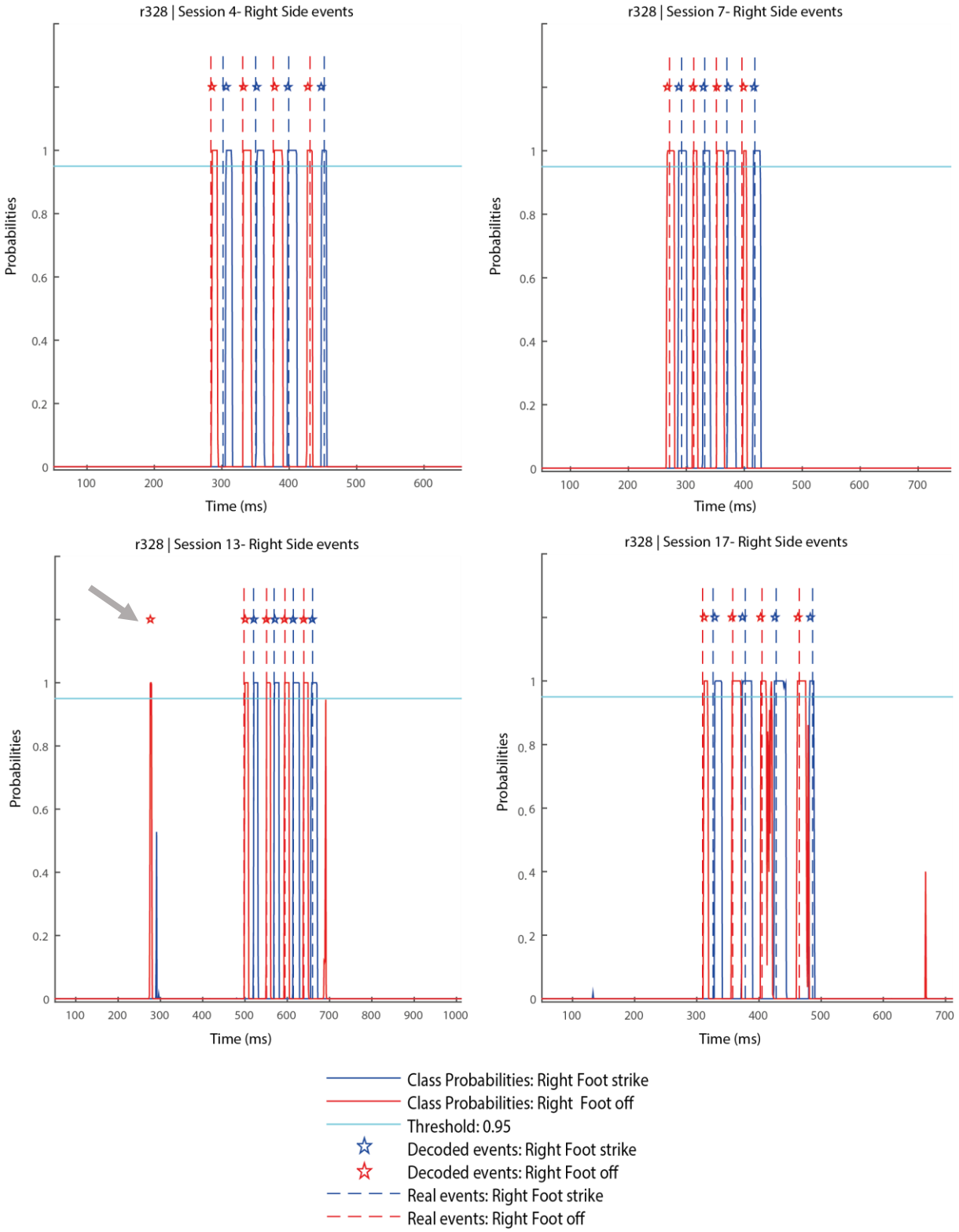

Figure 6.6: Class Probabilities of right side events from rat 328. The grey arrow points to a classification mistake.

Chapter 7

Discussion and Conclusion

State of the art neuro rehabilitation techniques have major potential in surpassing the own body's ability to recover from motor impairment due to nerve damage. One technique that has showed clinical efficacy in humans is epidural electrical stimulation with aid of pharmacology which works by promoting nerve's plasticity and therefore creating new nerve circuitries. In this thesis we explore the feasibility of a system that delivers time and space specific epidural electrical stimulation, focusing on obtaining proof of concept that we can obtain reliable locomotor primitives from neural activity that can be used to trigger this stimulation in rats. For this we recorded local field potentials from rats during gait and used it to train a predictive algorithm offline.

1. Extracted features from recorded neuronal activity

An initial overview of the raw LFPs that were recorded showed a very irregular signal with multiple artefacts that needed pre-processing. Considering that this signal was recorded from the sensorimotor cortex, an area that comprises both sensory and motor information this was somewhat to be expected. Data that corresponded to a time of an event would inescapably not only encode gait primitives but all sorts of concurrent sensory stimulus. However, since the algorithm is built on existing patterns, this does not by itself determine the usefulness of the data.

Firstly the signal was divided into two different components (see Methods) and we compared all the trials correspondent to each of the four events (LFO, LFS, RFO and RFS) to each other and baseline (Appendix A). It was possible to see a pattern in the neural activity values around the time of the event, although not always so evident. Also looking at the SNR we can identify the channels that give us the most information, by looking at the channels that had the highest SNR values, meaning that they had a higher difference from the baseline values. For r263 these were channels 15, 21, 29 and 31 and for r328, channels 17, 18, 28 and 30. Figure 7.1 shows the electrode sitemap and the location for these channels. Considering the small scale of the device and the animal model brain it is not possible to determine where these electrode locations refer to, in the sensorimotor cortex, without a posterior cortex dissection. Furthermore we see that RFO and LFS and that LFO and RFS overlap which makes sense considering the gait cycles phases.

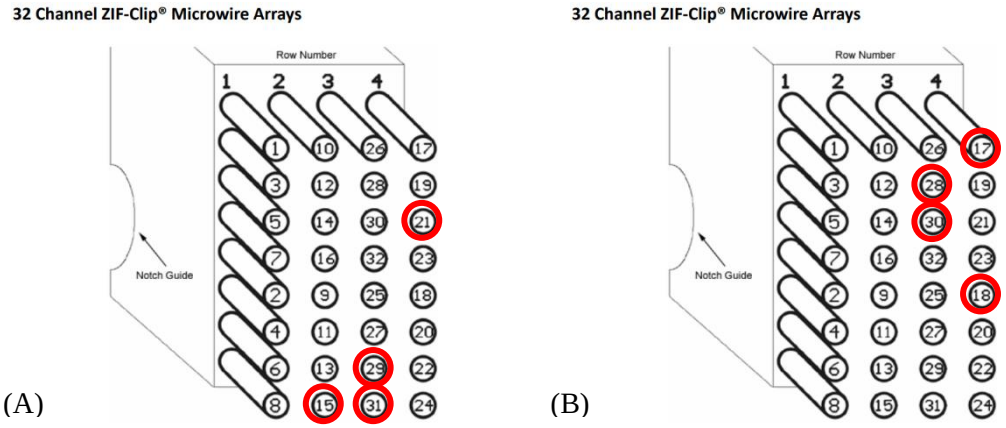

Figure 7.1: (A) Site map for electrodes of cortical microarray implanted in r263.The red circles show the channels with the highest SNR values. (B) Site map for electrodes of cortical microarray implanted in r328.The red circles show the channels with the highest SNR values. Adapted from [42]

Finally, we extracted two different signal components from the TRFT data, by searching which frequencies ranges showed the highest SNR. These frequencies are described in Table 6.1. Looking at the frequency values we see that the TRFT-low range (3~21Hz) covers two known motor-related brain wave oscillations in rats, beta (12 – 40 Hz)[43] and theta (4 – 8 Hz)[44]. On the other hand the TRFT-high range (39 ~700 Hz) matches the gamma wave band (30 Hz - 100 Hz)[45]. This neural wave has also been associated with various cognitive and motor functions.

When comparing the LPC, TRFT-low and TRFT-high spectrograms we see that TRFT-low seems to show more information around the time of the event, then the TRFT-high and finally the LPC, see Figure 7.2. Although this is an exception to the rule since the highest frequency component usually can give us the most information.

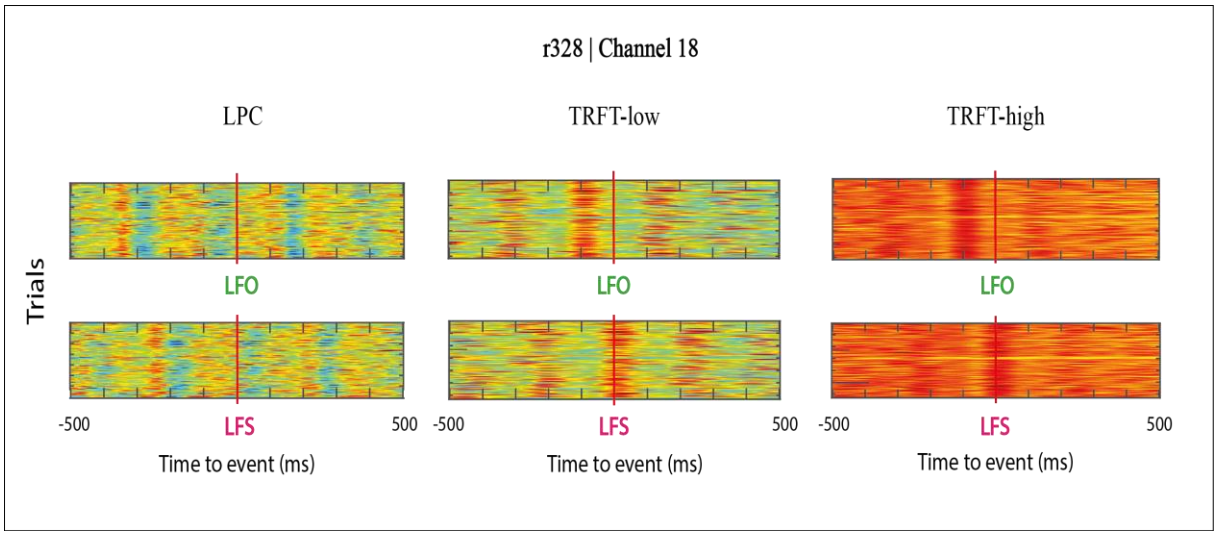

Figure 7.2: All trials from LFO and LFS after extracting the three signals (the LPC, the TRFT-low and the TRFT-high) from the raw neural activity of r328, channel 18.

2. Decoding performance

Four different decoding algorithms were built, one for each rat left/right side events. At end when searching for the optimum parameters that gave us a higher value of mutual information, see Appendix B, we realise that they are essentially the same parameters, independent of the subject and side. However this is a particularity of the data that we had, so we cannot make a generalisation.

The mutual information values regarding the decoding from left and right side, of both rats (see Table 6.2, Table 6.3, Table 6.6 and Table 6.7) tell us that the decoding algorithm is more accurate for the left side events than for the right side events. The implanted array that recorded the neural signals was placed in the right motor cortex in both rats, which therefore implies that there is more information in the signal regarding activity from the left motor system due to the pyramidal decussation which changes the side of the encoding pathways from the sensorimotor cortex.

Additionally there is also a significant difference between the mutual information values from r263 and r328, see Table 7.1. The reason for this can be extrapolated from watching the recording videos provided by the Vicon system, where we can clearly see that r263 had a more lethargic and irregular gait pattern than r328. The video frames show a much more steady and strong gait from r328.

An analysis to some of the most common misclassification errors shows that they occur at the beginning or very end of the session or in between extremely close succession of detections. These type of errors that usually happen at the beginning or end of every session relate to times when the rat would move his hindlimb legs to accommodate his posture and without necessarily performing a complete step cycle with a swing and stance stage. As for the second case, when events happened too close to each other there was a higher risk of misclassification happening, denoting that some event related information was being masked and maybe a setup of 32 electrodes was not enough.

As for the time bias that the decoder showed (see Table 6.4 and Table 6.8) where the detected events appeared between 25 ms to 30 ms before the actual events on average, can be intuitively justified by the fact that the neural activity encoded the intention of movement and not the physical execution of it.

Table 7.1: Comparison between mutual information values

Relative difference between mutual information value from left and right side events of r263	Relative difference between mutual information value from left and right side events of r328
24%	25 %
Relative difference between mutual information value from r263 and r328, left side events	**Relative difference between mutual information value from r263 and r328, right side events**
34%	32%

3. Future developments

It is possible to accurately decode the two stages of gait from the neural activity of an intact rat, however the algorithm has still its weaknesses. The overall highest value of mutual information obtained was 0.6017, which means that around forty percent of the events are still not being accurately detected. This can be improved by working on a better detection model and by using more data to train and test it, preferably from multiple days of recording.

Future work on the rat BSI, moving from just proof-of-concept would imply building a decoder on healthy rats, then performing a lesion and finally providing epidural stimulation controlled by stimulation protocols triggered by the decoded locomotor primitives. Also the possibility of building a decoder which could detect the four events should be tested. This was tested in the development of this project however this work was not carried out because the primary goal was to focus on each individual side, although it showed promise.

The idea of a brain-machine interface for restoration of hindlimbs or forelimbs has been widely researched in this past years though not all research focuses on restoration by promoting new circuitry using existing undamaged neurons. We are confident on the pursuit of this path since it has already proven efficacy. Nevertheless it is important to better understand how all systems integrate to guarantee motor functions in a healthy state in order to deal with neuropathologies that compromise them. So, further and more extensive studies on animal subjects need to happen, such as rats and mice, since they are more cost and time effective and provide more access to a wider range of immunohistochemistry techniques. Still, translation has to be kept in mind and additional studies need to be implemented in human subjects with different degrees of incomplete and complete lesions to answer the question if space and time-specific stimulation, with aid of pharmacology, provide a more efficient and effective epidural electrical stimulation with clinical significance than other neuron regenerative techniques.

References

[1] P. T. Trent Stephens Rod Seeley, *Essentials of Anatomy and Physiology*. McGraw-Hill Science/Engineering/Math; 6 edition, 2006.

[2] S. Harkema, Y. Gerasimenko, J. Hodes, J. Burdick, C. Angeli, Y. Chen, C. Ferreira, A. Willhite, E. Rejc, R. G. Grossman, and others, "Effect of epidural stimulation of the lumbosacral spinal cord on voluntary movement, standing, and assisted stepping after motor complete paraplegia: a case study," *The Lancet*, vol. 377, no. 9781, pp. 1938–1947, 2011.

[3] R. Van Den Brand, J. Heutschi, Q. Barraud, J. Digiovanna, K. Bartholdi, M. Huerlimann, L. Friedli, I. Vollenweider, E. M. Moraud, S. Duis, N. Dominici, S. Micera, P. Musienko, and G. Courtine, "Restoring Voluntary Control of Locomotion after Paralyzing Spinal Cord Injury," *Science*, vol. 336, no. 6085, pp. 1182–1185, 2012.

[4] M. Capogrosso, T. Milekovic, D. Borton, F. Wagner, E. M. Moraud, J.-B. Mignardot, N. Buse, J. Gandar, Q. Barraud, D. Xing, and others, "A Brain–Spinal Interface Alleviating Gait Deficits after Spinal Cord Injury in Primates," *Nature*, vol. 539, no. 7628, p. 284, 2016.

[5] E. R. Kandel, J. H. Schwartz, T. M. Jessell, S. A. Siegelbaum, and A. J. Hudspeth, *Principles of neural science*, vol. 4. McGraw-hill New York, 2000.

[6] "Everything You Need to Know About the Parts of the Brain," *Johns Hopkins Medicine Health Library*. [Online]. Available: http://www.hopkinsmedicine.org/healthlibrary/conditions/nervous_system_disorders/anatomy_of_the_brain_85,P00773/. [Accessed: 11- May- 2017].

[7] "Upper motor neuron," *Wikipedia*. Wikimedia Foundation [Online]. Available: https://en.wikipedia.org/wiki/Upper_motor_neuron. [Accessed: 12- May- 2017].

[8] "Issues | Brain | Oxford Academic," *Oxford University Press*. Oxford University Press [Online]. Available: https://academic.oup.com/brain/issue. [Accessed: 10- May- 2017].

[9] "Spinal Cord Vertebrae Anatomy," *Human Anatomy Diagram*. 2016 [Online]. Available: http://human-anatomy101.com/spinal-cord-vertebrae-anatomy/. [Accessed: 12- May- 2017].

[10] StudyBlue, "PSYCH 3313 Study Guide (2013-14 Wenk) - Instructor Wenk at The Ohio State University," *STUDYBLUE*. 2013 [Online]. Available: https://www.studyblue.com/notes/note/n/psych-3313-study-guide-2013-14-wenk/deck/8697168. [Accessed: 11- May- 2017].

[11] "Hodgkin-Huxley Model." EPFL | SPNM [Online]. Available: http://icwww.epfl.ch/ gerstner/SPNM/node14.html. [Accessed: 12- May- 2017].

[12] "Action potential," *Wikipedia*. Wikimedia Foundation [Online]. Available: https://en.wikipedia.org/wiki/Action_potential. [Accessed: 12- May- 2017].

[13] Boundless, "Skeletal Muscle Fibers - Boundless Open Textbook," *Boundless*. Boundless, 2017 [Online]. Available: https://www.boundless.com/biology/textbooks/boundless-biology-textbook/the-musculoskeletal-system-38/muscle-contraction-and-locomotion-218/skeletal-muscle-fibers-824-12067/. [Accessed: 12- May- 2017].

[14] "School of Engineering," *Gait Lab*. [Online]. Available: https://www2.warwick.ac.uk/fac/sci/eng/meng/nongps/rnd/gait/. [Accessed: 12- May- 2017].

[15] S. Harkema, Y. Gerasimenko, J. Hodes, J. Burdick, C. Angeli, Y. Chen, C. Ferreira, A. Willhite, E. Rejc, R. G. Grossman, and others, "Effect of epidural stimulation of the lumbosacral spinal cord on voluntary movement, standing, and assisted stepping after motor complete paraplegia: a case study," *The Lancet*, vol. 377, no. 9781, pp. 1938–1947, 2011.

[16] "Understanding spinal cord injury," *Living with Attendant Care: Spinal Cord injury : Understanding spinal cord injury*. [Online]. Available: http://www.living-with-attendant-care.info/Content/Spinal_Cord_Injury_c_Understanding_spinal_cord_injury.html. [Accessed: 12- May- 2017].

[17] "ASIA Impairment Scale and the ISNCSCI Motor and Sensory Exam," *Spinal Cord Injury Research Evidence*. [Online]. Available: http://scireproject.com/outcome-measures/outcome-

measure-tool/american-spinal-injury-association-impairment-scale-ais-international-standards-for-neurological-classification-of-spinal-cord-injury/#1467983894080-2c29ca8d-88af. [Accessed: 12- May- 2017].
[18] V. Dietz and K. Fouad, "Restoration of sensorimotor functions after spinal cord injury," *Brain*, vol. 137, no. 3, pp. 654–667, 2014.
[19] J. B. Zimmermann and A. Jackson, "Closed-loop control of spinal cord stimulation to restore hand function after paralysis," *Frontiers in Neuroscience*, vol. 8, no. 87, 2014.
[20] N. Wenger, E. M. Moraud, J. Gandar, P. Musienko, M. Capogrosso, L. Baud, C. G. Le Goff, Q. Barraud, N. Pavlova, N. Dominici, and others, "Spatiotemporal neuromodulation therapies engaging muscle synergies improve motor control after spinal cord injury," *Nature medicine*, vol. 22, no. 2, p. 138, 2016.
[21] "Scales in recording from the brain." Neurotechnology, University of Freiburg [Online]. Available: http://www.neurotechnology.uni-freiburg.de/research/clinic/bmi-overview/box-bmi-scales. [Accessed: 10- May- 2017].
[22] T. J. Hastie, R. J. Tibshirani, and J. H. Friedman, *The elements of statistical learning*. New York: Springer, 2009.
[23] "Analytics-driven embedded systems, part 2 " Developing analytics and prescriptive controls," *Embedded Computing Design*. [Online]. Available: http://embedded-computing.com/articles/analytics-driven-embedded-systems-part-2-developing-analytics-and-prescriptive-controls. [Accessed: 13- May- 2017].
[24] L. F. Nicolas-Alonso and J. Gomez-Gil, "Brain computer interfaces, a review," *Sensors*, vol. 12, no. 2, pp. 1211–1279, 2012.
[25] R. Plonsey and R. C. Barr, *Bioelectricity: a quantitative approach*. Springer Science & Business Media, 2007.
[26] U. Chaudhary, N. Birbaumer, and A. Ramos-Murguialday, "Brain-computer interfaces for communication and rehabilitation," *Nature Reviews Neurology*, vol. 12, no. 9, pp. 513–525, 2016.
[27] C. E. Bouton, A. Shaikhouni, N. V. Annetta, M. A. Bockbrader, D. A. Friedenberg, D. M. Nielson, G. Sharma, P. B. Sederberg, B. C. Glenn, W. J. Mysiw, and others, "Restoring cortical control of functional movement in a human with quadriplegia," *Nature*, vol. 533, no. 7602, pp. 247–250, 2016.
[28] M. Alam, X. Chen, Z. Zhang, Y. Li, and J. He, "A brain-machine-muscle interface for restoring hindlimb locomotion after complete spinal transection in rats," *PloS one*, vol. 9, no. 8, p. e103764, 2014.
[29] I. R. Minev, P. Musienko, A. Hirsch, Q. Barraud, N. Wenger, E. M. Moraud, J. Gandar, M. Capogrosso, T. Milekovic, L. Asboth, R. F. Torres, N. Vachicouras, Q. Liu, N. Pavlova, S. Duis, A. Larmagnac, J. Vörös, S. Micera, Z. Suo, G. Courtine, and S. P. Lacour, "Electronic dura mater for long-term multimodal neural interfaces," *Science*, vol. 347, no. 6218, pp. 159–163, 2015.
[30] G. S. Ramakrishnan A Udoekwere UI Song W, "Multiple Types of Movement Related Information Encoded in Hindlimb/Trunk Cortex in Rats and Potentially Available for Brain Machine Interface Controls.," *IEEE transactions on bio-medical engineering.*, vol. 56(11 Pt 2):2712–2716. doi:10.1109/TBME.2009.2026284., 2009.
[31] A. Manohar, R. D. Flint, E. Knudsen, and K. A. Moxon, "Decoding Hindlimb Movement for a Brain Machine Interface after a Complete Spinal Transection," *PLoS ONE*, vol. 7, no. 12, pp. 1–14, 2012.
[32] J. Rigosa, A. Panarese, N. Dominici, L. Friedli, R. van den Brand, J. Carpaneto, J. DiGiovanna, G. Courtine, and S. Micera, "Decoding bipedal locomotion from the rat sensorimotor cortex," *Journal of Neural Engineering*, vol. 12, no. 5, p. 056014, 2015.
[33] R. D. Flint, M. R. Scheid, Z. A. Wright, S. A. Solla, and M. W. Slutzky, "Long-term stability of motor cortical activity: implications for brain machine interfaces and optimal feedback control," *Journal of Neuroscience*, vol. 36, no. 12, pp. 3623–3632, 2016.
[34] R. D. Flint, Z. A. Wright, M. R. Scheid, and M. W. Slutzky, "Long term, stable brain machine interface performance using local field potentials and multiunit spikes," *Journal of neural engineering*, vol. 10, no. 5, p. 056005, 2013.

[35] H. L. R. Sarma A A Bacher D Masse N Y Simeral J D Sorice B Oakley E M Blabe C Pandarinath C Gilja V Cash S S Eskandar E N Friehs G Henderson J M Shenoy K V Donoghue J P Jarosiewicz B, "Virtual typing by people with tetraplegia using a self-calibrating intracortical brain-computer interface.," *Neurotecnhology*, vol. 7 Issue 313 313ra179, 2015.
[36] J. C. Kao, P. Nuyujukian, S. I. Ryu, and K. V. Shenoy, "A high-performance neural prosthesis incorporating discrete state selection with hidden Markov models," *IEEE Transactions on Biomedical Engineering*, vol. 64, no. 4, pp. 935–945, 2017.
[37] J. Jung, B. K. Kwak, A. M. Reddy, B. C. Ha, H. J. Shim, J. S. Byun, S. H. Kang, and E. S. Park, "Characterization of photothrombotic cerebral infarction model at sensorimotor area of functional map in rat," *J Neurol Sci-Turk*, vol. 30, pp. 617–628, 2013.
[38] J. Steinier, Y. Termonia, and J. Deltour, "Smoothing and differentiation of data by simplified least square procedure," *Analytical Chemistry*, vol. 44, no. 11, pp. 1906–1909, 1972.
[39] B. P. F. Saul A. Teukolsky William T. Vetterling William H. Press, *Numerical Recipes: The Art of Scientific Computing*. Cambridge University press, 2007.
[40] J. L. Semmlow and B. Griffel, *Biosignal and medical image processing*. CRC press, 2014.
[41] T. Milekovic, T. Ball, A. Schulze-Bonhage, A. Aertsen, and C. Mehring, "Detection of error related neuronal responses recorded by electrocorticography in humans during continuous movements," *PloS one*, vol. 8, no. 2, p. e55235, 2013.
[42] "TDT | Zip-Clip microarray Manual." Tucker-Davis Technologies [Online]. Available: http://www.tdt.com/files/manuals/Sys3Manual/ZIFArrays.pdf. [Accessed: 12- Sep- 2017].
[43] I. Avila, L. C. Parr-Brownlie, E. Brazhnik, E. Castaneda, D. A. Bergstrom, and J. R. Walters, "Beta frequency synchronization in basal ganglia output during rest and walk in a hemiparkinsonian rat," *Experimental neurology*, vol. 221, no. 2, pp. 307–319, 2010.
[44] J. Jacobs, "Hippocampal theta oscillations are slower in humans than in rodents: implications for models of spatial navigation and memory," *Philosophical Transactions of the Royal Society of London B: Biological Sciences*, vol. 369, no. 1635, 2013.
[45] J. Csicsvari, B. Jamieson, K. D. Wise, and G. Buzsaki, "Mechanisms of gamma oscillations in the hippocampus of the behaving rat," *Neuron*, vol. 37, no. 2, pp. 311–322, 2003.

Appendix A

A.1. Spectrograms of all trials for each event with a time window of 500 ms for all individual channels.

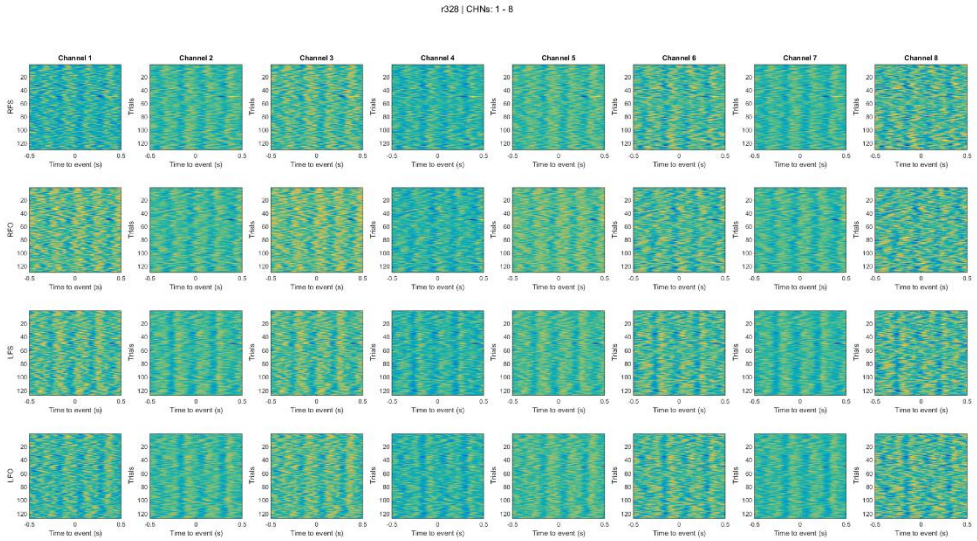

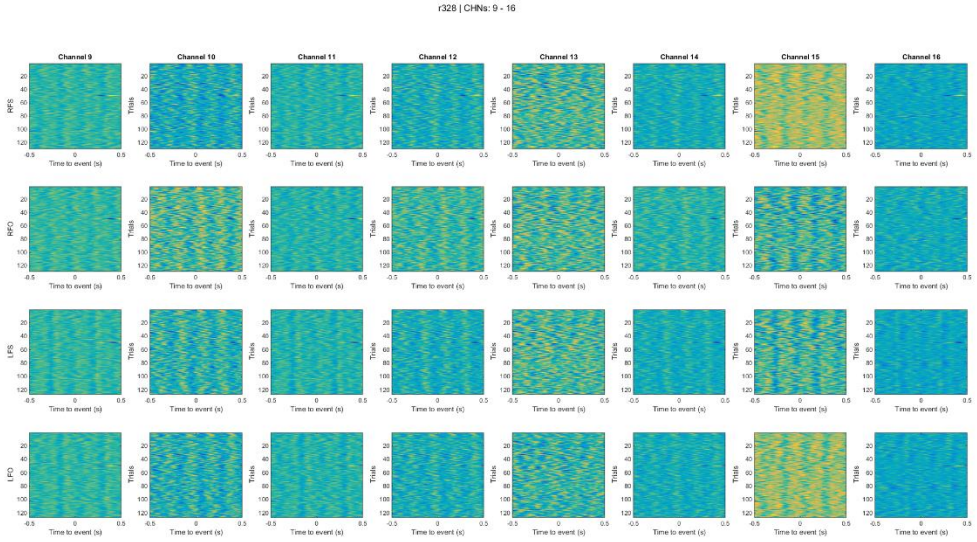

r328 | CHNs: 17 - 24

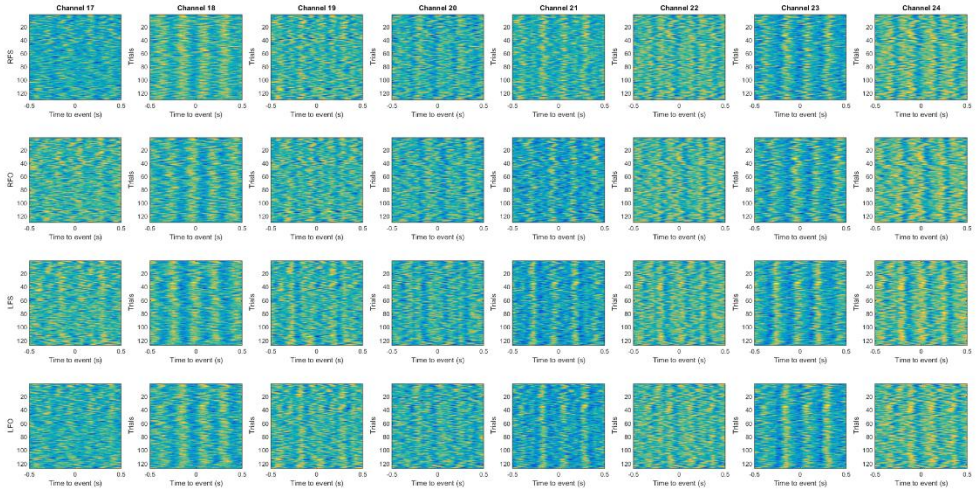

r328 | CHNs: 25 - 32

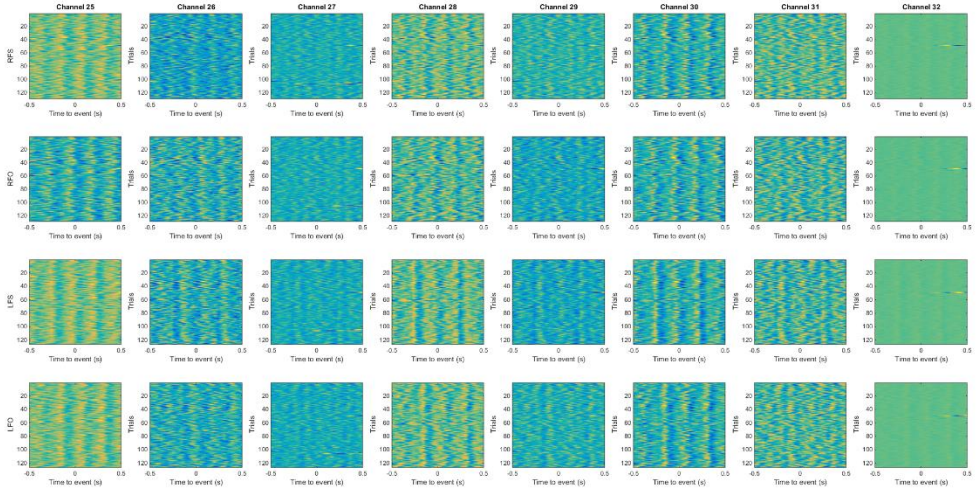

r263| CHNs: 1 - 8

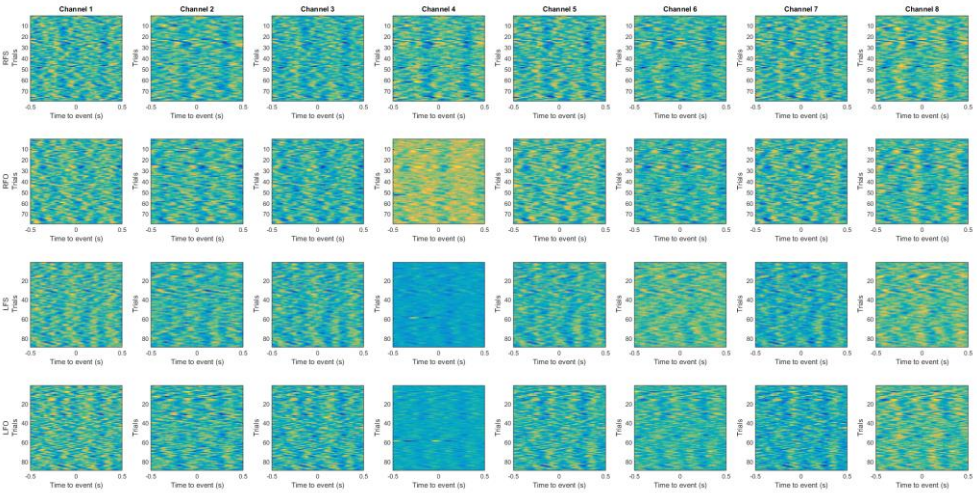

r263| CHNs: 9 - 16

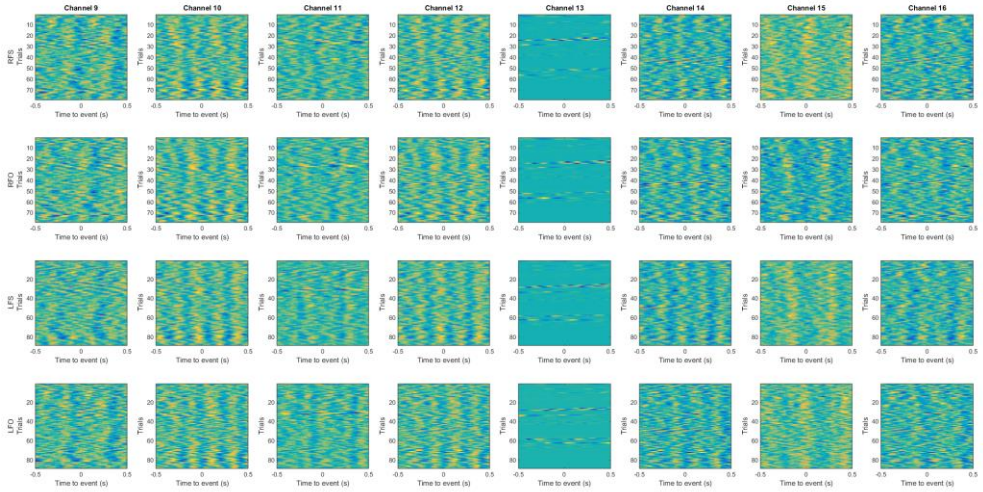

r263 | CHNs: 17 - 24

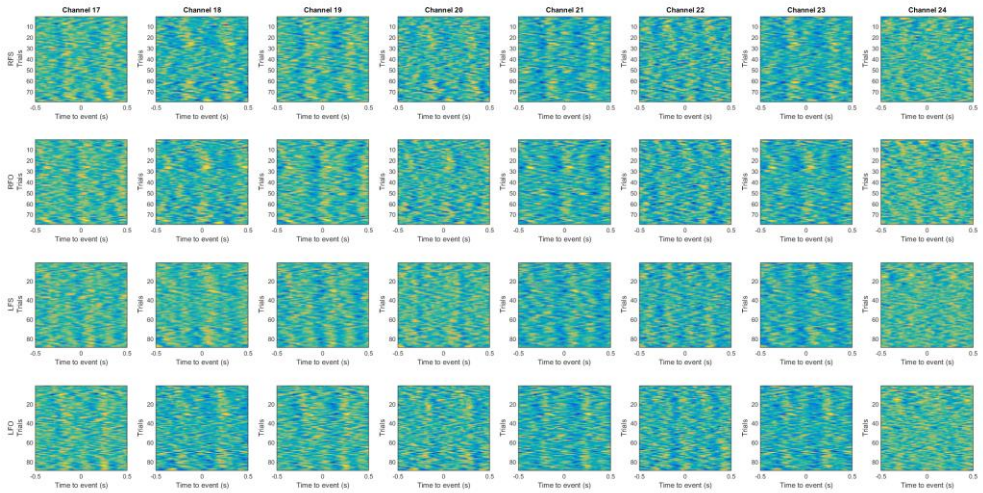

r263 | CHNs: 25 - 32

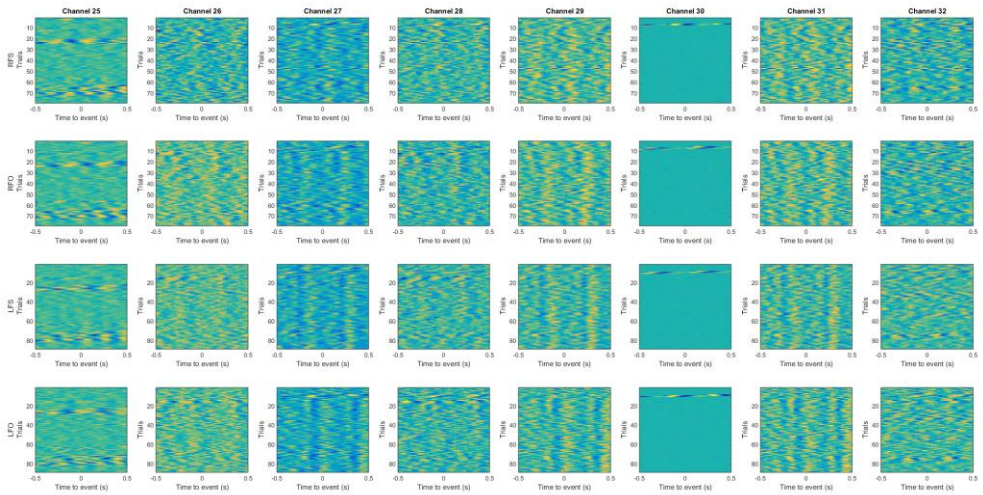

A.2.1. Average SNR values of all trials for all four events (RFO, RFS, LFS and LFO) with a time window of 500 ms for all individual channels for the data that was low pass filtered.

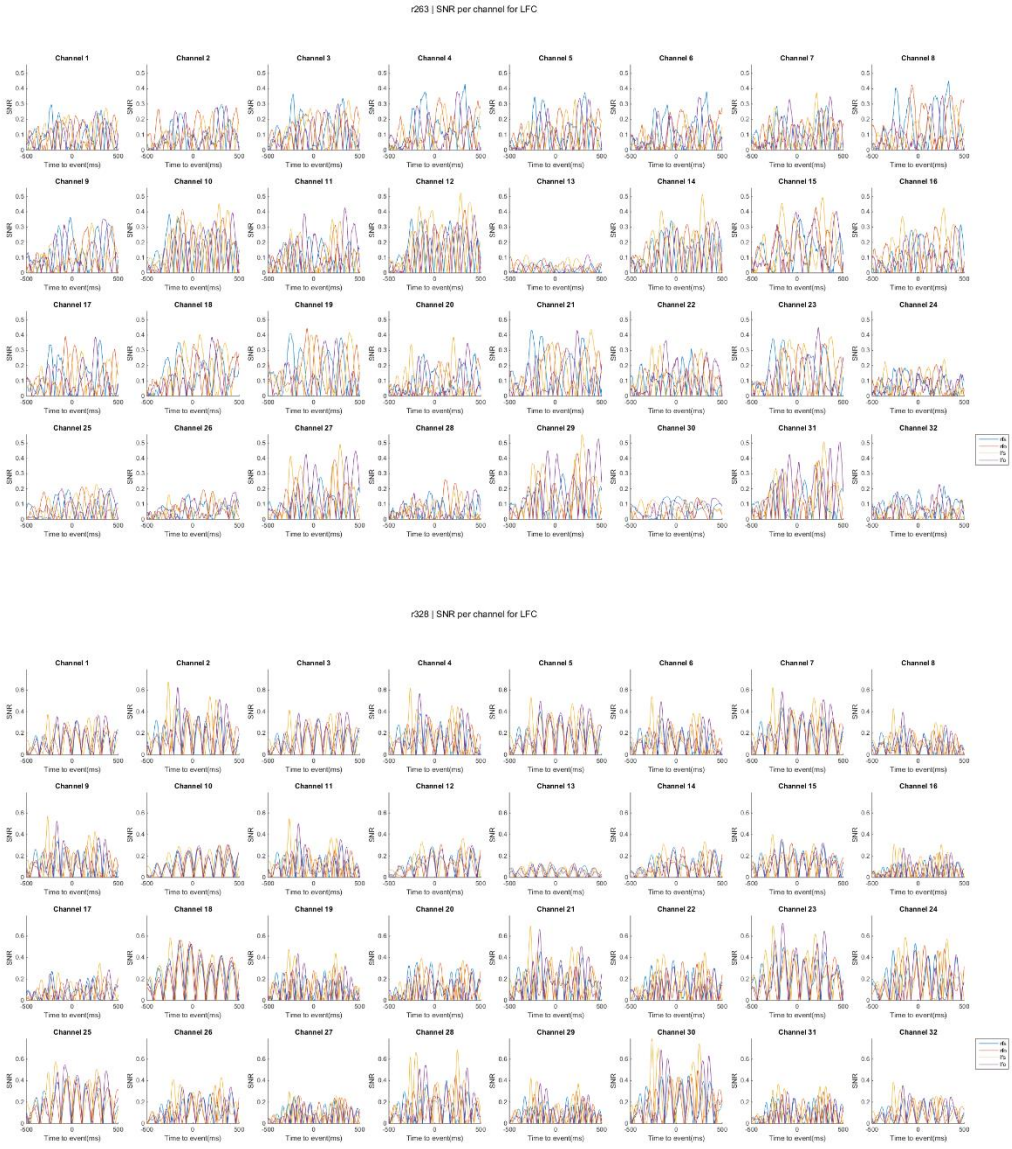

A.2.2. Average SNR values of all trials for all four events (RFO, RFS, LFS, and LFO) with a time window of 500 ms for all individual channels for data that went through the TRFT.

Appendix B

B.1. Data from r328. Mutual information values obtained in cross-validation procedures using different model parameters (feature length, number of features per each channel, regularization coefficient) and tolerance windows. For the cross-validation dataset division three different scenarios were used: halves, thirds and tenths.

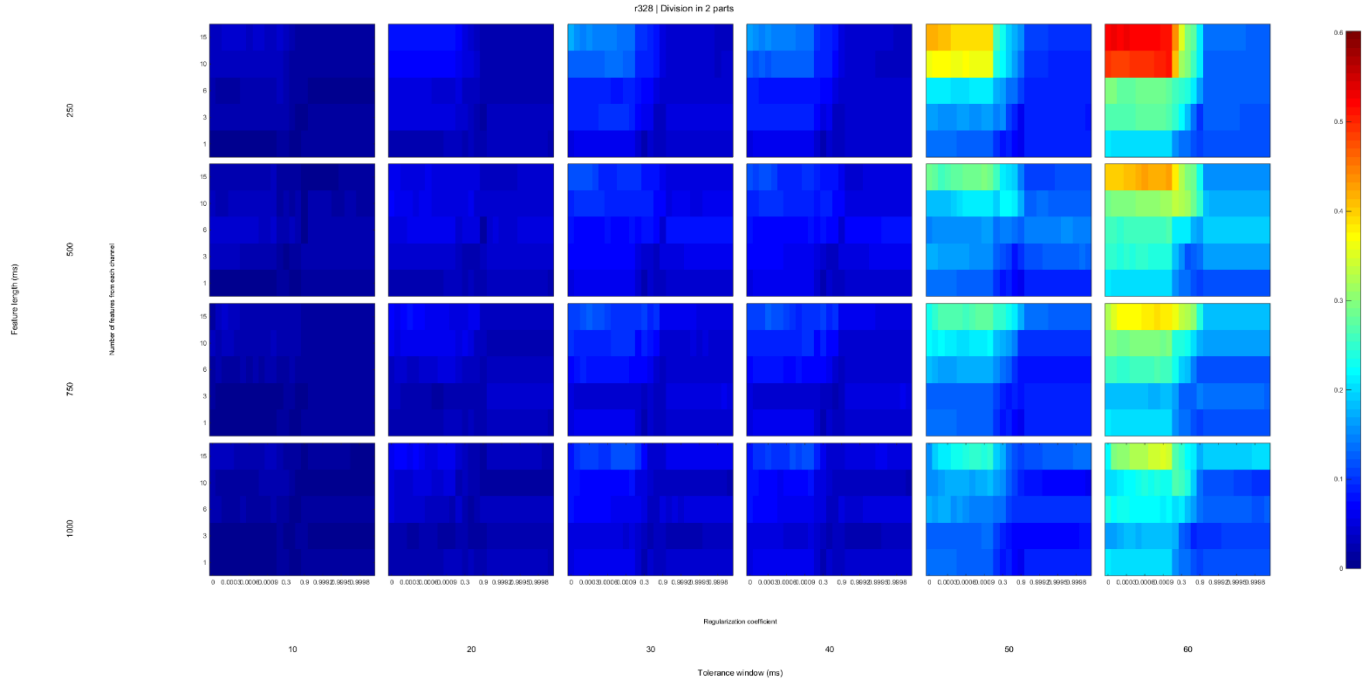

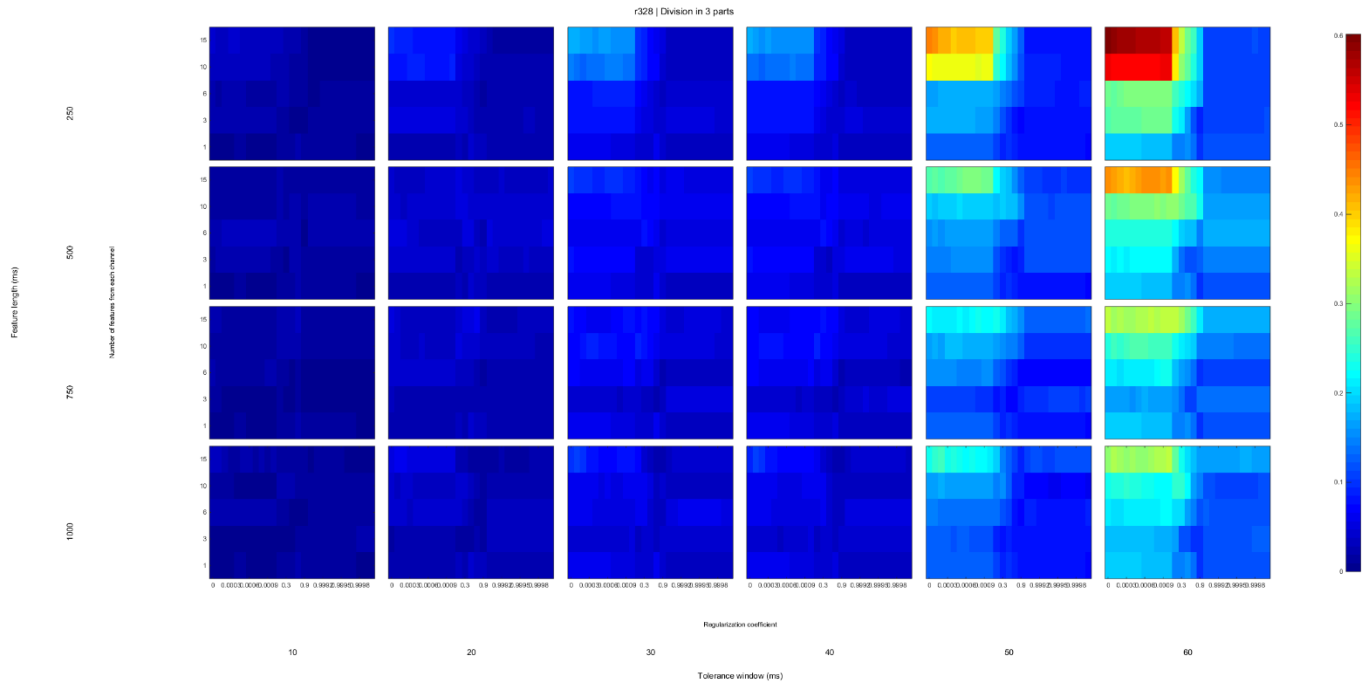

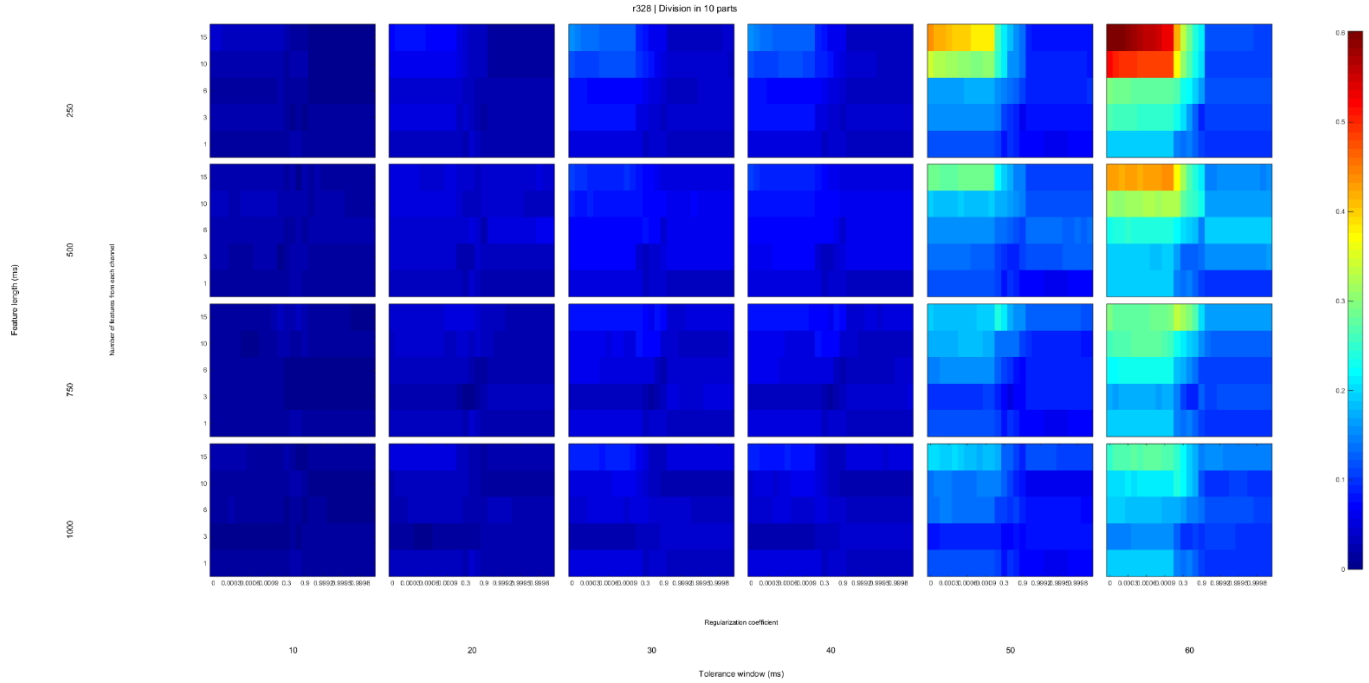
r328 | Division in 10 parts
Feature length (ms)
250
500
750
1000
Number of features from each channel
Regularization coefficient
10
20
30
40
50
60
Tolerance window (ms)

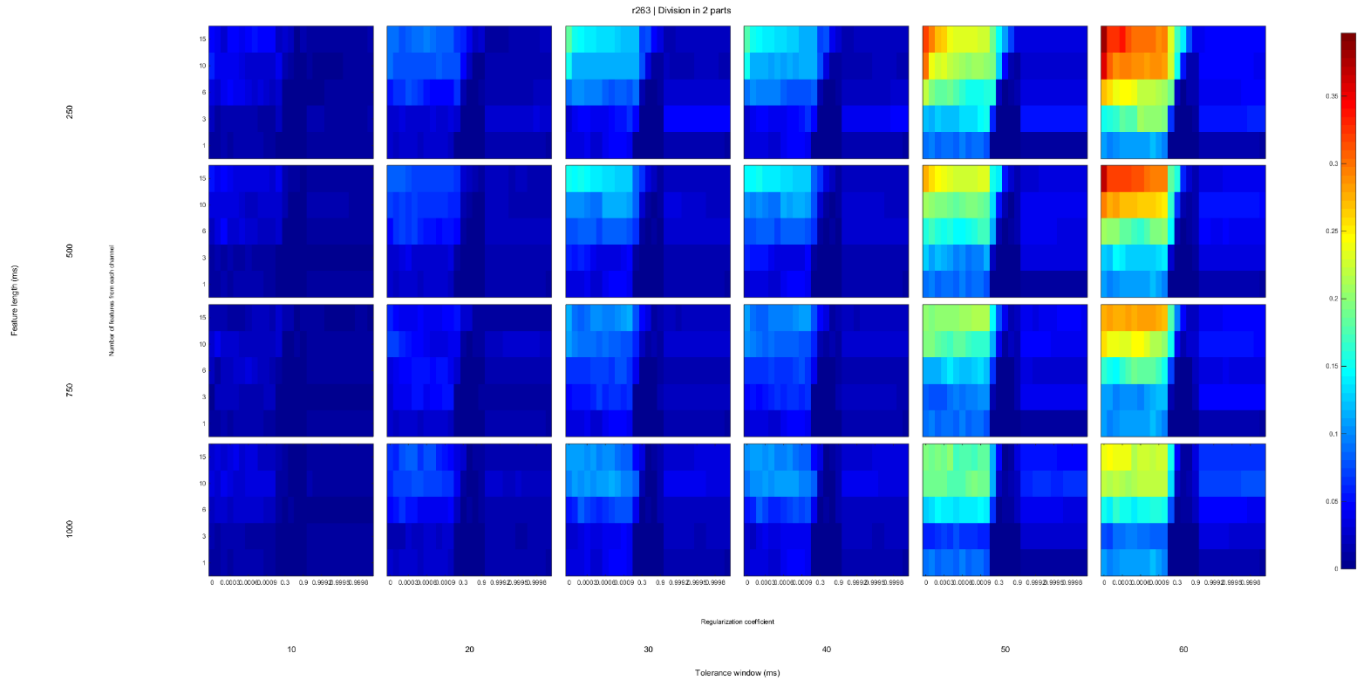
r263 | Division in 2 parts
Feature length (ms)
250
500
750
1000
Number of features from each channel
Regularization coefficient
10
20
30
40
50
60
Tolerance window (ms)

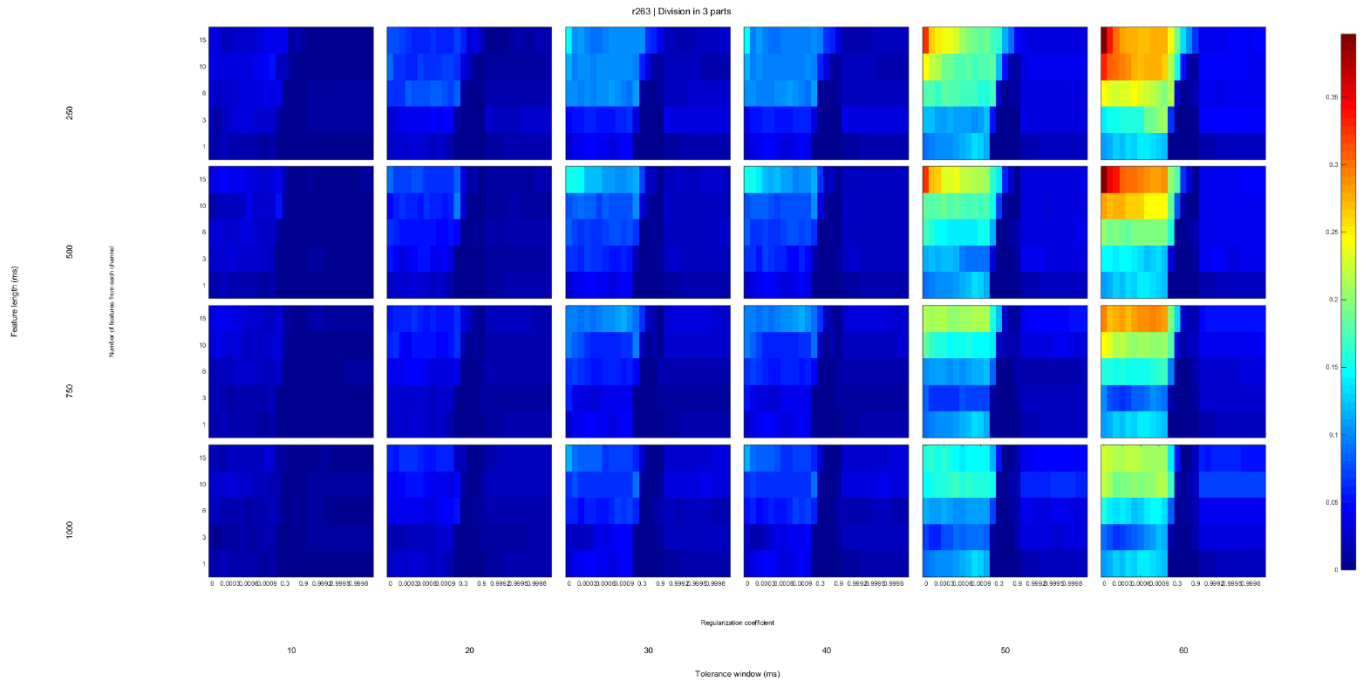
r263 | Division in 3 parts
Feature length (ms)
250
500
750
1000
Number of features from each channel
Regularization coefficient
Tolerance window (ms)
10
20
30
40
50
60

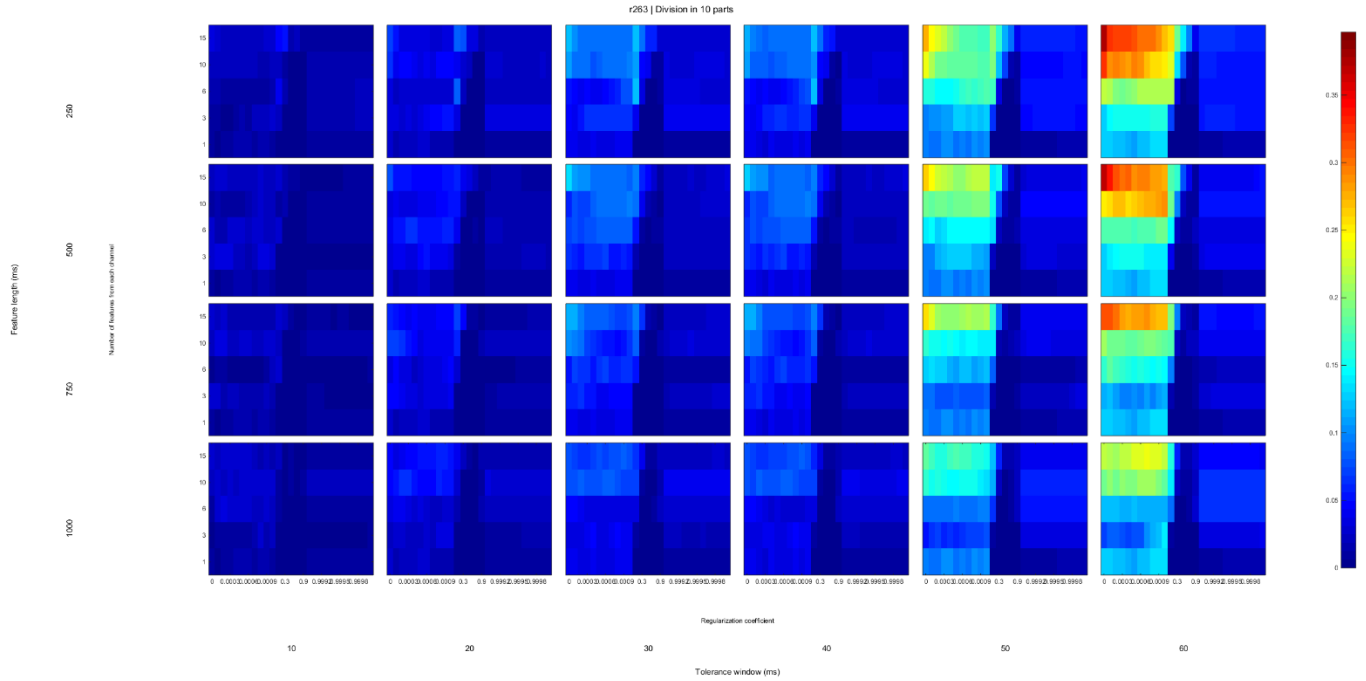
r263 | Division in 10 parts
Feature length (ms)
250
500
750
1000
Number of features from each channel
Regularization coefficient
Tolerance window (ms)
10
20
30
40
50
60

B.2. Data from r263. Mutual information values obtained in cross-validation procedures using different model parameters (feature length, number of features per each channel, regularization coefficient) and tolerance windows. For the cross-validation dataset division three different scenarios were used: halves, thirds and tenths.

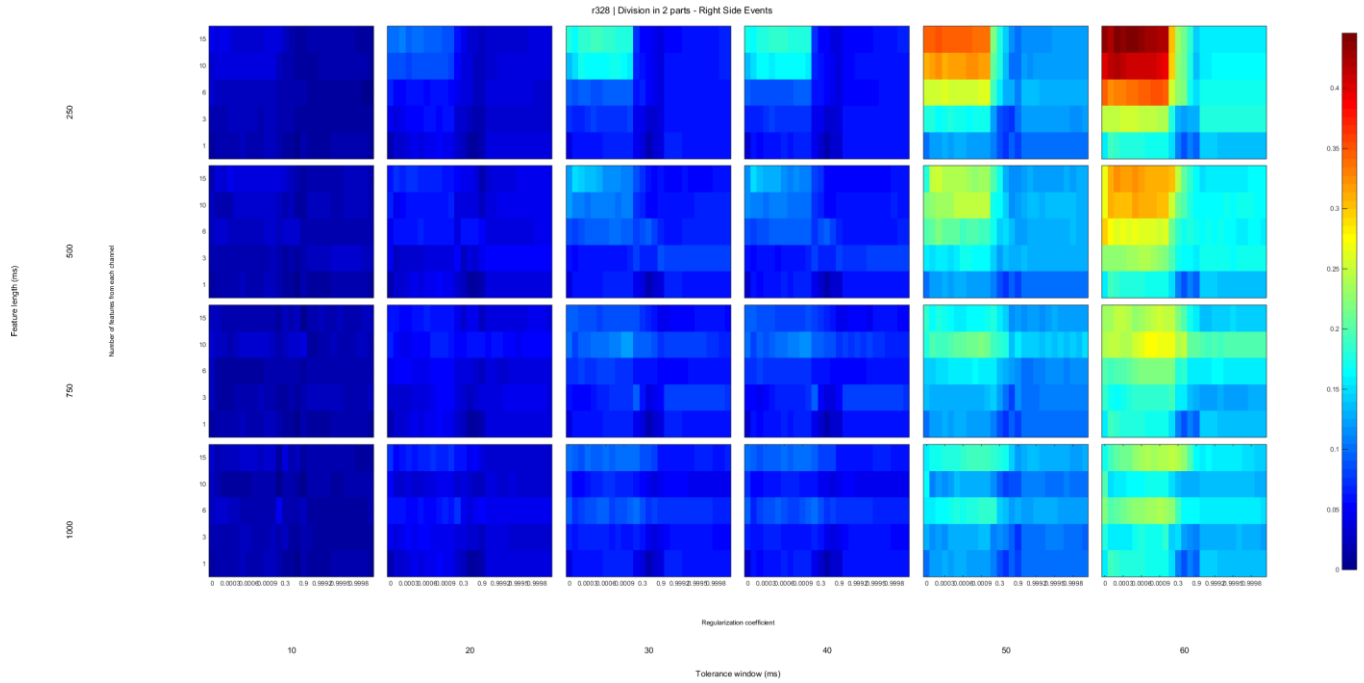

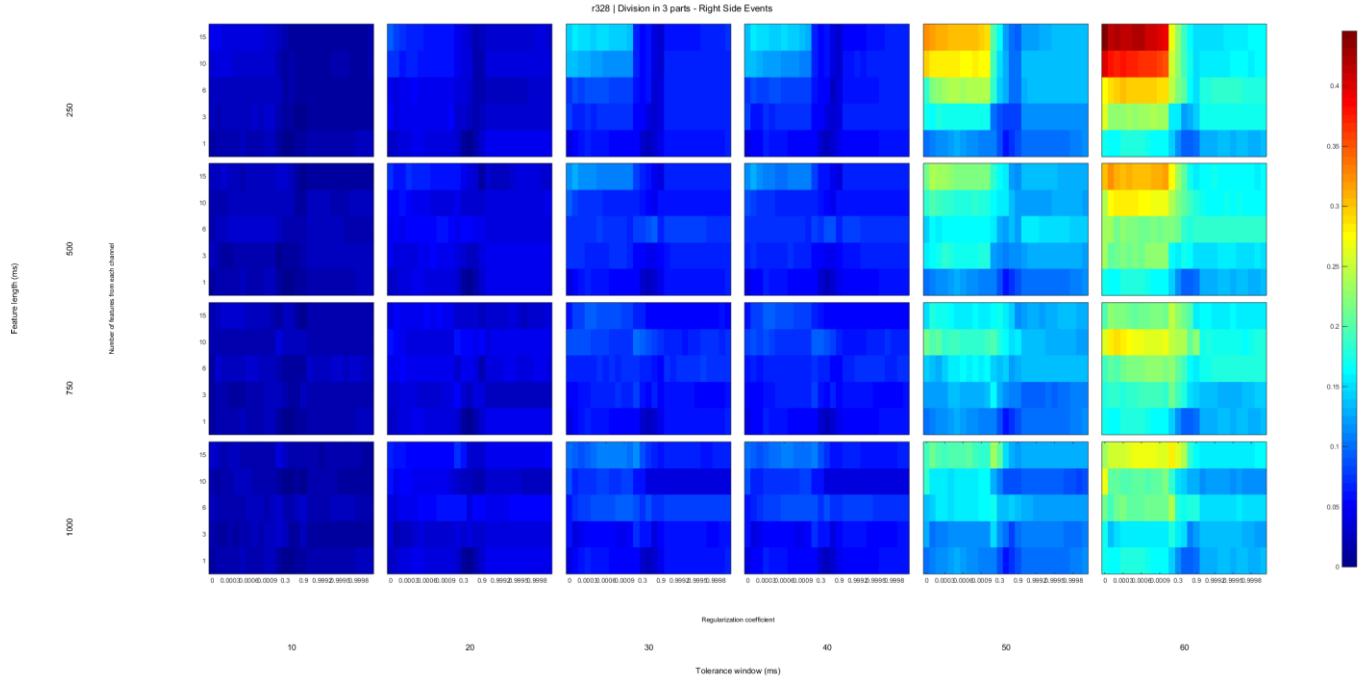

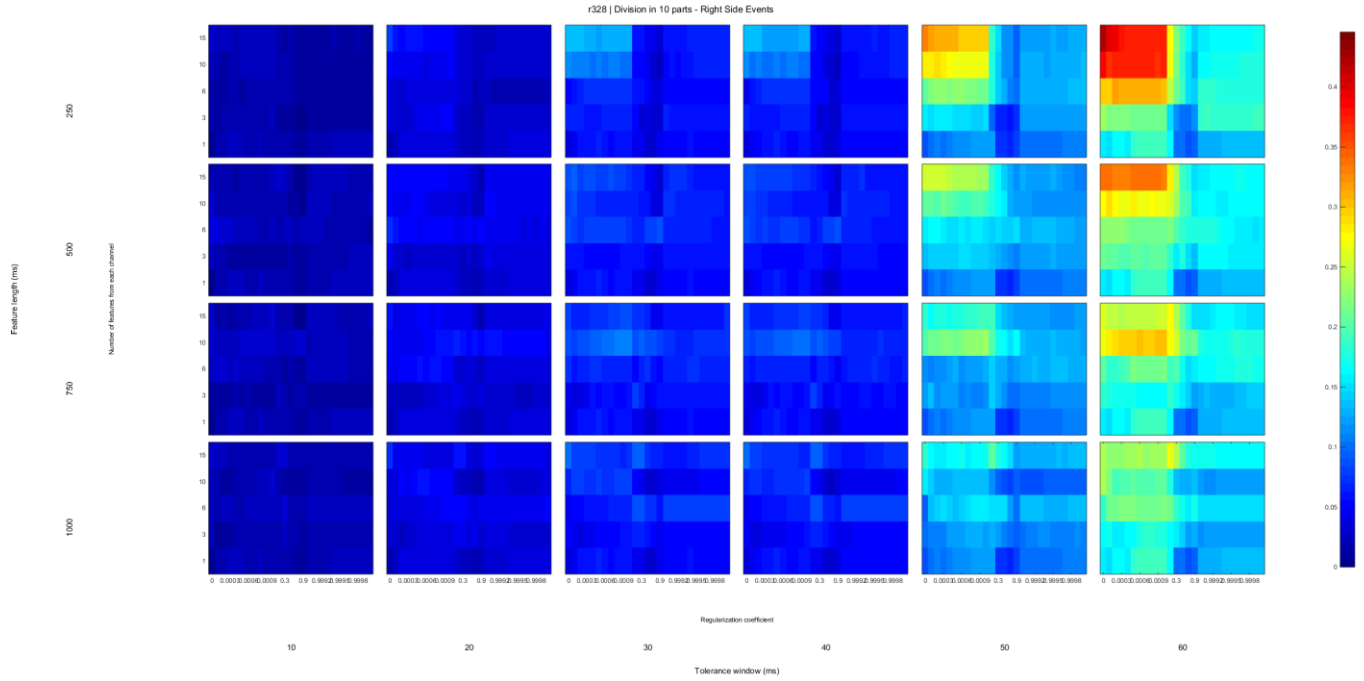
r328 | Division in 10 parts - Right Side Events
Feature length (ms)
Number of features from each channel
Regularization coefficient
Tolerance window (ms)
10
20
30
40
50
60

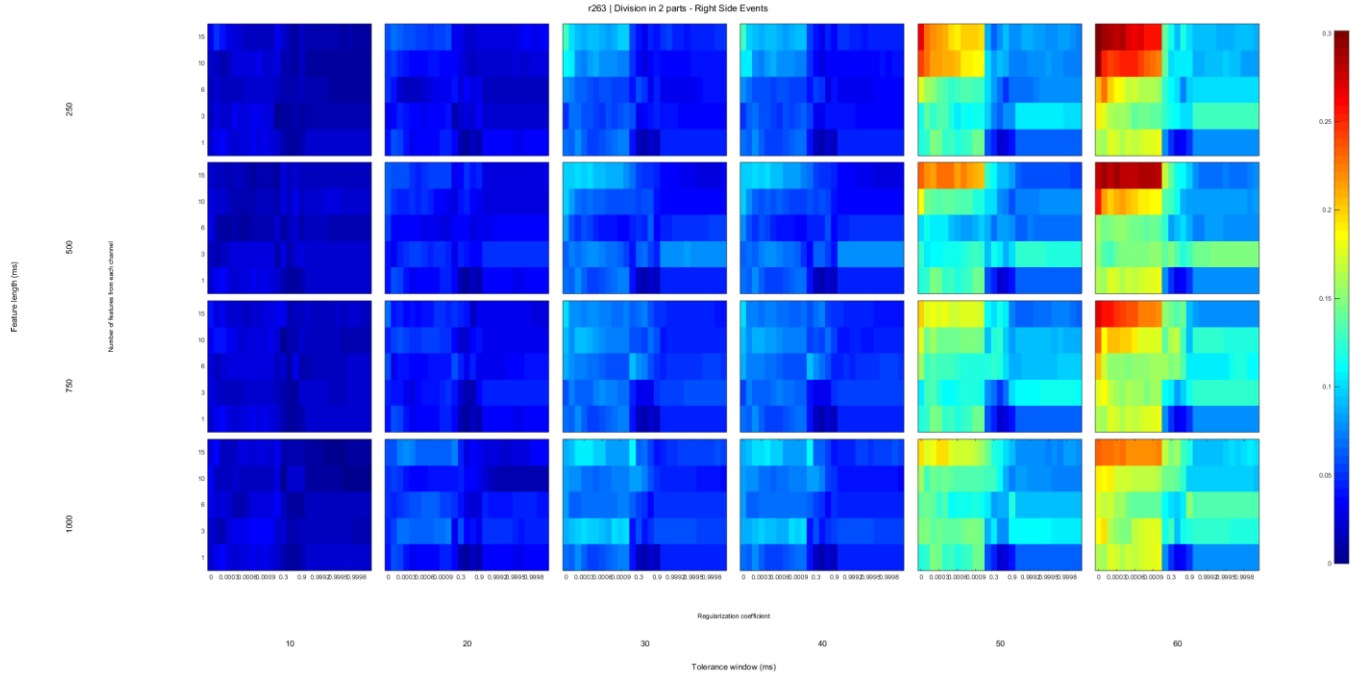
r263 | Division in 2 parts - Right Side Events
Feature length (ms)
Number of features from each channel
Regularization coefficient
Tolerance window (ms)
10
20
30
40
50
60

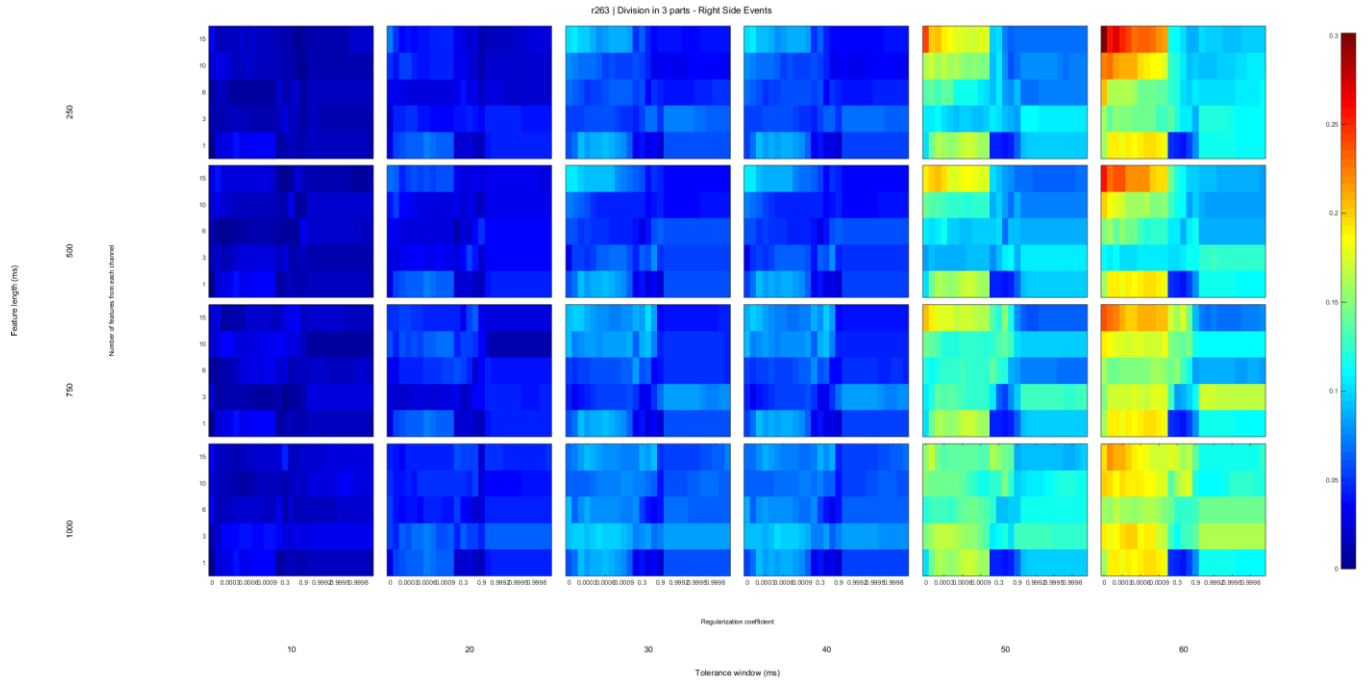
r263 | Division in 3 parts - Right Side Events
Feature length (ms)
250
500
750
1000
Number of features from each channel
Regularization coefficient
10
20
30
40
50
60
Tolerance window (ms)

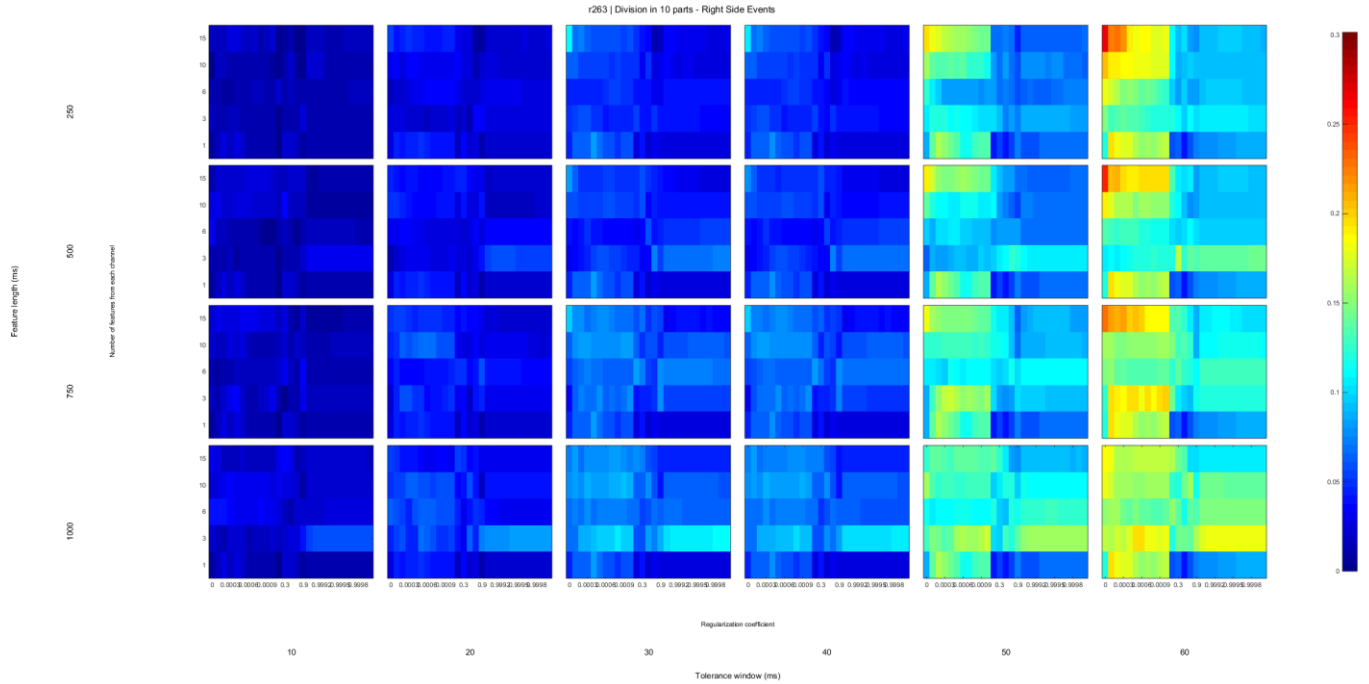
r263 | Division in 10 parts - Right Side Events
Feature length (ms)
250
500
750
1000
Number of features from each channel
Regularization coefficient
10
20
30
40
50
60
Tolerance window (ms)